

**TOWSON UNIVERSITY
OFFICE OF GRADUATE STUDIES**

**USING HIGH-FREQUENCY DATA AND CONCENTRATION-DISCHARGE
RELATIONSHIPS TO DESCRIBE SOLUTE MOBILIZATION AND
TRANSPORT IN SUBURBAN AND URBAN WATERSHEDS**

by

Melinda Marsh

A thesis

Presented to the faculty

of Towson University

in partial fulfillment

of the requirements for the degree

Master of Science

Department of Environmental Science

Towson University

Towson, MD

21252

August, 2021

Thesis Approval Page

DocuSign Envelope ID: 87CBD0C3-AE06-4B7E-9B86-4104BC972EAF



Office of Graduate Studies

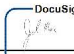
Thesis Approval Page Form

This is to certify that the thesis prepared by Melinda Marsh

titled Using High-Frequency Data and Concentration-Discharge Relationships to Describe Solute Mobiliza

has been approved by the thesis committee as satisfactorily completing the thesis requirements for
the degree of Master of Science

(i.e., Doctor of Science)

DocuSigned by:
 _____ Joel Moore 07/12/21
8EA359973CA3466

Chairperson, Thesis Committee Signature Printed Name Date

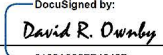
DocuSigned by:
 _____ Alexis Navarre-Sitchler 07/13/21
1DA9FD22EC5B40F

Committee Member Signature Printed Name Date

DocuSigned by:
 _____ Jonathan Duncan 07/13/21
D4DEAA89655E4AD

Committee Member Signature Printed Name Date

☒ Thesis has been submitted to Graduate Studies

DocuSigned by:
 _____ David R. Ownby 07/14/21
0109A385FE4043B

Dean of Graduate Studies Signature Printed Name Date

Acknowledgments

I would like to thank my advisor, Joel Moore, for his support and guidance during this project. I would also like to thank my committee members, Jonathan Duncan and Alexis Navarre-Sitchler, for their time and feedback. I thank the members of the Moore Lab for their support. In particular, I thank Patrick McMahon, Kathleen Hohweiler, Ginny Jeppi, and Emily O'Donnell for their assistance in the field and laboratory. I thank Nico Werps and Kyle Bucher for creating the site maps for this project. I also thank Cassie Cosans for her time and assistance with water isotope analyses and Mark Monk for his invaluable help with analytical instrumentation and troubleshooting.

Abstract

Using High-Frequency Data and Concentration-Discharge Relationships to Describe Solute Mobilization and Transport in Suburban and Urban Watersheds

Melinda Marsh

Event-scale and long-term C-Q patterns of multiple dissolved constituents were examined for three small watersheds—one mostly forested suburban and two urban—in Maryland using discrete sampling and high-frequency specific conductance data. Despite differences in land use and hydrology, the watersheds exhibited remarkably similar behavior for individual solutes across timescales, albeit with higher concentrations and fluxes for the urban watersheds. Geogenic and exogenous solutes exhibited dilution, while biologically associated solutes showed enrichment with increasing discharge. Concentrations showed much less variability than discharge, suggesting near-chemostatic behavior may be characteristic of urbanized watersheds, similar to forested/agricultural watersheds. Regardless of dilution or enrichment in event concentrations, solute fluxes increased during all storm events and were substantially higher at the urban sites. Baseflow was a significant contributor to event flow at the suburban site, while quickflow contributions dominated at the urban sites. Across all sites, most of the solute load was exported during baseflow.

Table of Contents

List of Tables	vii
List of Figures	ix
1. Introduction.....	1
1.1 Urban Watersheds.....	1
1.2 Concentration-Discharge (C-Q) Relationships	4
1.3 Factors Driving C-Q Relationships.....	9
2. Materials and Methods.....	13
2.1 Site Description.....	13
2.2. Sample Collection and Analysis	14
2.2.1 Baseflow and Stormflow Sampling	14
2.2.2 End Member Sampling	15
2.2.3 Sample Analysis.....	15
2.3 Discharge and Specific Conductance Data Collection	17
2.4 High-Frequency Time Series Datasets for Major Ions	18
2.5 Hydrograph Separation	19
2.6 Solute Flux and Solute Load Calculations.....	20
2.7 Storm Delineation	21
2.8 Calculation of Hysteresis Metrics	22
2.8.1 Hysteresis Index.....	22

2.8.2 Flushing Index	24
2.8.3 Power Laws and Coefficient of Variation	25
2.8.4 Classification of C-Q Behavior.....	26
2.9 End Member Mixing Analysis.....	27
3. Results and Discussion	28
3.1 High-Frequency Discharge and Specific Conductance Data.....	28
3.2 Baseflow Water Chemistry – Discrete Samples	30
3.3 Stormflow Water Chemistry – Discrete Samples	33
3.4 Storm Event Specific Conductance-Discharge Relationships	36
3.5 Event-Scale Concentration-Discharge Relationships	41
3.5.1 Biologically Associated Solutes	42
3.5.2 Geogenic and Exogenous Solutes.....	45
3.6 Event-Scale Flux-Discharge Relationships.....	52
3.7 Long-term Solute Behavior.....	53
3.8 Hydrograph Separation for Calculation of Solute Loads.....	56
3.9 End Member Mixing Analysis.....	60
4. Conclusions.....	60
5. Tables	62
6. Figures.....	78
7. References.....	102
8. Curriculum Vitae	120

List of Tables

Table 1: Study site characteristics	62
Table 2: Regression models for high-frequency solute concentration datasets	63
Table 3: Summary statistics for high-frequency discharge	64
Table 4: Summary statistics for high-frequency specific conductance	65
Table 5: Median cation concentrations of discrete baseflow and stormflow samples ..	66
Table 6: Median anion concentrations of discrete baseflow and stormflow samples ...	67
Table 7: Median [DOC], [TDN], and [SiO ₂] of discrete baseflow and stormflow samples	68
Table 8: Concentrations of dissolved constituents in precipitation samples and direct surface runoff from a stormflow drainpipe at HERR.....	69
Table 9: Summary statistics for storm event peak discharge	70
Table 10: Specific conductance-discharge patterns and percentages observed during storm events.....	71
Table 11: Median FI and HI by season for storm event SC-Q relationships	72
Table 12: Median FI, HI CV_C/CV_Q and C-Q slope (b) for discretely sampled storm events at BARN.....	73

Table 13: Median FI, HI CV_C/CV_Q and C-Q slope (b) for discretely sampled storm events at HERR	74
Table 14: Median FI, HI CV_C/CV_Q and C-Q slope (b) for discretely sampled storm events at PTRG.....	75
Table 15: Long-term CV_C/CV_Q , C-Q slopes (b), and power law regression coefficients for BARN, HERR, and PTRG.....	76
Table 16: Results from baseflow separation showing the fraction of the total load of individual solutes attributed to nonwinter, winter, quickflow, and baseflow.	77

List of Figures

Figure 1: Representations of hysteresis patterns showing (A) general characteristics, including rotational direction, slope, and amplitude, and (B) interpretations of slope. Figure modified from Long (2017)	78
Figure 2: (A) An example of a three-component end member mixing model adapted from Liu et al. (2004) showing hydrograph contributions of overland flow, interflow, and baseflow over time. (B) Theoretical hysteresis patterns that were proposed by Evans and Davies (1998)	79
Figure 3: Watershed land cover map of (A) Baisman Run (BARN), (B) Plumtree Run (PTRG), and (C) West Branch Herring Run (HERR); (D) land cover map of the Baltimore metropolitan region.	80
Figure 4: High-frequency discharge normalized to watershed area by season	81
Figure 5: High-frequency specific conductance by season ($\mu\text{S}/\text{cm}$).....	82
Figure 6: Concentrations of select dissolved constituents from discrete samples collected during baseflow and stormflow at BARN, HERR, PTRG.	83
Figure 7: Hysteresis index (<i>HI</i>) versus flushing index (<i>FI</i>) of specific conductance-discharge (SC-Q) relationships at BARN	84

Figure 8: Hysteresis index (<i>HI</i>) versus flushing index (<i>FI</i>) of specific conductance-discharge (SC-Q) relationships at HERR.....	85
Figure 9: Hysteresis index (<i>HI</i>) versus flushing index (<i>FI</i>) of specific conductance-discharge (SC-Q) relationships at BARN	86
Figure 10: Storm event flushing index (<i>FI</i>) versus the logarithm of peak discharge for 75, 219, and 209 individual events at BARN, HERR, and PTRG, respectively	87
Figure 11: Example of the first flush effect during a moderately-sized storm event at PTRG.....	88
Figure 12: Comparison of C-Q behavior characterization for an example event at BARN using A) the C-Q slope (<i>b</i>) of the log(C)-log(Q) regression and B) the flushing index (<i>FI</i>).....	89
Figure 13: C-Q slope (<i>b</i>) versus CV_C/CV_Q of dissolved solutes for discretely sampled storm events at A) BARN, B) HERR, and C) PTRG.....	90
Figure 14: Median <i>HI</i> versus median <i>FI</i> of dissolved solutes for discretely sampled storm events at A) BARN, B) HERR, and C) PTRG.....	91
Figure 15: Concentration-discharge behavior of select geogenic and exogenous solutes during discretely sampled winter storm events at A) BARN and B) HERR	92
Figure 16: Fluxes (g/s) of select dissolved constituents for a discretely sampled storm event on 10-11-2020 at BARN, HERR, and PTRG.	93
Figure 17: Total dissolved solids (TDS) flux for the smallest storm events (peak $Q < 10$ th percentile) and the largest storm events at BARN, HERR, and PTRG.	94

Figure 18: Long-term C-Q behavior of dissolved constituents at BARN compared to the C-Q behavior of individual storm events	95
Figure 19: Long-term C-Q behavior of dissolved constituents at HERR compared to the C-Q behavior of individual storm events.	96
Figure 20: Long-term C-Q behavior of dissolved constituents at PTRG compared to the C-Q behavior of individual storm events	97
Figure 21: Comparison of event-scale and long-term (4-year) C-Q slopes (b) of dissolved constituents at BARN, HERR, and PTRG	98
Figure 22: Results from hydrograph separation showing the fraction of total load and total load ($\times 10^5$ kg) attributed to nonwinter and winter periods, and baseflow and quickflow components as determined from baseflow separation	99
Figure 23: A) Median event-scale C-Q slope (b) versus the fraction of export attributed to quickflow for each solute at BARN, HERR, and PTRG; B) Median event-scale CV_C/CV_Q versus the fraction of solute export attributed to quickflow.....	100
Figure 24: Discharge for an individual storm event in 2020 at A) BARN and B) HERR demonstrating baseflow separation results using the <i>EcoHydRology</i> package in R ...	101

1. Introduction

1.1 Urban Watersheds

Urban areas are one of the most rapidly growing land-use types in the United States with over 80% of the population residing in cities as of 2019 (The World Bank Group, 2019). Urban development and associated human activities can have adverse impacts on Earth's Critical Zone (CZ), which extends from the periphery of the vegetation canopy to the deepest freely circulating groundwater/bedrock interface (Chorover et al., 2017; Minor et al., 2020; National Research Council, 2001). In the CZ, interactions between air, water, soil, bedrock, and living organisms drive essential processes, including soil generation, nutrient cycling, decomposition of organic matter, water infiltration and storage, and evapotranspiration (Chorover et al., 2017; Lin, 2010; Minor et al., 2020). Urbanization can alter CZ fluxes through the loss of vegetation and expansion of impervious surface cover (ISC), which reduce infiltration of precipitation, diminish groundwater recharge and baseflow, and increase overland flow (Minor et al., 2020; O'Driscoll et al., 2010; Walsh et al., 2005). Soil compaction resulting from urbanization can further alter the hydrologic flow regime through the reduction of infiltration and the lowering of soil storage capacity. Consequently, even if precipitation can infiltrate soils, saturation is achieved more rapidly, and runoff will occur as Horton overland flow or saturation-excess overland flow rather than via subsurface flow processes (D B Booth & Jackson, 1997; Dunne & Black, 1970). Artificial drainage (e.g., gutters, drains, and storm drains) can efficiently convey surface runoff to stream channels, altering the rainfall-runoff response and causing flashier behavior relative to

forested watersheds (D B Booth & Jackson, 1997; J. D. Miller & Hess, 2017). Increased peak flows and runoff volumes, decreased lag times, and sharper ascending and descending limbs of the hydrograph are characteristic of urbanized watersheds (Walsh et al., 2005). For any given rate and duration of precipitation, peak discharge in urban watersheds has been found to be 2 to 5 orders of magnitude greater than in forested watersheds (D B Booth & Jackson, 1997). Furthermore, the frequency with which discharge events occur in urban watersheds has been shown to increase by a factor of 10 or more relative to forested catchments (Derek B Booth, 1991).

In addition to the changes in hydrology caused by urbanization, non-point source contributions from urban runoff can alter and degrade the water quality of urban streams and downstream receiving water bodies (McGrane, 2016). Inputs from atmospheric deposition, road salt, anthropogenic materials (e.g., weathering of concrete), and septic and sanitary sewer systems have been linked to elevated alkalinity and concentrations of major ions and nutrients in urban watersheds (Sujay S. Kaushal et al., 2011, 2017; Moore et al., 2017; Peters, 2009; Taka et al., 2017). Flushing from urban surfaces can also contribute organic material, sediments, metals, and other pollutants to urban waterways (Masoner et al., 2019; Nicolau et al., 2012; Peters, 2009). The transport of dissolved and particulate species is commonly expedited in urban watersheds as a result of increased ISC coupled with the hydraulic efficiency of artificial drainage systems. Storm events can exacerbate urban water quality degradation as storm runoff bypasses subsurface retention and is routed directly to receiving streams (Blaszczak et al., 2019; McGrane, 2016; J. D. Miller & Hess, 2017). The initial period of a storm event may be marked by increases in

temperature and concentrations of dissolved and particulate species as heat and constituents from impervious surfaces are rapidly delivered to streams, a phenomenon referred to as ‘first-flush’ (Bach et al., 2010; Taka et al., 2017). Furthermore, storm events may be the primary mobilizer of solutes in urban watersheds. For example, in a small, urban Mediterranean watershed, stormflow accounted for more than 70% of the annual output of dissolved organic carbon (DOC) and nitrate along with 39-65% of the annual output of major ions (Na^+ , K^+ , Mg^{2+} , Ca^{2+} , Cl^- , and SO_4^{2-}) (Nicolau et al., 2012). Storm runoff discharging into urban and suburban streams adversely affects aquatic organisms, particularly the community composition, abundance, and biomass of benthic macroinvertebrates (Goldyn et al., 2018; Masoner et al., 2019; Pratt et al., 1981; Walsh et al., 2001).

While elevated concentrations of metals and suspended solids in urban stormwater are well documented, less attention has been paid to the occurrence and temporal variability of major ion concentrations either individually or as a whole through their role in increased conductivity (Blaszczak et al., 2019; Fovet et al., 2018; Moore et al., 2020; Taka et al., 2017). Stream chemistry reflects the integration of watershed hydrological and biogeochemical processes that occur in the CZ over varied spatial and temporal scales. As water is transported through the CZ, the chemical composition may be changed by anthropogenic inputs as well as the CZ components with which it interacts (e.g., soil pores, bedrock, hyporheic zones) before its emergence at the stream channel (Chorover et al., 2017; Olshansky et al., 2018). The extent to which the chemical composition is changed is dictated by residence times and by thermodynamic and

kinetically limited reactions, e.g., microbial transformation of nutrients, decomposition of organic matter, ion exchange, and mineral weathering (Chorover et al., 2017; Olshansky et al., 2018). Insight into the watershed hydrologic and biogeochemical processes driving changes in water chemistry can be gained through the examination of solute concentration and discharge (C-Q) relationships.

1.2 Concentration-Discharge (C-Q) Relationships

Variations in the connectivity, compositions, and contributions of hydrologic flow paths in the CZ can produce a range of C-Q responses during precipitation events (Chorover et al., 2017). At the storm event timescale, solute concentrations often exhibit nonlinear, hysteretic responses to varying hydrological conditions that are characterized by concentrations on the rising limb differing from those on the falling limb at a given discharge rate (Evans & Davies, 1998) (Figure 1a). When stream discharge increases, solute concentrations may increase (flushing or enrichment behavior), decrease (dilution behavior), or exhibit minimal change (chemostatic behavior) (Evans & Davies, 1998; Herndon et al., 2015; Hoagland et al., 2017) (Figure 1b). During storm events, solute concentrations may be substantially higher during the initial period of stormwater runoff due to the flushing of contaminants from impervious surfaces (i.e., first flush). Alternatively, stormwater runoff may dilute more concentrated groundwater sources (Hatt et al., 2004; Lee et al., 2002).

C-Q relationships can improve our understanding of the processes governing solute mobilization and transport to downstream ecosystems and can be used to infer potential sources and their distribution in watersheds. For example, clockwise hysteresis

occurs when concentrations on the rising limb exceed those on the falling limb, which suggests rapid solute mobilization and/or sources proximal to the sampling location. Conversely, counterclockwise hysteresis reflects higher falling limb concentrations, suggesting longer transport times (e.g., deeper subsurface sources), higher concentration sources distant from the sampling location, and/or delayed subsurface connectivity (Aguilera & Melack, 2018; L. A. Rose et al., 2018; Vaughan et al., 2017; Zuecco et al., 2019). Solutes that increase in concentration with rising discharge are considered transport-limited because discharge (or water flux) determines their mobilization. Flushing behavior has been attributed to several factors, including the mixing of more concentrated sources (e.g., surface runoff) with more dilute stream water, rising water tables that connect carbon- and nutrient-rich shallow soils to the stream, and increased hydrological connectivity between upland sources and the stream during high flow conditions (Hoagland et al., 2017; L. A. Rose et al., 2018; Vaughan et al., 2017). Solutes that decrease in concentration with rising discharge are considered source-limited due to a finite supply that is rapidly depleted. Dilution behavior may also result from the mixing of less-concentrated meteoric water with water stored in the catchment, shorter residence times in the contributing flow paths, or slow reaction rates (Duncan et al., 2017; Herndon et al., 2015; Hoagland et al., 2017; L. A. Rose et al., 2018; Vaughan et al., 2017). Chemostasis cannot be explained simply by the mixing of various sources, but instead has been attributed to large solute reservoirs and/or fast chemical reaction rates (Godsey et al., 2009; Olshansky et al., 2018; Vaughan et al., 2017).

Early studies on C-Q relationships focused on classifying and proposing explanations for different event-scale hysteresis patterns. Evans and Davies (1998) proposed that patterns in C-Q hysteresis could be explained using a three end-member mixing model (Figure 2a) consisting of surface event water (overland flow), soil water (interflow), and groundwater (baseflow). They presented six theoretical single-loop hysteresis patterns (Figure 2b) based on the fixed volume, timing, and composition of each end-member, and each pattern was characterized by rotation (clockwise/counterclockwise), slope (positive/negative), and curvature (convex/concave) based on the relative contribution of each end-member (Evans & Davies, 1998). Chanet et al. (2002) expanded on the Evans and Davies (1998) study and found that interpretations of C-Q patterns can be confounded by real-world hydrological variability. For example, modeled C-Q responses to variations in end-member volume, timing, and composition revealed that more than one of the C-Q patterns described by Evans and Davies (1998) could be generated for a given rank order of end-member contributions (Chanat et al., 2002; Hornberger et al., 2001). Other studies have found that a simple two end-member mixing model consisting of surface and shallow subsurface runoff and baseflow adequately explains the observed C-Q responses in their respective watersheds (Evans & Davies, 1998; Murphy et al., 2012; S. Rose, 2003). Complex patterns in event-scale C-Q hysteresis were identified by Williams (1989) and further classified by Zuecco et al. (2016), including the single-line-with-loop and multi-looped figure-of-eight patterns, and were attributed to variations in species storage, availability, and

transportability. The types of observed hysteresis patterns and the approach used to classify and interpret them will vary by watershed.

In addition to event-scale hysteresis, concentration-discharge studies have been performed across a range of timescales, including seasonal (Duncan et al., 2017; Fovet et al., 2018; Vaughan et al., 2017; Zuecco et al., 2016), interannual (Aguilera & Melack, 2018; Baker & Showers, 2019; L. A. Rose et al., 2018), and composite scales (i.e., all samples in the observation record) (Godsey et al., 2009; Musolff et al., 2015). While C-Q relationships developed from long-term, low-frequency data reflect the average characteristics of a watershed, they provide limited insight into hydrological processes and solute dynamics occurring on finer scales. Traditionally, temporal changes in stream chemistry have been examined through the collection of discrete samples (manual or automatic) across a range of stream discharge. Recent studies have employed high-frequency in-situ sensors to examine C-Q relationships for DOC, nitrate, and turbidity at finer temporal scales (Baker & Showers, 2019; Duncan et al., 2017; Lloyd et al., 2015; Vaughan et al., 2017). High-frequency sensors provide much higher resolution than discrete samples, allowing rapid changes in water chemistry to be captured and for much larger datasets across multiple storm events.

The processes controlling observed C-Q hysteresis patterns often can be explained by chemical and isotopic mixing models. If attributable to particular end members, isotopic and geochemical tracers can be used to quantify runoff sources and the dominant runoff-producing components contributing to stormflow, which can dictate C-Q behavior. Tracer studies typically utilize either hydrograph separation or end-member mixing

analysis (EMMA) techniques. Hydrograph separation commonly relies on a mass-balance approach to temporally separate the hydrograph into two source components. Two-component mass-balance models separate the hydrograph into pre-event and event components using a single tracer. Pre-event water is generally represented as the combination of soil and groundwater and is considered to be equivalent to the baseflow concentration before an event using the assumption that contributions from soils are minimal or chemically equivalent to groundwater (Pinder & Jones, 1969). Event water is represented by surface runoff and/or precipitation. In comparison to hydrograph separation techniques, EMMA uses least square regression or principal component analysis (PCA) to separate source components from a mixture with no restriction on the number of tracers used (Barthold et al., 2011; Christophersen & Hooper, 1992). Both methods require several assumptions, including 1) the solutes or tracers used behave conservatively, i.e., the tracers do not react during transport; 2) the mixing process is linear; 3) the chemical composition of each end-member is distinct; and 4) the chemical composition of each end-member is time- and space-invariant and is only altered during in-channel mixing (Barthold et al., 2011; Inamdar et al., 2013). Commonly used tracers include stable water isotopes ($\delta^{18}\text{O}$ and $\delta^2\text{H}$), cations (Na^+ , K^+ , Mg^{2+} , and Ca^{2+}), anions (Cl^- and SO_4^{2-}), alkalinity, acid-neutralizing capacity (ANC), dissolved silica, and electrical conductivity (Barthold et al., 2011; Inamdar et al., 2013; Liu et al., 2017). Individual tracers may not be appropriate for all watersheds, for example, sodium, chloride, and electrical conductivity may not be suitable tracers in watersheds receiving inputs of road salt during winter months. Potential end-members contributing to

streamflow include precipitation, throughfall, soil water, hillslope water, hyporheic water, shallow groundwater, and deep groundwater, amongst others; however, not all will be significant contributors to flow in every watershed.

1.3 Factors Driving C-Q Relationships

C-Q relationships may vary by land use, season, storm event, and chemical species. Behavior differences among individual solutes have been attributed to landscape heterogeneity, solute mass stores within a catchment, antecedent watershed conditions, and changes in hydrologic connectivity during varying flow regimes, amongst others (Herndon et al., 2015; Musolff et al., 2015; L. A. Rose et al., 2018). While explanations for behavior differences are often site-specific, they provide valuable insight into the hydrological and hydrochemical processes governing solute export in watersheds. An overview of the factors influencing C-Q relationships follows.

In forested and, to a lesser extent, agricultural watersheds, C-Q behavior can vary between groups of solutes from different sources such as mineral weathering versus biologically cycled or shallow versus deep soils. At both composite and interannual scales, Godsey et al. (2009) found that concentrations of solutes associated with mineral weathering (e.g., Ca, Na, Si) exhibited nearly chemostatic patterns for 59 geochemically diverse forested watersheds, suggesting similar concentrations of these solutes in all areas contributing to streamflow and/or rates of solute production and mobilization that are proportional to that of discharge. On a similar temporal scale, Herndon et al., (2015) found that, in three forested watersheds, patterns of vegetation and soil organic matter resulted in contrasting C-Q patterns due to heterogeneous distributions of dissolved

organic carbon in soils. Solutes concentrated in organic-rich soils (e.g., Ca, K) or that form strong complexes with DOC (e.g., Al) exhibited enrichment or dilution behavior with increasing discharge depending on the watershed, while solutes concentrated in soil minerals or that form weak complexes with DOC (e.g., Na, Mg, Si) showed chemostatic behavior (Herndon et al., 2015). In a Mid-Atlantic watershed comprised mostly of agricultural and forested land, Rose et al., 2018 identified distinct C-Q relationships for biologically associated species and geogenic/exogenous species. Across interannual and event scales, biologically associated species (e.g., DOC, total phosphorous) often showed counterclockwise flushing behavior due to the sequence and timing of flow path contributions while geogenic (e.g., Ca, Na) and exogenous (e.g., NO₃) species often exhibited clockwise dilution behavior (L. A. Rose et al., 2018). Aguilera and Melack (2018) reported similar flushing behavior for DOC but more variable behavior for NO₃ in forested and agricultural watersheds of southern California with NO₃ commonly exhibiting counterclockwise enrichment patterns in addition to clockwise dilution.

In primarily forested watersheds, the timing of contributions from different source areas can drive stream chemistry during high discharge events as upland sources become more hydrologically connected to the stream. Inputs may also shift from groundwater and riparian zones during the initial part of the event to hillslope runoff during higher flows as soil layers become saturated. For example, Rose et al. (2018) found that groundwater was the primary contributor to stormflow during the initial and final stages of storm events, while precipitation and soil water contributions dominated during the storm peak. Stream chemistry and C-Q behavior also can vary based on antecedent conditions in the

watershed. In a snowmelt-dominated forested watershed, Zhi et al. (2019) showed that groundwater contributions dominated under dry, low flow conditions while soil water was the dominant contributor during wet (snowmelt) conditions. Concentrations of geogenic species (e.g., Na, Ca, and Mg) and Cl were highest under dry conditions and diluted during snowmelt by increasing contributions of less-concentrated soil water, resulting in dilution C-Q patterns. In contrast, concentrations of solutes abundant in shallow soils (e.g., DOC, TN) exhibited flushing patterns in response to the rising water table tapping organic-rich soils (Zhi et al., 2019).

Similar event-scale variability in solute behavior has been observed in urban watersheds. For example, in a Michigan watershed, sodium and chloride commonly exhibited flushing patterns during the winter season but showed chemostatic patterns during non-salting periods due to substantial mass stored in the subsurface (Long et al., 2015, 2017). Conversely, only dilution patterns for Cl^- and Na^+ were observed in an Atlanta, GA watershed, where deicing salt application can be presumed to be much lower (S. Rose, 2003). As in forested and agricultural watersheds, NO_3 often shows mixed responses during storm events, with studies reporting clockwise dilution, counterclockwise flushing, and chemostatic C-Q patterns (Aguilera & Melack, 2018; Duncan et al., 2017; Vaughan et al., 2017). Duncan et al. (2017) identified a discharge threshold dictating NO_3 behavior in a Maryland watershed. Smaller storm events dominated by groundwater contributions gave rise to counterclockwise patterns and increasing rising limb concentrations, while larger storms dominated by inputs of precipitation and overland flow resulted in clockwise dilution patterns. Other solutes in

urban watersheds have been shown to exhibit more consistent C-Q responses, whether flushing (e.g., DOC, K, PO₄) or dilution (e.g., SiO₂) (Gwenzi et al., 2017; Long et al., 2017; S. Rose, 2003; Vaughan et al., 2017; Vaughan & Schroth, 2019).

As described above, the C-Q behaviors of nutrients, dissolved organic carbon, and to a lesser extent, major ions have been intensively studied at the event scale and longer. However, most previous work has been conducted in forested and agricultural watersheds, and information about C-Q in urban watersheds is sparse. The altered hydrology of urban watersheds suggests that transport of solutes should differ from forested and agricultural streams, but little investigation of solute dynamics in urban watersheds, particularly beyond nutrients, has been done to date. Investigation of C-Q relationships for multiple solutes in urban watersheds is likely to provide insight into transport and dynamics that are not accessible by looking only at nutrients or specific conductance (SC). To address this gap in research, we examined C-Q relationships in one mostly forested suburban watershed and two urban watersheds for multiple dissolved species using a combination of high-frequency SC data and discrete storm event and baseflow sampling. Our main objective is to quantify the relationship between stream discharge and concentrations of major ions (Na⁺, K⁺, Mg²⁺, Ca²⁺, Cl⁻, NO₃⁻, HCO₃⁻, SO₄²⁻, and PO₄³⁻), DOC, total dissolved nitrogen (TDN), and dissolved silica (DSi) during storm events to understand how solute export is affected by urbanization. The following questions will be addressed:

How do event-scale C-Q responses of SC, major ions, and DOC compare among watersheds of differing land use, and do predominant responses exist for each constituent?

1. How do long term C-Q relationships of major ions compare to event-scale C-Q responses?
2. What percentage of each dissolved constituent is exported in baseflow versus stormflow, and do these amounts differ between watersheds?
3. Based on end-member mixing analysis, what are the dominant sources and flow paths for individual dissolved constituents and stream runoff, and how do these compare among the study watersheds?

2. Methods

2.1 Site Descriptions

Three small ($<7 \text{ km}^2$) watersheds in the Baltimore, MD metropolitan area were selected to examine event-scale concentration-discharge relationships in urbanized watersheds: 1) Baisman Run (BARN), a primarily forested suburban watershed with septic systems located in Baltimore County, MD (Figure 3A), 2) Plumtree Run (PTRG), a highly urban watershed with sewer systems located in Harford County, MD (Figure 3B), and 3) West Branch Herring Run (HERR), a highly urban watershed with sewer systems located in Baltimore County, MD (Figure 3D). Pond Branch (POBR), a 100% forested watershed draining into BARN was used to compare water chemistry. All watersheds lie within the Piedmont physiographic province and are primarily underlain by silica-rich metamorphic schist or gneiss (Crowley et al., 1975; Southwick & Owens, 1968) (Table

1). In Plumtree Run, the headwaters are underlain by mafic, gabbroic bedrock, and in West Branch Herring Run, 33% of the watershed is underlain by coastal plain sediments derived from the surrounding bedrock (Crowley et al., 1975; Southwick & Owens, 1968). While land-use characteristics are similar between the two urban watersheds, watershed morphology and channel characteristics differ. West Branch Herring Run is partially channelized, i.e., substantial portions of the channel are lined with concrete, which likely contributes to its flashy hydrological response to precipitation events. Plumtree Run is non-channelized. In a 2015 study comparing the hydrologic response of 11,840 watersheds, West Branch Herring Run was determined to be the ninth flashiest gaged stream in the contiguous United States (Smith & Smith, 2015).

2.2 Sample Collection and Analysis

2.2.1 Baseflow and Stormflow Sampling

Sample collection took place immediately upstream of the USGS gage station at each study site. Baseflow water samples were collected approximately every two weeks as manual grab samples filtered in-field with a 0.45 μm polypropylene filter. Water temperature, pH, and SC were recorded at the time of baseflow sampling using a Thermo Orion A325 field meter calibrated less than 24 hours previous to each sampling event. Stormflow sampling occurred during precipitation events using ISCO automated water samplers. Samples were collected on the rising limb, at or near peak discharge, and on the recession limb to capture each storm event fully; therefore, sampling intervals ranged from 15 minutes to >1 hour depending on predicted storm length and magnitude, as well as watershed response. Manual grab samples were collected at or near baseflow before

and immediately following each storm event. Samples were filtered within 24 hours of collection using 0.45 μm polypropylene filters. Samples for alkalinity, major ion, and dissolved silica analyses were collected in low-density polyethylene (LDPE) bottles triple-rinsed with filtered sample water. Samples for DOC and TDN were collected in pre-ashed (500°C for >4 hours) amber glass vials. Samples for water isotopes were collected in 4-mL glass vials. Alkalinity, DOC, and water isotope samples were collected without headspace to minimize the effects of storage. All samples were stored at 4°C until analyzed.

2.2.2 End Member Sampling

Surface runoff (overland flow), shallow soil water, and groundwater are the most likely dominant end members contributing to stormflow in each watershed. Precipitation was collected as a composite sample across the duration of several storm events and used to represent the isotopic composition and solute concentrations of surface runoff. Urban runoff was collected directly from the stormwater outflow discharging into West Branch Herring Run when possible. Stream baseflow samples collected before each storm event were considered representative of groundwater chemistry.

2.2.3 Sample Analysis

All water chemistry analyses were performed in the Towson University Urban Environmental Biogeochemistry Laboratory (UEBL) except water isotope analysis. Alkalinity or dissolved inorganic carbon (DIC) was calculated as mg/L bicarbonate via the Gran method following titration with a Mettler-Toledo G20 automatic titrator. Accuracy was monitored through titration of a gravimetrically prepared Na_2CO_3 check

standard with every round of samples. Concentrations of major cations (Na^+ , K^+ , Mg^{2+} , and Ca^{2+}) and anions (Cl^- , NO_3^- , SO_4^{2-} , and PO_4^{3-}) were measured with a Dionex ICS-5000 ion chromatograph. Concentrations of TDN and DOC (as non-purgeable organic carbon) were measured with a Shimadzu TOC-Vcsh NC analyzer. Dissolved silica was measured colorimetrically with a SEAL AQ1 discrete analyzer using the molybdosilicate method. For all analyses, check standards were measured every 10-15 samples to ensure data quality. Samples were reanalyzed if check standard concentrations differed by $>10\%$ from the expected concentration. Similarly, samples were reanalyzed if charge balance error exceeded $\pm 10\%$.

Water samples were analyzed for $^{18}\text{O}/^{16}\text{O}$ and $^2\text{H}/^1\text{H}$ using a Los Gatos Research Liquid Water Isotope Analyzer (LGR LWIA) Off-Axis Integrated Cavity Output Spectroscopy system at Johns Hopkins University. Data post processing was performed using the LGR LWIA post analysis software version 2.1 with USGS standards 46, 47, and 48. The isotope ratios (R) are reported in delta notation ($\delta^{18}\text{O}$, $\delta^2\text{H}$) using the relationship:

$$\text{delta value} = \left(\frac{R_{\text{sample}} - R_{\text{standard}}}{R_{\text{standard}}} \right) \times 1000 \text{ ‰} \quad (1)$$

where the standard is the Vienna Standard Mean Ocean Water (V-SMOW). Samples were run with six replicates with the first two discarded to prevent carry over issues. A standard was run every four samples.

2.3 Discharge and Specific Conductance Data Collection

High-frequency discharge at all three sites were collected by the USGS. USGS stream discharge records were recorded at 15-minute intervals at Baisman Run until June 2020, after which measurements were recorded at 5-minute intervals. Discharge measurements were recorded at 5-minute intervals at Plumtree Run and West Branch Herring Run. High-frequency SC data were collected by the author at 15-minute or 5-minute intervals (corresponding with discharge) from January 2019 through January 2021 at BARN, the mostly forested, suburban site. At the two urban sites, high-frequency SC data were collected at 5-minute intervals from January 2018 through January 2021 at HERR by the author and at Plumtree Run by the USGS. All data recorded at the USGS gage stations were downloaded from the USGS National Water Information System (NWIS) database using the *dataRetrieval* library in R. HOBO conductivity loggers deployed by the author at Baisman Run and West Branch Herring Run measured and recorded SC at 15- and 5-minute intervals, respectively. After June 2020, SC was recorded at 5-minute intervals at BARN. Data was downloaded from the HOBO conductivity loggers biweekly to monthly and calibrated to electrical conductivity and temperature measured with a calibrated Thermo Orion A325 field meter at the time of data collection.

High-frequency SC data were manually checked for data quality and anomalous data points were removed from the datasets. Anomalous data arose during periods when the conductivity logger was buried under sediment or no longer submerged due to low discharge or displacement during storms. Gaps in the high-frequency SC data were filled

via interpolation if 1) gaps were <1 day and no new discharge events occurred during the period or 2) gaps were >1 day and discharge remained at baseflow conditions for the entire period. High-frequency SC data covered 89%, 76%, and 99% of the study period at BARN, HERR, and PTRG, respectively. Interpolation of missing SC data provided additional coverage at BARN and HERR, bringing coverage up to 94% and 82% at each site, respectively.

2.4 High-Frequency Time Series Datasets for Major Ions

High-frequency time series for major ions were determined based on regression models. Solute-specific regression models were developed using discrete concentration measurements from baseflow and stormflow samples and either SC or discharge.

Regression models based on SC were developed for 1) the entire dataset, 2) winter (Dec-Mar) and nonwinter (Apr-Nov) months, and 3) using a threshold value for SC.

Regression models based on discharge were developed by fitting a linear trendline to the log transformed solute concentration and discharge data. Models with $R^2 \geq 0.60$ were used to generate high-frequency concentration datasets (Table 2). If models were a poor fit, the median solute concentration was used for the entire timeseries. If regression equations generated negative solute concentrations, calculated concentrations less than one-half of the lowest discretely measured concentration were replaced with one-half of the lowest discrete value.

2.5 Hydrograph Separation

For each study site, the instantaneous streamflow record was separated into baseflow and quickflow (i.e., event water) components using the `BaseflowSeparation` function within the *EcoHydrology* package in R (Fuka et al., 2018). This package uses a single parameter digital recursive filter outlined in Nathan & McMahon (1990) to separate high-frequency (quickflow) signals from low-frequency (baseflow) signals using the following equation:

$$q_k = \alpha q_{k-1} + \frac{(1+\alpha)}{2} (y_k - y_{k-1}), \quad (2)$$

where q_k is the filtered quickflow at time step k , q_{k-1} is the filtered quickflow at time step $k-1$, y_k is the total streamflow at time step k , y_{k-1} is the total streamflow at time step $k-1$, and α is the filter parameter which influences the attenuation of the separation. The filtered baseflow (b_k) is defined as $y_k - q_k$.

A filter parameter value of 0.925 is recommended by Nathan & McMahon (1990); however, the parameter can range from 0.90-0.99. The filter is typically passed through the dataset three times (forward-backward-forward) when using daily flow data but can be varied based on the time step of the dataset. For example, nine passes were found to be appropriate for hourly flow data (Ladson et al., 2013; Nathan & McMahon, 1990). In this study, nine passes with a filter parameter of 0.925 produced reasonable results at all sites for the 5- to 15-minute interval datasets.

2.6 Solute Flux and Solute Load Calculations

For each site, high-frequency solute loads were calculated as follows:

$$L_k = C_k * Q_k * T, \quad (3)$$

where L_k is the solute load in mg at timestep k , C_k is the concentration in mg/L of the given solute at timestep k , Q_k is the discharge in L/s at timestep k , and T is the time in seconds between each timestep. At each timestep, the concentration was multiplied by the baseflow and quickflow fractions obtained from the hydrograph separation to determine the load transported in each component.

For select storm events, concentrations of total dissolved solids (TDS) were estimated using high-frequency SC data as follows:

$$TDS_k = 0.7 * SC_k, \quad (4)$$

where TDS_k is the TDS concentration in mg/L at timestamp k , 0.7 is the correction factor commonly used for freshwater systems, and SC_k is the specific conductance in $\mu\text{S}/\text{cm}$ (Walton, 1989). TDS flux was then calculated as follows:

$$TDS_F = TDS_k * Q_k, \quad (5)$$

where TDS_F is the TDS flux in mg/s at timestep k , TDS_k is the calculated TDS concentration in mg/L at timestep k , and Q_k is the discharge in L/s at timestep k .

2.7 Storm Delineation

For each study site, the SC-discharge time series were manually delineated into individual storm events. Storm events were defined as any hydrological response to rainfall where peak discharge increased above baseflow by a minimum of 100%. The timestamp prior to the initial discharge increase was selected as the starting point for each storm event. For this study, the following criteria were used for the selection of storms: 1) the event had complete SC and discharge data, 2) the storm returned to pre-event or inter-event discharge values, or if impacted by a subsequent rain event, the hydrograph receded by at least 90% relative to peak discharge, and 3) the storm did not have more than three distinct discharge peaks since large, multi-peaked storms often exhibit convoluted C-Q responses that are difficult to characterize. When possible, multi-peaked storms were separated into individual events if the hourly change in discharge recession was $\leq 0.1 \text{ ft}^3/\text{s}$ ($0.003 \text{ m}^3/\text{s}$) and SC had returned to 50% of its initial value prior the start of a subsequent rain event.

2.8 Calculation of Hysteresis Metrics

2.8.1 Hysteresis Index

For each storm event, we characterized SC-Q and/or C-Q hysteresis loops using the hysteresis index (*HI*) proposed by Lawler et al. (2006) and modified by Lloyd et al. (2016) and Vaughan et al. (2017) that allows for the quantification and comparison of solute hysteresis between watersheds and storms of varying magnitudes. The *HI* quantifies differences in solute concentration on the rising and falling hydrograph limbs using solute concentrations and discharges normalized to values between 0 and 1, as follows:

$$C_{i\text{ Norm}} = \frac{C_i - C_{min}}{C_{max} - C_{min}} \quad (6)$$

$$Q_{i\text{ Norm}} = \frac{Q_i - Q_{min}}{Q_{max} - Q_{min}}, \quad (7)$$

where C_i and Q_i are the concentration and discharge at timestep i , C_{min} and C_{max} are the minimum and maximum concentrations during the event, and Q_{min} and Q_{max} are the minimum and maximum discharge rates during the event (Lawler et al., 2006; Lloyd et al., 2016; Vaughan et al., 2017). While Lloyd et al. (2016) found that calculating *HI* at every 5% increment of normalized discharge allowed for robust characterization of 100% of storms with respect to loop shape and that the addition of more increments did not significantly alter the resulting *HI*, Vaughan et al. (2017) used 2% discharge intervals to characterize storm event hysteresis fully. Using high-frequency SC data, we found that interpolation at 2% of normalized discharge yielded a better fit to the observed hysteresis pattern in the urban watersheds of this study. Therefore, following the method outlined

by Vaughan et al. (2017), solute concentration C_j was interpolated via linear regression of $C_{i\text{ Norm}}$ at every 2% of the $Q_{i\text{ Norm}}$ range on both the rising and falling limbs using the two adjacent measurements containing interval j . For every 2% discharge interval j , the HI was calculated by subtracting the falling limb concentration from that of the rising limb, as follows:

$$HI_j = C_{j\text{ Rising limb}} - C_{j\text{ Falling limb}} \quad (8)$$

For each storm event, an overall HI was calculated by taking the mean of all HI_j values. HI values are scaled from -1 to 1 with negative and positive values indicating counterclockwise and clockwise hysteresis, respectively, and the magnitude reflecting the concentration differences between the rising and falling limbs. (Lloyd et al., 2016; Vaughan et al., 2017). An HI value of ~ 0 may represent little to no hysteresis (i.e., the C-Q relationship is linear). However, it may also be indicative of more complex figure-of-eight patterns, which emphasizes the need for additional hysteresis metrics or visual inspection to ensure accurate characterization (Lloyd et al., 2016). For example, the overall HI for a figure-of-eight hysteresis pattern is represented by the mean of the HI_j for discharge intervals with clockwise (positive HI_j) and counterclockwise (negative HI_j), which may yield an overall HI of 0 or near 0 depending on the loop symmetry (Lloyd et al., 2016).

2.8.2 Flushing Index

Storm event SC-Q and C-Q hysteresis loops were further characterized using the flushing index (*FI*) proposed by Vaughan et al., (2017) and similar to the concentration change (ΔC) metric used by Butturini et al., (2008). The *FI* reflects the slope of the concentrations on the rising limb of the hydrograph and was calculated using solute concentrations normalized to values between 0 and 1, as follows:

$$FI = C_{Qpeak\ Norm} - C_{0\ Norm}, \quad (9)$$

where $C_{Qpeak\ Norm}$ and $C_{0\ Norm}$ are the normalized solute concentrations at peak discharge and the start of the storm, respectively. *FI* values are scaled from -1 to 1, with negative and positive values indicating a diluting and flushing effect on the rising limb, respectively. A *FI* value of ~0 indicates static concentrations on the rising limb (Butturini et al., 2006, 2008; Vaughan et al., 2017).

2.8.3 Power Laws and Coefficient of Variation

Concentration-discharge relationships have been extensively characterized using a power law relationship:

$$C = aQ^b \quad (10)$$

where a and b are constants. Log transformation of Equation 10 allows parameters a and b to be fit using a linear regression as follows:

$$\log(C) = b * \log(Q) + \log(a) \quad (11)$$

where a is the intercept value and b represents the slope of the relationship between concentration and discharge. Values of b approaching 0 reflect constant concentrations with variable discharge. Values of b approaching 1 and -1 reflect direct and inverse C-Q relationships, respectively, and indicate discharge is the dominant control on solute concentrations (Musolff et al., 2015; Thompson et al., 2011). In recent work, a more detailed characterization of C-Q relationships was proposed based on the $\log(C)$ - $\log(Q)$ regression slope b and ratio of coefficients of variation for concentration and discharge:

$$\frac{CV_C}{CV_Q} = \frac{\mu_Q \sigma_C}{\mu_C \sigma_Q} \quad (12)$$

where μ and σ are the mean and standard deviation of solute concentration (C) and discharge (Q), respectively (Musolff et al., 2015; Thompson et al., 2011). Combining these approaches is particularly useful for characterizing C-Q relationships where $b \approx 0$. While a slope approaching 0 would otherwise be considered chemostatic, high CV_C/CV_Q would indicate chemodynamic behavior. Following Thompson et al. (2011), chemostatic

behavior is defined as $|b| \leq 0.2$ and/or small variations in concentration compared to discharge ($CV_c/CV_Q \ll 1$). Chemostasis suggests a consistent source and implies that discharge variation is the primary driver of solute transport, i.e., variation in load (Thompson et al., 2011). Chemodynamic behavior is defined as $|b| > 0.2$ and/or large variations in concentration relative to discharge ($CV_c/CV_Q \geq 1$) with positive and negative b values indicating enrichment and dilution behavior, respectively. High CV_c/CV_Q values indicate episodic transport dynamics, which may be driven by input timing or threshold-based transport (Musolff et al., 2015).

2.8.4 Classification of C-Q Behavior

In this study, event-scale C-Q behavior was classified primarily using the power law regression slope b and CV_c/CV_Q . Concentration-discharge relationships were classified as dilution when $b < -0.2$ and flushing/enrichment when $b > 0.2$. When $-0.2 \leq b \leq 0.2$, the C-Q relationship was classified as chemostatic when $CV_c/CV_Q < 1$ and chemodynamic when $CV_c/CV_Q > 1$. Hysteresis patterns were classified according to values of the HI using a method similar to that of Aguilera and Melack (2018). Hysteresis rotation was categorized as counterclockwise when $HI < -0.05$ and clockwise when $HI > 0.05$. When $-0.05 \leq HI \leq 0.05$, the hysteresis pattern were categorized as either complex or having no hysteresis based on visual inspection (Aguilera & Melack, 2018). As a secondary comparison of C-Q behavior, concentration-discharge relationships were classified as dilution when $FI < -0.10$ and flushing/enrichment when $FI > 0.10$. When $-0.10 \leq FI \leq 0.10$, the C-Q relationship was classified as chemostatic. Calculations of hysteresis metrics and the classification of hysteresis patterns were performed using R.

2.9 End Member Mixing Analysis

A two-end member mixing analysis using stable water isotopes will be conducted for selected storms to determine the relative contributions of source waters to stormflow. While this approach is similar to the digital recursive filter hydrograph separation, it aims to separate the hydrograph into physical source components (e.g., precipitation, overland flow, groundwater) rather than temporal components (e.g., pre-event, event). Furthermore, this method may provide greater detail on the mixing of sources that cannot be inferred from hydrograph separation alone. For example, a non-linear two-end member mixing model may indicate an additional end member (e.g., soil water) contributing to stormflow. The following equations will be used to calculate the proportional contributions of each end member (equations shown for two-end member mixing):

$$Q_t = Q_p + Q_g \quad (13)$$

$$Q_t C_t = Q_p C_p + Q_g C_g \quad (14)$$

$$Q_p = Q_g \frac{C_t - C_g}{C_p - C_g} \quad (15)$$

where Q represents the discharge of each component, C represents the isotopic composition, and the subscripts t , p , and g indicate total discharge, precipitation, and groundwater, respectively (Sklash & Farvolden, 1979).

3. Results & Discussion:

3.1 High-Frequency Discharge & Specific Conductance Data

Baseflow discharge was similar across all sites while discharge peaks were substantially higher at the urban watersheds. During the study period, discharge ranged by >2 orders of magnitude from 0.014 to 4.05 m³/s at BARN. At the urban sites, discharge measurements spanned >3 orders of magnitude, ranging from 0.010 to 59.7 m³/s at HERR and from 0.014 to 64.3 m³/s at PTRG. When normalized to watershed area (m/yr), median discharge was similar across all sites (Table 3, Figure 4). Winter months exhibited higher median discharge, while the lowest and highest discharge values occurred during nonwinter months (Figure 4).

Specific conductance increased with increasing urbanization. Median specific conductance at BARN, the mostly forested suburban watershed, was ~8x greater than POBR, the 100% forested reference site, which had median SC ~27µS/cm. Specific conductance was substantially higher at the urban watersheds compared to BARN (Figure 5). Median specific conductance was ~3-4x greater in the urban watersheds and was highest at HERR, followed by PTRG (Table 4). Median specific conductance was elevated during winter in the urban watersheds but showed no significant difference during winter and nonwinter periods at BARN. SC showed more variability during winter, particularly at the urban watersheds. During the study period, SC measurements spanned >1, >2, and >3 orders of magnitude at BARN, PTRG, and HERR, respectively. At all sites, the highest SC measurements were recorded during winter.

Annual precipitation is similar across all sites and equally distributed throughout the year; therefore, seasonality in baseflow discharge is influenced by groundwater recharge and evapotranspiration (Hershfield, 1971). Groundwater recharge is greatly reduced during summer months when evapotranspiration is highest, resulting in lower water tables and reduced baseflow discharge (Figure 4). Conversely, higher median discharge in winter (Figure 4) reflects low evapotranspiration and increased groundwater recharge (Hershfield, 1971). Shorter, high-intensity precipitation events that are characteristic of summer months generate higher discharge peaks relative to winter months which are generally characterized by longer, lower-intensity events. Higher nonwinter and winter discharge peaks at the urban sites reflect reduced infiltration of precipitation and greater inputs of surface runoff during storm events due to greater impervious cover (O'Driscoll et al., 2010). Similarly, lower discharge values (e.g., discharge minimums) at the urban sites reflect increased evaporation and reduced infiltration of precipitation, particularly during nonwinter months (O'Driscoll et al., 2010).

Elevated SC was previously reported at BARN and HERR in Moore et al. (2017), and at PTRG in Moore et al. (2020). Increasing salinization of freshwater systems of the northern and northeastern United States has been widely documented (Corsi et al., 2015; S. S. Kaushal et al., 2005; Moore et al., 2017, 2020). Elevated SC has been shown to be highly correlated with increasing impervious cover across multiple U.S. geographic regions, particularly those where deicing salts are regularly applied during winter (Moore et al., 2020). Inputs of deicing salts and weathering of anthropogenic materials (e.g.,

concrete and other impervious surfaces) contribute to increases in major ion concentrations that elevate SC in suburban and urban watersheds. Even watersheds with minimal anthropogenic influence (e.g., BARN with ~1% ISC) exhibit elevated SC relative to undisturbed sites like POBR (Moore et al., 2017). Higher winter SC (Figure 5, Table 4) and strong correlations between SC, $[\text{Na}^+]$, and $[\text{Cl}^-]$ (Table 2) suggest deicing salts are the primary driver of elevated SC at the study sites.

3.2 Baseflow Water Chemistry – Discrete Samples

Baseflow concentrations of dissolved species, including major cations and anions, DOC, TDN, and SiO_2 increased with increasing urbanization. Baseflow concentrations of all major ions were >50-100% greater at BARN, the mostly forested suburban watershed, compared to POBR, the 100% forested reference site (Table 5, 6). At the urban sites, median solute concentrations were significantly higher than at BARN, apart from K^+ at PTRG and NO_3^- at HERR which showed no significant difference ($p < 0.001$, Figure 6). Median solute concentrations were significantly different between the two urban watersheds, except for Cl^- , Mg^{2+} , and DOC ($p < 0.001$, Figure 6).

Baseflow concentrations of most major cations were substantially higher in the urban watersheds compared to the mostly forested, suburban watershed (Table 5, Figure 6E, F). Except for $[\text{Mg}^{2+}]$, which was highest at PTRG, concentrations of major cations were highest at HERR. Median $[\text{Na}^+]$ was highest at all sites, followed by $[\text{Ca}^{2+}]$, $[\text{Mg}^{2+}]$, and $[\text{K}^+]$ (Table 5). At the urban sites, median $[\text{Na}^+]$, $[\text{Mg}^{2+}]$, and $[\text{Ca}^{2+}]$ were >2x, >3x, and 5-6x greater than the suburban site, respectively. Median $[\text{Na}^+]$ was similar to median $[\text{Ca}^{2+}]$ at the urban sites but not at the suburban site, where median $[\text{Na}^+]$ was >2x greater

than median $[\text{Ca}^{2+}]$. Median $[\text{K}^+]$ at HERR was 2.5x higher than BARN and PTRG, which had similar low median $[\text{K}^+]$. At all sites, $[\text{Na}^+]$ showed the most variability relative to other cations.

Like cations, baseflow concentrations of major anions, DOC, TDN, and SiO_2 were higher in the urban watersheds compared to the suburban site (Table 6, Figure 6). Median $[\text{Cl}^-]$ was highest at all sites, followed by $[\text{HCO}_3^-]$, $[\text{SO}_4^{2-}]$, and $[\text{NO}_3^-]$ (Table 6). At the urban sites, median $[\text{Cl}^-]$ and $[\text{SO}_4^{2-}]$ were >3x and >7x higher than the suburban site, respectively (Figure 6A, C). Relative to the suburban site, median $[\text{HCO}_3^-]$ was >3x and >5x higher at PTRG and HERR, respectively (Figure 6B). At all sites, $[\text{Cl}^-]$ showed the most variability relative to other anions. Although highest at PTRG, median $[\text{NO}_3^-]$, $[\text{DOC}]$ and $[\text{TDN}]$ were relatively similar (<3 mg/L) across all sites (Table 7, Figure 6D, G)). Median $[\text{SiO}_2]$ was substantially higher at PTRG compared to BARN and HERR (Figure 6H).

Bedrock geology is similar across all sites; therefore, differences in stream baseflow chemistry are primarily driven by differences in land use. Concentrations of all dissolved solutes were elevated relative to the 100% forested reference site (POBR) and generally increased with urban land use and impervious surface cover (Table 5, 6, Figure 6). Elevated concentrations of dissolved constituents relative to POBR were previously reported for BARN and HERR in Moore et al. (2017). The relationship between urbanization and elevated alkalinity, and concentrations of major ions, nutrients, and DOC has been well documented (Sujay S. Kaushal et al., 2017; Moore et al., 2017; O'Driscoll et al., 2010; Walsh et al., 2005). Anthropogenic non-point source inputs are

the most likely driver of concentration increases in the suburban and urban watersheds. Direct inputs and watershed storage of deicing salts are likely responsible for elevated $[\text{Na}^+]$ and $[\text{Cl}^-]$ observed in with increasing impervious cover. Similar relationships between $[\text{Na}^+]$, $[\text{Cl}^-]$, and %ISC have been observed in other temperate suburban and urban watersheds that receive inputs of deicing salts during winter months (Corsi et al., 2015; Moore et al., 2020). Cation exchange processes resulting from inputs of deicing salts may explain elevated $[\text{Ca}^{2+}]$ and $[\text{Mg}^{2+}]$, particularly at the urban sites. High concentrations of Na^+ in soil pore water resulting from the addition of NaCl road deicers can displace Ca^{2+} and Mg^{2+} from soil exchange sites, allowing for their removal by surface and subsurface flows (Sujay S. Kaushal et al., 2017; J. B. Shanley, 1994). Enhanced weathering of silicate bedrock and weathering of carbonate-rich urban infrastructure (e.g., concrete, cement) can contribute additional Ca^{2+} and Mg^{2+} , and may contribute to elevated $[\text{HCO}_3^-]$, $[\text{SO}_4^{2-}]$, and $[\text{SiO}_2]$ in the urban watersheds (Carey & Fulweiler, 2012; Sujay S. Kaushal et al., 2017). Weathering of mafic bedrock containing Mg-rich orthopyroxene (hypersthene) likely contributes to the higher concentrations of Mg^{2+} and SiO_2 observed at PTRG relative to the other sites. The urban signal was not as pronounced for biologically associated solutes. While $[\text{K}^+]$, $[\text{NO}_3^-]$, and $[\text{DOC}]$, generally increased with urbanization, median baseflow concentrations were relatively similar across the suburban and urban sites, suggesting similar inputs and rates of biological uptake and processing (Table 5, 6, 7).

3.3 Stormflow Water Chemistry – Discrete Samples

Discrete samples were collected during 19 storm events, including five at BARN, the mostly forested suburban site, ten at HERR and four at PTRG, the two urban sites. At BARN, peak discharges of sampled storm events ranged from 50% to 97% of the event peak discharges measured between January 2019 and January 2021. Peak discharges of sampled storms at HERR and PTRG represented 39-89% and 48-96% of the event peak discharges measured between January 2018 and January 2021, respectively.

Concentrations of major cations and anions in precipitation samples were low (<1 mg/L) (Table 8). Concentrations of most dissolved solutes decreased during stormflow, reflecting mixing of concentrated baseflow with less-concentrated precipitation and surface runoff. At all sites, median concentrations of major cations decreased during stormflow (Table 5). Decreases in cation concentrations were more substantial in the urban watersheds relative to the suburban site (Figure 6E, F). At BARN, median stormflow $[\text{Na}^+]$, $[\text{Mg}^{2+}]$, and $[\text{Ca}^{2+}]$ were significantly lower than baseflow with concentration decreases ranging from 18-22% ($p < 0.001$). Median stormflow $[\text{K}^+]$ was not significantly different from baseflow at BARN. At the urban sites, concentrations of major cations were significantly lower during stormflow compared to baseflow except for $[\text{K}^+]$ at PTRG ($p < 0.001$). At HERR, median concentrations decreased by 44%, 55%, and 48% for $[\text{Na}^+]$, $[\text{Mg}^{2+}]$, and $[\text{Ca}^{2+}]$, respectively. At PTRG, median concentrations of $[\text{Na}^+]$, $[\text{Mg}^{2+}]$, and $[\text{Ca}^{2+}]$ decreased by 60-61%. Median $[\text{K}^+]$ showed the smallest decreases in median concentrations, with 33% and 16% reductions at HERR and PTRG, respectively.

Median concentrations of major anions decreased during stormflow at the urban sites and showed variable behavior at the suburban site (Table 6). Except $[\text{HCO}_3^-]$, changes in anion concentrations were more substantial in the urban watersheds relative to the suburban site and were largest at PTRG (Figure 6A-D). At BARN, median stormflow $[\text{HCO}_3^-]$ increased by 19% and was significantly higher than baseflow ($p < 0.01$, Figure 6B). Median $[\text{Cl}^-]$ and $[\text{NO}_3^-]$ decreased by 17% and 33%, respectively, and were significantly lower than baseflow ($p < 0.001$). Median stormflow $[\text{SO}_4^{2-}]$ was not significantly different from baseflow at BARN (Figure 6C). At the urban sites, concentrations of all major anions were significantly lower during stormflow compared to baseflow ($p < 0.001$). At HERR, median concentrations of $[\text{Cl}^-]$, $[\text{NO}_3^-]$, and $[\text{SO}_4^{2-}]$ decreased by 52-57%. At PTRG, median concentrations of $[\text{Cl}^-]$, $[\text{NO}_3^-]$, and $[\text{SO}_4^{2-}]$ decreased by 72%, 71%, and 59%, respectively. Median $[\text{HCO}_3^-]$ showed the smallest decreases in concentration with 34%, and 20% reductions at HERR and PTRG, respectively.

At all sites, median concentrations of DOC increased and concentrations of TDN and SiO_2 decreased during stormflow (Table 7, Figure 6G-H). Except [DOC], changes in median concentrations were larger in the urban watersheds relative to the suburban site. At all sites, median [DOC] was significantly higher during stormflow compared to baseflow with increases in median [DOC] ranging from 104% at PTRG to 150% at HERR ($p < 0.001$, Figure 9). At all sites, median stormflow [TDN] and $[\text{SiO}_2]$ were significantly lower than baseflow ($p < 0.001$). Median [TDN] decreased by 27%, 35%, and

58% and median $[\text{SiO}_2]$ decreased by 14%, 48%, and 47% at BARN, HERR, and PTRG, respectively.

Although the urban watersheds exhibited greater decreases in concentration during stormflow, median solute concentrations often remained significantly higher than those at BARN, the mostly forested suburban site (Figure 6). Exceptions to this include NO_3^- , TDN, and SiO_2 which showed either no significant difference or significantly lower median stormflow concentrations relative to BARN (Figure 6D, H). Similarly, median stormflow concentrations of Na^+ , Cl^- , and K^+ were not significantly different between PTRG and BARN.

Changes in stream chemistry during storm events are reflected in the hysteresis behavior of solutes, as discussed below. More substantial differences between baseflow and precipitation chemistry and greater volumes and more rapid inputs of overland flow likely contribute to the more pronounced decreases in median solute concentrations at the urban sites relative to BARN, the mostly forested suburban site (O'Driscoll et al., 2010). Comparatively smaller changes in stormflow chemistry at BARN may reflect greater influence of enriched groundwater or soil water contributions during storm events (Olshansky et al., 2018; L. A. Rose et al., 2018). Small storm events (lower 50% of discharge peaks) were underrepresented in the discrete stormflow dataset at all sites. As discussed in detail below, SC-Q patterns suggest this underrepresentation should have little influence on median stormflow concentrations at BARN. Conversely, median stormflow concentrations at the urban sites based on discrete samples could be skewed toward lower values due to the frequency with which SC exhibited chemostatic or

enrichment behavior during small storm events. Differences in stormflow ion behavior between the urban watersheds may be attributable to different timing of storm sampling. At HERR, three out of the ten sampled events occurred during winter months which may result in higher median stormflow concentrations of solutes associated with road salt (Na^+ , Cl^-). Conversely, no winter storms were sampled at PTRG which may explain why median stormflow $[\text{Na}^+]$ and $[\text{Cl}^-]$ are similar to BARN.

3.4 Storm Event Specific Conductance-Discharge Relationships

Event scale specific conductance-discharge relationships were examined for 75, 219, and 209 storm events at BARN, HERR, and PTRG, respectively. Of these storms, roughly one-third occurred during winter. Peak stormflow values were substantially higher at the urban sites compared to the suburban site (Table 9). At HERR and PTRG, median peak stormflow was >4x higher and maximum peak stormflow was more than an order of magnitude greater than at BARN.

Across all sites and seasons, SC commonly decreased during storm events. Dilution patterns accounted for 84%, 70%, and 67% of the SC-Q patterns characterized at BARN, HERR, and PTRG, respectively (Table 10). Median flushing indices for SC were negative, indicating dilution on the storm rising limb (Table 11). Dilution was most pronounced ($FI \ll 0$) at BARN, followed by HERR and PTRG. Winter months showed significantly less dilution (higher median FIs) than nonwinter months at all sites ($p < 0.001$, Table 11). Clockwise hysteresis ($HI > 0.05$) was the dominant pattern type at all sites, accounting for 60%, 72%, and 53% of the SC patterns examined at BARN, HERR, and PTRG, respectively (Table 10). Median HI values were similar across all

sites and exhibited a narrow range of positive values reflecting higher SC on the rising limb relative to the falling limb. Median HI during winter was lower at the suburban site and higher at the urban sites, but not significantly different from nonwinter (Table 11). Counterclockwise ($HI < -0.05$) patterns and complex, figure-of-eight, patterns each accounted for roughly 20% of the examined SC-Q patterns at BARN and PTRG and 12% at HERR (Table 10).

Flushing patterns in which SC increased with discharge were observed more frequently in the urban watersheds. Flushing patterns ($FI > 0.1$) accounted for 12% of the observed SC-Q patterns at BARN (Table 10). Flushing patterns at BARN were observed only during winter months when peak stormflow exceeded the 25th percentile (0.116 m³/s) (Figure 7). At HERR, 17% of the examined storm events exhibited flushing patterns for SC (Table 10). Of these, 53% were observed during winter months and 47% during nonwinter months, which was defined as the period from April through November. Flushing patterns at HERR occurred only during smaller storm events when peak stormflow was below the median value (1.22 m³/s) with counterclockwise patterns occurring more frequently than clockwise or complex (Figure 8). Similar behavior was observed at PTRG with 15% of the of the examined storms showing flushing for SC; however, complex flushing patterns occurred more often (Figure 9, Table 10).

Chemostatic patterns in which minimal SC change occurred with increasing rising limb discharge were observed more frequently in the urban watersheds. Chemostatic patterns ($-0.1 < FI < 0.1$) accounted for 4%, 13%, and 18% of the SC patterns at BARN, HERR, and PTRG, respectively (Table 10). At BARN, chemostatic patterns occurred

only with a counterclockwise rotation and during small winter events when peak stormflow was lower than the median value ($0.257 \text{ m}^3/\text{s}$) (Figure 7). Conversely, chemostatic patterns were observed across seasons and a range of storm sizes in the urban watersheds. At HERR, clockwise chemostatic patterns occurred $>2\times$ as often as counterclockwise with the latter associated with small nonwinter storm events during which peak stormflow was less than the 25th percentile (Figure 8). SC did not exhibit chemostatic patterns when peak stormflow exceeded the 75th percentile ($4.43 \text{ m}^3/\text{s}$). SC showed similar behavior at PTRG; however, counterclockwise patterns occurred roughly twice as often as clockwise (Figure 9).

Although the altered hydrology of urban watersheds suggests solute transport should differ from forested or mostly forested sites, our analysis shows broadly similar SC-Q behavior across all sites where SC decreases as Q increases, albeit with a smaller SC decrease at the urban sites. At all sites, negative median *FI* and positive median *HI* values (Table 11) suggest a source limitation of the solutes contributing to SC which implies 1) concentrated near-channel sources are rapidly mobilized and depleted during most storm events and/or 2) solute-rich groundwater sources are progressively diluted during storm events by low concentration precipitation, soil, and surface runoff inputs entering the stream (Knapp et al., 2020; L. A. Rose et al., 2018; Wymore et al., 2019). As stormflow recedes, conductivity increases and eventually returns to pre-event levels as groundwater progressively becomes the dominant flow source. As indicated by predominantly clockwise hysteresis ($HI > 0.1$), higher rising limb SC may reflect the flushing of solutes stored in soils and riparian zones and/or those accumulated on

impervious surfaces (Wymore et al., 2019). Similar, albeit less variable SC-Q behavior was reported in forested and agricultural watersheds (A. Miller et al., 2021; Wymore et al., 2019).

While the median behavior of SC was similar across all sites, examination of individual storm event SC behavior revealed a greater degree of complexity at the two urban sites relative to the mostly forested suburban site. The urban sites exhibited substantial inter-event SC-Q variability that corresponded with storm event size but did not correspond with season (Figure 10). Higher median *FIs* during both winter and nonwinter periods at the urban sites (Table 11) reflect the greater number of events in which SC either increased or remained nearly constant (chemostatic) on the storm rising limb and suggests urbanization influences storm event SC behavior (Table 10). The flushing of deicing salts from impervious surfaces likely drives SC enrichment and chemostasis during winter storm events at all sites, although no clear seasonal relationship was apparent due to the episodic nature of road salt application (Lakoba et al., 2021; Long et al., 2017). Greater impervious cover, and therefore, more widespread distribution of deicing salts throughout the watersheds likely explains the higher frequency of SC enrichment and chemostatic patterns during winter months at the urban sites. Lakoba et al. (2021) reported similar variability in SC-Q behavior for an urban watershed also receiving deicing salt inputs; storm event *FIs* and *HIs* ranged from negative to positive, and no seasonal relationship was found for either index.

SC enrichment and chemostasis during nonwinter storm events occurred only at the urban sites. These patterns were associated with small storm events and showed either

constant SC or slight increases in SC on the storm rising limb that may reflect the flushing of solutes accumulated on watershed surfaces (Figure 8, 9). This first-flush effect may only be apparent during small storm events, where discharge sufficiently increases to mobilize solutes but does not increase enough to dilute or deplete these sources. Nonwinter enrichment and chemostatic patterns were often associated with counterclockwise hysteresis (Figure 8, 9), reflecting higher falling limb SC that may be explained by longer transport times of solutes flushed from the headwaters and/or late contributions from subsurface flow paths. These behaviors also may reflect greater fractions of enriched subsurface water contributing to stormflow, given that small storm events are likely to produce less overland flow (Benettin et al., 2017; Duncan et al., 2017). Larger storm events in which discharge increases substantially may have a clear first flush based on visual inspection of event data but for which that first flush is not apparent in *FI* and *HI* indices (Figure 11). Many studies have documented a first flush effect during storm events, and this effect is often associated with urban watersheds containing substantial impervious cover (Flint et al., 2007; Inserillo et al., 2017; Koenig et al., 2017; Sansalone et al., 2005).

3.5 Event-Scale Concentration-Discharge Relationships

Solute behavior generally fell into two categories, with some exceptions: 1) biologically associated solutes, including DOC and K^+ , that exhibited flushing or chemostatic behavior, and 2) geogenic solutes, including HCO_3^- , Mg^{2+} , Ca^{2+} , and SiO_2 , and exogenous solutes commonly associated with anthropogenic inputs, including Na^+ , Cl^- , NO_3^- , SO_4^{2-} , and TDN, that exhibited chemostatic or dilution behavior. Distinctly different behavior was observed for HCO_3^- and SO_4^{2-} at BARN relative to the urban sites.

Solute behavior was characterized primarily using the slope of the power law regression (hereafter referred to as the C-Q slope) and the ratio of coefficients of variation for concentration and discharge (CV_c/CV_Q). Although this method is commonly used to describe C-Q behavior over longer timescales, it provided a better characterization of event scale solute dynamics than FI values. An artifact of the FI calculation is its potential to inflate the magnitude of enrichment or dilution on the storm rising limb. For example, a small decrease in concentration on the storm rising limb can yield a highly negative FI if the initial concentration and the concentration at peak discharge approach the maximum and minimum values during the storm event, respectively. The resulting high FI could be interpreted as substantial solute dilution; however, a C-Q regression may show relatively invariant concentrations with increasing discharge (Figure 12).

3.5.1 Biologically Associated Solutes

Median C-Q slopes for DOC and K^+ (biologically associated solutes) at BARN were positive ($b > 0.2$), reflecting enrichment behavior (Table 12, Figure 13A). Higher CV_C/CV_Q values for these solutes indicated greater variation in concentration relative to other solutes at BARN, particularly for DOC (Table 12). Enrichment behavior was supported by strongly positive median FIs ($FI > 0.50$) while median HIs were negative, indicating counterclockwise hysteresis or higher falling limb concentrations (Figure 14A). At the urban sites, DOC exhibited similar behavior to BARN, albeit to a lesser degree, as reflected in lower C-Q slopes, and CV_C/CV_Q values (Figure 13B, C). Like BARN, DOC exhibited counterclockwise hysteresis at PTRG (Figure 14C). At HERR, the median HI reflected complex hysteresis due to DOC exhibiting clockwise, counterclockwise, and complex figure-of-eight patterns during separate storm events (Figure 14B). K^+ showed different behavior at the urban sites (Figure 13B, C). Instead of the enrichment seen at BARN, C-Q slopes indicated chemostatic behavior ($|b| < 0.20$). At the urban sites, median FIs for K^+ were variable, ranging from -0.08 at PTRG to -0.63 at HERR, and median HIs were positive, reflecting clockwise hysteresis and higher rising limb concentrations (Table 13, 14; Figure 14B-C).

Urbanization can potentially alter dissolved organic carbon loading in streams due to shifts in organic carbon sources and abundance. In forested watersheds, dissolved organic carbon is sourced primarily from decomposing organic matter accumulated in soils. While soils may still be a significant pool of organic carbon in urban watersheds, contributions may be subordinate to grass clippings from lawns and organic litter

deposited on impervious surfaces, including stormwater pipes and roadside gutters that may promote decomposition of accumulated organic matter (Fork et al., 2018; Newcomer et al., 2012).

Despite potentially varying sources of DOC, relatively similar event scale behavior was observed across all study sites, albeit with higher DOC concentrations at baseflow and stormflow at the urban sites. DOC routinely exhibited enrichment behavior during individual storm events (Figure 13). Concentrations of DOC often peaked after stream discharge, resulting in positive C-Q slopes and *FIs*, and predominantly counterclockwise hysteresis (Figure 14). Enrichment behavior on the storm rising limb suggests abundant, rapidly mobilized sources of DOC proximal to the stream, with a substantially larger portion of the urban watersheds considered hydrologically proximal due to the prevalence of overland flow and stormwater infrastructure (L. A. Rose et al., 2018; Vaughan et al., 2017). For example, during the onset of a storm event at HERR, the concentration of DOC in stormwater entering the channel was >12x greater than the median baseflow concentration (Table 7, 8). Higher falling limb concentrations (counterclockwise hysteresis) suggest delayed contributions from distal DOC sources due to upland sources becoming hydrologically connected and/or longer transport times from headwaters regions (Koenig et al., 2017). Similar relationships between DOC and flow have been documented across a range of watershed land uses, including forested, agricultural, suburban, and urban, which suggests similar processes control DOC export regardless of variations in land use or potential sources (Koenig et al., 2017; Newcomer et al., 2012; Raymond & Saiers, 2010; L. A. Rose et al., 2018; Vaughan et al., 2017).

However, substantially higher discharge rates and typically higher concentrations result in high DOC fluxes from the urban watersheds, as discussed in depth below.

Much like DOC, K^+ can be sourced from the decomposition of organic matter; however, K^+ may also be derived from a variety of natural and anthropogenic sources, including weathering of silicate bedrock and soil minerals, cation exchange, agricultural and lawn fertilizers, and deicing salts, that have been shown to complicate its relationship with discharge across catchments (Long et al., 2017; L. A. Rose et al., 2018; Siwek et al., 2017). At BARN, a strong positive correlation between [DOC] and [K^+] ($R^2 = 0.81$, $p < 0.001$) and similar event-scale enrichment behavior suggest these solutes were largely coupled in transport (Figure 13A). By contrast at the urban sites, [DOC] and [K^+] were not well correlated. Across all sites, individual storm event C-Q slopes for K^+ ranged from slight dilution to enrichment (Figure 13) and often exhibited a weaker relationship with discharge when compared to other major ions, suggesting contributions from multiple sources may generate complex responses and substantial inter-event variability (L. A. Rose et al., 2018). For example, early mobilization of K^+ accumulated on impervious surfaces can contribute to enrichment or chemostatic behavior on the storm rising limb, as evidenced by stormwater runoff entering the stream channel at HERR that contained substantially elevated [K^+] relative to precipitation during the onset of a nonwinter storm event (Table 8). Similarly, K^+ showed strong positive correlations ($R^2 = 0.99$, $p < 0.001$) with the flushing of Na^+ and Cl^- following the application of deicing salts during a winter storm event at HERR. Mobilization of geogenically and biologically sourced K^+ from groundwater and soils may further contribute to enrichment or

chemostatic behaviors, particularly at BARN where contributions from overland flow are likely minimal due to low watershed ISC. Inter-event variability in K^+ behavior may be influenced by antecedent conditions and/or source abundance. For example, Long et al. (2017) found that C-Q behavior transitioned from enrichment to chemostatic to dilution during consecutive storm events as K^+ was progressively flushed from the system.

3.5.2 Geogenic and Exogenous Solutes

Median C-Q slopes indicated chemostatic behavior for predominantly geogenic species at BARN (Table 12). Except for HCO_3^- ($b \approx 0$), median C-Q slopes were weakly negative ($b \leq -0.20$) and concentrations of these solutes showed little variation relative to discharge ($CV_C/CV_Q \leq 0.20$) (Figure 13A). Median *HIs* were positive, indicating clockwise hysteresis or higher rising limb concentrations except for HCO_3^- which had a median *HI* of -0.20 (Table 12, Figure 14A). At the urban sites, median *HIs* for geogenic solutes were similar to those observed at BARN (Figure 14B-C); however, C-Q slopes for these solutes were lower at the urban sites ($-0.21 \geq b \geq -0.34$), indicating moderate dilution with increasing discharge (Table 13, 14). At all sites, HCO_3^- exhibited higher median C-Q slopes and less variability relative to other geogenic solutes. For any given geogenic solute, the urban watersheds exhibited greater variability in concentration relative to discharge compared to BARN (Figure 13).

Exogenous species species—defined as those associated with significant anthropogenic inputs, including Na^+ , Cl^- , NO_3^- , SO_4^{2-} , and TDN—exhibited behavior similar to geogenic species at each site. At BARN, SO_4^{2-} and TDN showed chemostatic behavior and low CV_C/CV_Q , while Na^+ , Cl^- , and NO_3^- exhibited dilution behavior and

higher CV_C/CV_Q (Table 12, Figure 13A). Median HIs for these solutes were positive (clockwise hysteresis), except for SO_4^{2-} which exhibited counterclockwise hysteresis (Table 12, Figure 14A). At the urban sites, C-Q slopes indicated moderate dilution of exogenous solutes with increasing discharge with dilution greater than that of exogenous solutes at BARN (Figure 13B-C). Across all sites and solutes, NO_3^- exhibited the most dilution with increasing discharge with C-Q slopes ranging from -0.29 at BARN to -0.64 at PTRG. TDN showed comparatively less dilution than NO_3^- with C-Q slopes ranging from -0.14 at BARN to -0.28 at PTRG. Exogenous species, particularly Cl^- and NO_3^- , showed more pronounced variation in concentration relative to discharge at the urban sites (Figure 13B-C).

Some geogenic and exogenous species exhibited inter-event variability in C-Q response. While dilution of geogenic and exogenous species was the dominant response at all sites, a winter storm event at BARN showed flushing behavior for Na^+ and Cl^- (Figure 15A). Higher falling limb concentrations reflect longer transport times from the headwaters where most development is located at BARN. Similarly, a winter storm event at HERR showed strong flushing behavior for Na^+ and Cl^- and chemostatic to slight flushing behavior for Ca^{2+} and SO_4^{2-} (Figure 15B). None of these solutes exhibit flushing patterns during discretely sampled nonwinter storm events; however, $[Na^+]$ and $[Cl^-]$ exhibited chemostatic behavior during a single discretely sampled nonwinter event at HERR. While winter storms were not discretely sampled at PTRG, high-frequency SC suggests similar behavior is likely. Although a seasonal trend was not apparent, NO_3^- exhibited substantial variability between events, with C-Q slopes ranging from weak

enrichment behavior to strong dilution. Regardless of event-scale behavior, substantially higher discharge rates and typically higher concentrations result in high fluxes of geogenic and exogenous solutes from the urban watersheds, as discussed in depth below.

The event-scale behavior of geogenic solutes at our study sites were largely in agreement with similar studies conducted in forested, agricultural, and urban watersheds (Arora et al., 2020; Gwenzi et al., 2017; Knapp et al., 2020; Long et al., 2017; L. A. Rose et al., 2018). While Na^+ and Cl^- are considered exogenous in this study due to inputs of deicing salts, studies conducted in forested and agricultural watersheds typically consider these solutes to be predominantly geogenic or atmospheric in origin. Across all sites, negative C-Q slopes (Figure 13) suggest a source limitation of most geogenic solutes during storm events as enriched groundwater is progressively diluted during storm events through mixing with lower concentration sources, e.g., soil water or overland flow (Knapp et al., 2020). Positive median *HIs* for most geogenic solutes (Figure 14) indicate concentrations are higher on the storm rising limb and may reflect flushing of these solutes from soils and/or those accumulated on impervious surfaces. For example, surface runoff collected from a stormwater outflow at HERR contained elevated $[\text{HCO}_3^-]$ and $[\text{Ca}^{2+}]$ relative to precipitation (Table 8).

Over longer timescales, concentrations of geogenic solutes in forested watersheds have been shown to be relatively invariant with increased discharge due to large subsurface stores and production/mobilization rates that change proportionally with discharge (Godsey et al., 2009). At BARN, the mostly forested suburban site, C-Q slopes of geogenic solutes were generally higher when compared to the urban sites (Figure 13).

While the processes controlling production and mobilization of geogenic solutes are likely similar across all the study sites, impervious cover associated with urban land use induces greater variability in discharge, resulting in a greater degree of dilution during high flow events. Increased CV_Q at the urban sites compared to the forested site would be expected to result in decreased CV_C/CV_Q values for geogenic solutes; however, we observed the opposite effect. Higher CV_C for geogenic solutes at the urban sites suggests multiple sources and/or flow paths contributing to stormflow concentrations of these solutes.

The event-scale behavior of HCO_3^- was markedly different from that of other geogenic solutes at BARN and, to a lesser extent, at the urban sites (Figure 13, 14). Contrary to the clockwise dilution behavior commonly exhibited by geogenic solutes, HCO_3^- at BARN exhibited counterclockwise enrichment behavior (Figure 14A). Concentrations of HCO_3^- increased on the storm rising limb and peaked on the storm falling limb before gradually decreasing to pre-event values. To the best of our knowledge, HCO_3^- enrichment has not been reported in other C-Q studies. Instead, HCO_3^- has been shown to exhibit chemostatic or dilution behavior closely tied to SiO_2 and has been attributed to contributions from deep groundwater pathways (Arora et al., 2020; Olshansky et al., 2018; Zhong et al., 2017). Across all sites, HCO_3^- exhibited less dilution than SiO_2 during storm events. Although the mechanism for HCO_3^- enrichment remains unclear, a possible explanation is contributions from shallow soil pathways where HCO_3^- can accumulate due to plant and microbial respiration (Finlay, 2003). At

the urban sites, HCO_3^- may show less dilution than other geogenic solutes due to inputs from concrete weathering (Sujay S. Kaushal et al., 2017; Moore et al., 2017).

Similarities in event-scale behavior of geogenic and exogenous solutes suggest that exogenous solutes also have extensive subsurface stores within our study sites. Watershed storage of exogenous solutes associated with atmospheric deposition and the application of fertilizers and deicing salts has been widely documented (Baker & Showers, 2019; Corsi et al., 2015; Driscoll et al., 2016; Moore et al., 2020). These legacy stores can be released to the stream system over time through groundwater, resulting in elevated baseflow concentrations. Like geogenic solutes, negative C-Q slopes of exogenous solutes point to concentrated groundwater sources that are progressively diluted during storm events due to mixing with lower concentration sources. However, C-Q slopes and CV_C/CV_Q values of exogenous solutes generally indicated a greater degree of dilution and variability relative to geogenic solutes, suggesting greater heterogeneity in the spatial and/or temporal distribution of these solutes relative to weathering products (Figure 13).

The high variability in event-scale behavior of Na^+ and Cl^- observed at HERR and, to a lesser extent, BARN was primarily driven by deicing salt application (Figure 13A, B). At both sites, enrichment patterns were observed during winter storm events following the application of deicing salts, with greater enrichment observed at HERR (Figure 15). During one winter storm event at HERR, high CV_C/CV_Q resulted from a substantial first flush pulse of deicing salts at the storm onset followed by dilution once depleted (green squares, Figure 13B). Chemostatic rising limb behavior of Na^+ and Cl^-

during a nonwinter event at HERR likely results from subsurface storage of deicing salts with enriched groundwater inputs maintaining rising limb concentrations before being diluted through mixing with event water, although this is not a consistent behavior of nonwinter events (green squares, Figure 13B). At PTRG, where winter storm events were not discretely sampled, Na^+ and Cl^- exhibited less inter-event variability in C-Q behavior (Figure 13C).

The inter-event variability for NO_3^- reported in this study also has been observed in other urbanized watersheds (Duncan et al., 2017; Vaughan et al., 2017). Duncan et al. (2017) showed that event-scale NO_3^- behavior was influenced by storm event size. Smaller storm events exhibited counterclockwise hysteresis and increasing concentrations while larger storm events showed clockwise dilution. Chemostatic and weak rising limb enrichment of NO_3^- corresponded with small to moderately sized storm events at HERR (peak discharge 0.71-1.33 m/s) and may reflect rapid transport of any nitrate sources accumulated on impervious surfaces. Typically, NO_3^- exhibited greater dilution relative to all other solutes, particularly at the urban sites, suggesting the flow paths mixing with enriched groundwater (e.g., soil water, overland flow) contain lower concentrations of NO_3^- relative to other solutes and/or nitrate sources are rapidly depleted (Figure 13). The behavior of TDN showed a marked difference from that of NO_3^- , with higher median C-Q slopes indicating less dilution during storm events. While NO_3^- often showed substantial dilution with increasing discharge, TDN showed a dampened response due to increases in other N species, such as NH_4^+ which has been shown to have a positive response with

increasing discharge due to flushing from soils (McMahon et al., 2021; L. A. Rose et al., 2018).

The behavior of SO_4^{2-} , particularly at the most forested BARN site, is likely the result of subsurface legacy stores resulting from long-term atmospheric deposition to watersheds in the eastern US (Driscoll et al., 2016; Herlihy, 1993; Rice et al., 2014). Although reductions in SO_2 emissions have dramatically reduced atmospheric sulfate deposition since 1970, $[\text{SO}_4^{2-}]$ remains elevated in mid-Atlantic streams. Unglaciaded soils characteristic of the region exhibit thick, highly-weathered profiles that can retain SO_4^{2-} due to adsorption to clay minerals (Rice et al., 2014). At BARN, the higher falling limb $[\text{SO}_4^{2-}]$ observed during all sampled storm events may reflect the flushing of legacy SO_4^{2-} from soils. This effect was not apparent at the urban sites, which may be attributed to minimal contributions of soil water relative to surface runoff at these sites. Late contributions of SO_4^{2-} at BARN may also reflect inputs from septic systems located predominately in the headwaters. In the septic drain field, hydrogen sulfide (H_2S) present in septic tanks is readily oxidized to SO_4^{2-} , which can then enter soil and groundwater systems (Neurath, 2007). However, the event-scale behavior of SO_4^{2-} differed from that of Cl^- and NO_3^- which are also common indicators of domestic wastewater (Neurath, 2007). While this suggests that septic systems play a minimal role in sulfate additions and transport, additional and often more substantial sources of these solutes (e.g., deicing salts, lawn fertilizers) and biological cycling of NO_3^- may confound this relationship.

3.6 Event Scale Flux-Discharge Relationships

While solute concentrations often decreased with increasing discharge, solute fluxes generally increased with increasing discharge at all sites. For example, during a storm event sampled in October 2020, solute fluxes increased with discharge and were higher at the urban sites compared to the mostly forested, suburban site for equivalent event stages (Figure 16). At BARN, solute flux exhibited no to minimal hysteresis for most solutes. For example, at similar discharge values, Cl^- showed slightly higher rising limb fluxes while NO_3^- and SO_4^{2-} showed slightly higher falling limb fluxes. Conversely, at the urban sites, solute flux exhibited more pronounced hysteretic behavior with rising limb fluxes higher than those on the falling limb for all solutes. The magnitude of solute flux hysteresis was greatest for NO_3^- at the urban sites, and HCO_3^- fluxes showed the least hysteresis at all sites. Solute fluxes at all sites appear to increase with discharge regardless of storm size. Total dissolved solids (TDS) concentrations derived from high-frequency SC data indicate total solute flux increased with discharge during both small storm events (peak discharge < 10th percentile) and the largest storm event at each site (Figure 17).

Greater linearity (less hysteresis) in flux-discharge relationships compared to C-Q relationships reflects the lower variability of solute concentrations (CV_C) relative to discharge (CV_Q) observed in our study sites (Figure 13). Typically, variations in discharge were >1-2 orders of magnitude greater than variations in solute concentrations, which is in line with numerous studies that indicate most solute concentrations vary far less than discharge (Arora et al., 2020; Diamond & Cohen, 2018; Gwenzi et al., 2017; L.

A. Rose et al., 2018). Small decreases in solute concentration relative to increases in discharge result in greater solute fluxes at increasingly higher flows, and differences between rising and falling limb behaviors are reduced (Figure 16). Solutes associated with higher CV_C/CV_Q (e.g., NO_3^-) exhibit greater flux-discharge hysteresis (Figure 13, 16). While C-Q slopes indicated greater dilution of geogenic and exogenous solutes at the urban sites (Table 13, 14), higher stormflow discharge often resulted in substantially higher solute fluxes compared to the mostly forested suburban site (Figure 16). Although not shown, flux-discharge relationships persisted across the long-term record of baseflow and stormflow data. For any given solute, flux exhibited a much stronger relationship with discharge (higher R^2) than concentration, suggesting discharge may be used as a good predictor of solute load even in flashy, urban streams.

3.7 Long-term Solute Behavior

Across the four-year record of discrete baseflow samples and two- to three-year record of stormflow samples, solute behavior fell into groupings similar to the event-scale albeit with somewhat weaker correlation statistics. C-Q behavior of geogenic and exogenous solutes generally showed dilution, while C-Q behavior of biologically associated species ranged from chemostatic to weak mobilization. The strength of the regression relationships varied by site and solute (Table 15). The R^2 values of the power law regressions were low ($R^2 < 0.40$) for many solutes at BARN (Figure 18) and HERR (Figure 19) and were often substantially higher at PTRG (Figure 20). Biologically associated species (K^+ , DOC) and those with strong anthropogenic influence (Cl^- , Na^+)

tended to have weaker relationships compared to geogenic solutes (HCO_3^- , Mg^{2+} , Ca^{2+} , SiO_2).

C-Q behavior showed substantial variability at the event scale when compared to the long-term record of discrete samples, particularly for exogenous and biologically associated species (Figures 18, 19, 20). For example, Cl^- , Na^+ , Ca^{2+} , and SO_4^{2-} exhibited flushing, dilution, and chemostatic patterns based on changes in rising limb concentrations during separate discretely sampled storm events at HERR, while the long-term record showed dilution as the overall trend (Figure 19). The extent of inter-event variability in C-Q slopes differed between solutes and sites and tended to be greatest at HERR (Figure 21). No distinct trend in solute variability was observed across the sites. Despite the low R^2 values for the slopes of the long-term datasets, the four-year slopes were ± 0.2 of the median event-scale C-Q slopes for all solutes except DOC, NO_3^- , and K^+ at BARN (Figure 21). Additionally, for HCO_3^- and SO_4^{2-} at BARN though the median event-scale and four-year slopes were within 0.2, the four-year slope was outside the range of all events. Long term slopes were typically a close approximation of event-scale behavior for geogenic solutes, while exogenous species often showed a greater deviation between event and long-term behaviors. In most cases, long-term slopes of exogenous species indicated less dilution (higher b) relative to the event-scale, except at PTRG where long-term CQ-slopes indicated greater dilution. Note that stormflow samples constituted 60–70% of the long-term data for each site and so the differences between event-scale and long-term are not a function of “oversampling” at baseflow (e.g., N values in Table 6).

Across all sites, long term variations in solute concentration were orders of magnitude less than discharge. Long-term C-Q relationships indicated most individual solutes behaved similarly across the study sites despite event-scale variability and differences in land use. Across all sites, the long-term C-Q slopes of most geogenic (HCO_3^- , SiO_2 , Ca^{2+} , Mg^{2+}) and exogenous (Na^+ , Cl^- , NO_3^- , SO_4^{2-}) solutes were negative, indicating dilution was the dominant response to increasing discharge (Table 15). The typically stronger power-law relationships between geogenic solutes and discharge suggest a simple mixing of enriched groundwater diluted by less concentrated event water. In comparison, often weaker relationships between exogenous solutes and discharge reflect greater event-scale variability due to contributions from multiple flow paths or sources and/or spatial or temporal heterogeneity in the source distribution. The degree of solute dilution varied by site, with BARN often exhibiting less dilution (higher b) than the urban sites, suggesting concentrations are buffered by soil water inputs and/or less influence of dilute overland flow due to infiltration of precipitation. More substantial dilution ($b \leq -0.29$) at the urban sites reflects a greater influence of overland flow and is in contrast with recent work that reports chemostatic behavior ($b \approx 0$) to weak dilution ($-0.2 \leq b \leq 0$) of geogenic solutes over longer timescales (Creed et al., 2015; Diamond & Cohen, 2018; Godsey et al., 2009; Hunsaker & Johnson, 2017; Moatar et al., 2017). However, similar negative slopes were reported for some geogenic solutes in agricultural (L. A. Rose et al., 2018) and urban (Balerna et al., 2021) watersheds. Long-term behavior of biologically associated species (DOC , K^+) reflects chemostasis to weak

enrichment and is agreement with long term behaviors found in similar studies (Koenig et al., 2017; L. A. Rose et al., 2018).

While the long-term C-Q relationships of many solutes were chemodynamic, C-Q slopes and CV_C/CV_Q values were relatively low ($|b| < 1$; $CV_C/CV_Q \ll 1$). In particular, long-term CV_C/CV_Q values at the urban sites were notably lower than those observed on the event scale due to higher discharge variability over longer timescales (Table 15). Low C-Q slopes and CV_C/CV_Q values imply discharge controls solute flux; therefore, despite not meeting the somewhat arbitrary definition of chemostatic behavior, our results agree with studies showing long-term variations in solute concentration are orders of magnitude less than discharge (Creed et al., 2015; Godsey et al., 2009; Hunsaker & Johnson, 2017; L. A. Rose et al., 2018).

3.8 Hydrograph Separation for Calculation of Solute Loads

Estimated solute loads were calculated for the two-year period from January 2019 through December 2020 over which high-frequency data were available at all sites. Baseflow contributions accounted for the majority of solute export at all sites. On average, 86%, 70%, and 65% of major cation and anion export was attributed to baseflow at BARN, PTRG, and HERR, respectively (Table 16). Quickflow contributions showed little variation between solutes at BARN and more variability between solutes in the urban watersheds (Figure 22A, C, E). For example, HCO_3^- , K^+ , and Ca^{2+} showed higher than average quickflow contributions while NO_3^- showed greater baseflow contributions at HERR and PTRG (Table 16). Quickflow contributions to solute export were somewhat correlated with storm event C-Q slope (b) and, to a lesser extent, CV_C/CV_Q (Figure 23).

Higher C-Q slopes corresponded to greater quickflow export. Conversely, greater quickflow export was associated with lower CV_c/CV_Q , except at BARN which showed no correlation. Quickflow contributions were not correlated with median storm event FI or HI .

Seasonal solute export was similar across all sites. Approximately 60% of the total discharge at each site occurred during the nonwinter period (Apr-Nov). Total loads for most solutes in nonwinter months were similar to discharge (50-65%) except Cl^- and Na^+ which had higher winter exports at all sites (Figure 22, Table 16). Although winter months (Dec-Mar) only accounted for ~40% of total discharge at each site, winter contributions of Cl^- and Na^+ were 53 and 57% of total load at BARN, respectively, and 66–76% of total load at the urban sites. Despite similarities in seasonal distribution, loads of all solutes were substantially lower at BARN relative to the urban sites (Figure 22B, D, F, Table 16).

Higher baseflow contributions to discharge and solute export at BARN, the mostly forested suburban site, reflect greater infiltration of event water and the subsequent displacement of stored water within the catchment (Table 16). Studies employing various methods of hydrograph separation in forested watersheds have demonstrated similar behavior, with contributions to stormflow consisting predominantly of pre-event or “old” water relative to event or “new” water, which can be equated to quickflow (Buttle, 1994; Farrick & Branfireun, 2015; James B Shanley et al., 2002). In contrast, higher quickflow contributions at the urban sites reflect greater contributions from overland flow due to increased watershed ISC, which agrees with behavior

previously documented in urban watersheds (Inserillo et al., 2017; Pellerin et al., 2008). The differences in watershed hydrology between the mostly forested suburban and urban sites are illustrated by the event-scale results of the hydrograph separation performed at each site (Figure 24). During the same storm event, quickflow contributions to stormflow were $\sim 2\times$ higher at HERR relative to BARN, and this variation in source water was reflected in substantially higher peak flows at HERR. Surprisingly, despite having substantial contributions to stormflow on the event scale, quickflow contributions to total load were substantially lower than baseflow over long timescales, even at the urban sites where flashy responses to storm events are common (Table 16). Elevated baseflow concentrations of most solutes, particularly at the urban sites, and the episodic nature of precipitation events are the most likely explanations for greater solute export by baseflow/slowflow components over time.

Variations in quickflow contributions of individual solutes appear to reflect event-scale C-Q relationships (Figure 23). Solute enrichment behavior on the event scale are more likely to have substantial contributions from quickflow that allow for increasing concentrations with discharge (e.g., DOC). Similarly, groundwater-sourced solutes that exhibit less dilution relative to other groundwater-sourced solutes likely have quickflow sources that buffer concentrations from rapid dilution. The lack of correlation between *FI* and *HI* and hydrograph separation results suggests that C-Q slope and CV_c/CV_Q are likely more useful for characterizing solute behavior, at least in urban watersheds.

Seasonal export only varied for solutes with a strong seasonal component, such as Na^+ and Cl^- , which exhibited substantially higher loads during winter, particularly at the urban sites (Table 16). A substantial portion of Na^+ and Cl^- loading was attributed to baseflow, reflecting direct inputs of deicing salts and slow movement of accumulated salt through the stream system. Following the application of deicing salts, stream SC often remained elevated long after flow conditions returned to pre-storm values, behavior that is not observable when only considering solute transport during storm events but is clear when comparing seasonal data (e.g., $\geq 75^{\text{th}}$ percentile for winter versus nonwinter, Table 4). While NO_3^- can potentially have a strong seasonal component, we used the median concentration for the duration of the dataset due to weak regression relationships with SC and discharge (Table 2); therefore, NO_3^- loads follow discharge trends. Median concentrations were used for several other solutes (HCO_3^- and SO_4^{2-} at BARN; K^+ across all sites); therefore, total load calculations may substantially overestimate or underestimate actual loads.

Regardless, higher storm event discharge (Table 3) and solute concentrations (Table 5, 6, 7) result in substantially higher loads at the urban sites compared to BARN (Table 16). Solute loads at the urban sites were $>2\text{-}14\times$ higher than BARN, with Ca^{2+} showing the greatest increases. Higher Ca^{2+} loads at PTRG relative to BARN and HERR may be attributed to relatively weak regression relationships between Ca^{2+} and higher SC values (Table 2). Loads of Na^+ and Cl^- , which had the strongest regression relationships across all sites, were $7\text{-}8\times$ higher at the urban sites.

3.9 End Member Mixing Analysis

End member mixing calculations will be conducted in the future pending remaining isotope analyses results from collaborators at Johns Hopkins.

4. Conclusions

Despite the altered hydrology of the urban watersheds, our results show remarkably similar behavior for individual solutes across the suburban and urban sites. Solute response to increased discharge generally fell into the following groups: 1) Groundwater-sourced geogenic and exogenous species that exhibited dilution (source limitation) and 2) biologically associated species that exhibited chemostatic (invariant concentrations) or enrichment (transport limitation). Solute behavior was similar across temporal scales; however, substantial inter-event variability in solute response was commonly observed for exogenous and biologically associated species. We found that the C-Q slope (b) combined with CV_C/CV_Q provided a better characterization of geochemical and hydrological behavior compared to other C-Q metrics and allowed for comparison of solute behavior across timescales. While the HI remained useful for distinguishing between rising and falling limb solute behavior and, thus, transport processes, the FI had low utility for the study watersheds.

Across all sites and solutes, variations in discharge were >1-2 orders of magnitude greater than variations in concentration, suggesting near-chemostatic solute behavior may be characteristic of urban watersheds and thus C-Q patterns are similar despite large differences in Q responses compared to forested and agricultural watersheds. Regardless of event-scale behavior, low variation in solute concentration relative to discharge

resulted in increasing solute fluxes (and loads) during all storm events. Although event-scale behavior indicated a greater degree of dilution for most solutes, substantially higher storm discharge at the urban sites offsets any dilution, resulting in solute loads 2-14x higher than the mostly forested suburban watershed. Hydrograph separation results indicate quickflow (overland flow) is a significant contributor to stormflow at the urban sites, which likely drives the event-scale dilution observed for groundwater-sourced geogenic and exogenous solutes. In contrast, baseflow (groundwater, soil water) is the overwhelmingly dominant contributor to stormflow at the mostly forested suburban site. The increase in the fraction of water exported via quickflow at the urban sites was greater than the fraction of solute load exported during quickflow. Thus, across all sites, a substantial majority of the solute load is exported during baseflow.

5. Tables

Table 1: Study site characteristics

Study Site	Baisman Run (BARN)	West Branch Herring Run (HERR)	Plumtree Run (PTRG)
Drainage Basin Area (km ²) ¹	3.80	5.61	6.37
Forested Land Use (%) ²	63.4	2.09	5.38
Impervious Surface Area (%) ³	1.09	24.9	27.0
Urban Land Use (%) ³	25.2	87.3	82.3
Dominant Bedrock Lithology ^{4,5}	Loch Raven Schist	Baltimore Gneiss	Port Deposit Gneiss

¹USGS StreamStats, 2018. ²Maryland Land Use/Land Cover, 2010. ³National Land Cover Database, 2011. ⁴Maryland Geological Survey Cockeysville, MD Quadrangle (Crowley, 1975).

⁵Maryland Geological Survey Geologic Map of Harford County (Southwick, 1968).

Table 2: Regression models for high-frequency solute concentration datasets

Constituent	BARN		HERR		PTRG	
	Regression Model	R ²	Regression Model	R ²	Regression Model	R ²
HCO ₃ ⁻	N/A	N/A	Q	0.64	Q	0.65
SiO ₂	Q	0.68	Q	0.62	Q	0.74
Cl ⁻	SC	0.95	SC	0.99	SC	0.99
Na ⁺	SC Nonwinter	0.83	SC	0.99	SC	0.94
	SC Winter	0.87				
SO ₄ ²⁻	N/A	N/A	SC Nonwinter	0.72	Q	0.74
	N/A	N/A	SC Winter	0.89		
Ca ²⁺	SC Nonwinter	0.88	SC Nonwinter	0.72	SC Nonwinter	0.95
	SC Winter	0.73	SC Winter	0.92	SC Winter	0.46
Mg ²⁺	SC Nonwinter	0.90	SC < 1000	0.77	SC < 800	0.94
	SC Winter	0.69	SC > 1000	0.24*	SC > 800	0.15*
NO ₃ ⁻	N/A	N/A	SC < 1000	0.67	SC < 800	0.90
	N/A	N/A	SC > 1000	0.03*	SC > 800	0.29*
K ⁺	N/A	N/A	N/A	N/A	N/A	N/A

Regression models were developed using discrete concentration measurements from baseflow and stormflow samples. Winter (Dec-Mar) represents the period during which deicing salts are commonly applied. SC breakpoints (in $\mu\text{S}/\text{cm}$) were determined visually from regression plots. N/A and * denote models were not a good fit and median concentrations were used instead.

Table 3: Summary statistics for high-frequency discharge (m/yr)

Site	Season	10th Percentile	25th Percentile	Median	75th Percentile	90th Percentile	Maximum	<i>n</i>
BARN	Nonwinter	0.15	0.18	0.24	0.40	0.67	33.61	81126
	Winter	0.26	0.32	0.40	0.63	0.98	14.66	33447
HERR	Nonwinter	0.11	0.15	0.24	0.37	0.60	335.87	209638
	Winter	0.20	0.25	0.36	0.50	0.80	118.43	106624
PTRG	Nonwinter	0.14	0.20	0.32	0.48	0.98	318.23	210190
	Winter	0.24	0.33	0.46	0.63	1.09	37.43	105279

Table 4: Summary statistics for high-frequency specific conductance ($\mu\text{S}/\text{cm}$)

Site	Season	10th Percentile	25th Percentile	Median	75th Percentile	90th Percentile	Maximum	<i>n</i>
BARN	Nonwinter	149.50	169.50	184.40	190.70	193.40	287.40	73486
	Winter	157.60	172.50	183.70	195.10	300.30	2898.80	30011
HERR	Nonwinter	350.10	516.50	610.70	659.20	700.70	5985.20	155749
	Winter	497.50	616.10	712.10	1026.30	1762.60	22603.70	93411
PTRG	Nonwinter	280.00	440.00	534.00	593.00	634.00	3040.00	209524
	Winter	410.00	517.00	612.00	929.00	1500.00	8810.00	107514

Table 5: Median cation concentrations of discrete baseflow and stormflow samples (mg/L)

Site	Flow Condition	Median [Na ⁺]	Median [K ⁺]	Median [Mg ²⁺]	Median [Ca ²⁺]	<i>n</i>
BARN	Baseflow	16.84	1.65	4.70	7.52	70
	Stormflow	13.72*	1.64	3.81*	5.95*	113
HERR	Baseflow	47.49	4.19	13.88	45.41	54
	Stormflow	26.51*	2.80*	6.27*	23.43*	183
PTRG	Baseflow	40.59	1.57	14.42	37.49	57
	Stormflow	15.77*	1.32	5.76*	15.13*	87
POBR ¹	Baseflow	1.85	0.66	0.63	0.71	22

¹Median baseflow concentration data from Moore et al. (2017)

*: Denotes statistical significance between median baseflow and stormflow concentrations (p < 0.001) based on results of a two-sided unpaired Wilcoxon rank-sum test

Table 6: Median anion concentrations of discrete baseflow and stormflow samples (mg/L)

Site	Flow Condition	Median [HCO ₃ ⁻]	Median [Cl ⁻]	Median [NO ₃ ⁻]- N	Median [SO ₄ ²⁻]	<i>n</i>
BARN	Baseflow	16.60	38.31	1.69	3.18	70
	Stormflow	20.21**	31.67*	1.14*	2.97	113
HERR	Baseflow	96.75	127.16	1.74	23.45	54
	Stormflow	63.83*	61.36*	0.85*	11.11*	183
PTRG	Baseflow	56.06	128.60	2.51	22.66	57
	Stormflow	45.46*	36.28*	0.74*	9.25*	87
POBR ¹	Baseflow	9.76	2.53	0.15	1.41	22

¹Median baseflow concentration data from Moore et al. (2017)

*: Denotes statistical significance between median baseflow and stormflow concentrations (p < 0.001) based on results of a two-sided unpaired Wilcoxon rank-sum test

**: Denotes statistical significance between median baseflow and stormflow concentrations (p < 0.01) based on results of a two-sided unpaired Wilcoxon rank-sum test

Table 7: Median [DOC], [TDN], and [SiO₂] of discrete baseflow and stormflow samples (mg/L)

Site	Flow Condition	Median [DOC]	Median [TDN]	Median [SiO ₂]	<i>n</i>
BARN	Baseflow	1.07	1.80	10.20	59-68
	Stormflow	2.21*	1.31*	8.84*	106-112
HERR	Baseflow	1.65	2.06	11.60*	37-52
	Stormflow	4.12*	1.33*	6.23*	82-182
PTRG	Baseflow	1.83	2.66	17.93	54-57
	Stormflow	3.97*	1.08*	9.54*	81-87

DOC: Dissolved organic carbon; TDN: Total dissolved nitrogen

*: Denotes statistical significance between median baseflow and stormflow concentrations ($p < 0.001$) based on results of a two-sided unpaired Wilcoxon rank-sum test

Table 8: Concentrations of dissolved constituents in precipitation samples and direct surface runoff from a stormflow drainpipe at HERR (mg/L)

Constituent	Precipitation	Surface Runoff
[HCO ₃ ⁻]	n.m.	33.19
[Cl ⁻]	0.39	4.10
[NO ₃ ⁻]-N	0.14	0.05
[SO ₄ ²⁻]	0.40	2.40
[Na ⁺]	0.15	2.33
[K ⁺]	0.00	4.09
[Mg ²⁺]	0.15	2.37
[Ca ²⁺]	0.28	8.79
[SiO ₂]	0.09	10.08
[DOC]	n.m.	20.94
[TDN]	n.m.	0.67

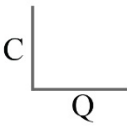







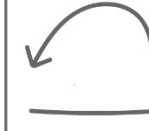

Precipitation data reflects the average of precipitation samples collected between 08/2020-11/2020 (n=3). Surface runoff was collected during a single event in 11/2020. n.m: not measured

Table 9: Summary statistics for storm event peak discharge (m³/s)

Site	10th Percentile	25th Percentile	Median	75th Percentile	90th Percentile	Max	<i>n</i>
BARN	0.08	0.12	0.25	0.52	0.99	4.05	75
HERR	0.12	0.25	1.22	4.43	13.66	59.75	219
PTRG	0.16	0.26	1.19	3.34	7.47	64.28	209

Summary statistics only include storm events for which specific conductance-discharge relationships were examined based on selection criteria.

Table 10: Specific conductance-discharge patterns and percentages observed during storm events

										
Site	CW Dilution	CCW Dilution	Complex Dilution	CW Flushing	CCW Flushing	Complex Flushing	CW Chemostatic	CCW Chemostatic	Complex Chemostatic	<i>n</i>
BARN	56%	11%	17%	4%	7%	1%	0%	4%	0%	75
HERR	58%	4%	8%	6%	9%	3%	8%	3%	1%	219
PTRG	47%	8%	11%	1%	7%	7%	4%	10%	4%	209

Storm event SC-Q behavior was classified using the calculated hysteresis index (*HI*) and flushing index (*FI*) and verified by visual inspection of the hysteresis pattern. Chemostatic indicates little to no change in concentration on the storm rising limb. *CW*: clockwise; *CCW*: counterclockwise

Table 11: Median FI and HI by season for storm event SC-Q relationships

Site	Season	Median FI	Median HI	<i>n</i>
BARN	Nonwinter	-0.70	0.15	48
	Winter	-0.37	0.08	27
HERR	Nonwinter	-0.55	0.15	150
	Winter	-0.22	0.22	69
PTRG	Nonwinter	-0.36	0.15	135
	Winter	-0.09	0.18	74

Table 12: Median FI , HI , CV_C/CV_Q and C-Q slope (b) for discretely sampled storm events at BARN

Constituent	Median FI	Median HI	Median CV_C/CV_Q	Median b	n
HCO_3^-	0.30	-0.20	0.10	0.06	5
Cl^-	-1.00	0.24	0.26	-0.28	5
NO_3^-	-0.85	0.29	0.29	-0.29	5
SO_4^{2-}	-0.37	-0.15	0.12	-0.12	5
Na^+	-0.94	0.27	0.29	-0.30	5
K^+	0.69	-0.21	0.34	0.27	5
Mg^{2+}	-0.86	0.29	0.20	-0.20	5
Ca^{2+}	-0.89	0.23	0.18	-0.19	5
SiO_2	-0.95	0.22	0.17	-0.20	5
DOC	0.91	-0.16	0.62	0.72	5
TDN	-0.79	0.32	0.19	-0.14	5

FI : flushing index; HI : hysteresis index; CV_C : coefficient of variation of concentration; CV_Q : coefficient of variation of discharge; b : slope of the $\log(C)$ - $\log(Q)$ regression

Table 13: Median FI , HI , CV_C/CV_Q and C-Q slope (b) for discretely sampled storm events at HERR

Constituent	Median FI	Median HI	Median CV_C/CV_Q	Median b	n
HCO_3^-	-0.88	0.24	0.27	-0.22	9
Cl^-	-0.71	0.34	0.60	-0.37	9
NO_3^-	-0.77	0.23	0.81	-0.47	9
SO_4^{2-}	-0.90	0.35	0.51	-0.37	9
Na^+	-0.64	0.33	0.60	-0.32	9
K^+	-0.63	0.29	0.28	-0.12	9
Mg^{2+}	-0.81	0.29	0.54	-0.34	9
Ca^{2+}	-0.73	0.28	0.47	-0.30	9
SiO_2	-0.82	0.19	0.34	-0.29	9
DOC	0.52	0.05	0.23	0.25	5
TDN	-0.76	0.29	0.43	-0.22	5

FI : flushing index; HI : hysteresis index; CV_C : coefficient of variation of concentration; CV_Q : coefficient of variation of discharge; b : slope of the $\log(C)$ - $\log(Q)$ regression

Table 14: Median FI , HI , CV_C/CV_Q and C-Q slope (b) for discretely sampled storm events at PTRG

Constituent	Median FI	Median HI	Median CV_C/CV_Q	Median b	n
HCO_3^-	-0.94	0.17	0.17	-0.21	4
Cl^-	-0.88	0.40	0.53	-0.39	4
NO_3^-	-0.90	0.26	0.67	-0.65	4
SO_4^{2-}	-0.92	0.37	0.45	-0.37	4
Na^+	-0.91	0.36	0.41	-0.37	4
K^+	-0.09	0.27	0.21	-0.01	4
Mg^{2+}	-0.85	0.37	0.44	-0.32	4
Ca^{2+}	-0.86	0.36	0.44	-0.32	4
SiO_2	-0.90	0.34	0.33	-0.30	4
DOC	0.57	-0.22	0.23	0.21	4
TDN	-0.89	0.25	0.33	-0.28	4

FI : flushing index; HI : hysteresis index; CV_C : coefficient of variation of concentration; CV_Q : coefficient of variation of discharge; b : slope of the $\log(C)$ - $\log(Q)$ regression

Table 15: Long-term CV_C/CV_Q , C-Q slopes (b), and power law regression coefficients for BARN, HERR, and PTRG

Constituent	BARN			HERR			PTRG		
	CV_C/CV_Q	b	R^2	CV_C/CV_Q	b	R^2	CV_C/CV_Q	b	R^2
HCO_3^-	0.18	-0.08*	0.12	0.05	-0.20*	0.64	0.06	-0.17*	0.65
Cl^-	0.23	-0.21*	0.41	0.39	-0.21*	0.06	0.29	-0.53*	0.62
NO_3^-	0.24	-0.18*	0.22	0.11	-0.43*	0.39	0.17	-0.82*	0.70
SO_4^{2-}	0.21	0.12*	0.18	0.11	-0.33*	0.45	0.12	-0.42*	0.74
Na^+	0.26	-0.13*	0.16	0.42	-0.16***	0.03	0.39	-0.48*	0.56
K^+	0.37	-0.14*	0.08	0.09	-0.16*	0.23	0.07	-0.02	0.00
Mg^{2+}	0.18	-0.22*	0.73	0.09	-0.34*	0.54	0.12	-0.40*	0.70
Ca^{2+}	0.18	-0.23*	0.80	0.09	-0.29*	0.45	0.12	-0.39*	0.70
SiO_2	0.14	-0.15*	0.68	0.08	-0.29*	0.62	0.09	-0.29*	0.74
DOC	0.65	0.16***	0.03	0.13	0.22*	0.18	0.11	0.26*	0.47
TN	0.17	-0.06**	0.07	0.07	-0.26*	0.35	0.11	-0.30*	0.66

*: Denotes significance $p < 0.0001$ **: Denotes significance $p < 0.001$ ***: Denotes significance $p < 0.01$

Table 16: Results from hydrograph separation showing the fraction of the total load (kg) of individual solutes attributed to nonwinter (NW), winter (W), quickflow (QF) and baseflow (BF). Total discharge (m/yr) and the fraction of discharge attributed to NW, W, QF, and BF are listed at the bottom. Nonwinter was defined as Apr-Nov; winter was defined as Dec-Mar. Load estimates were calculated using high-frequency concentration datasets generated from solute-specific regression models based on discrete concentration measurements and either SC or discharge. Load estimates reflect the period from Jan. 2019 through Dec. 2020.

Constituent	BARN					HERR					PTRG				
	Fraction of Total				Total Load (kg)	Fraction of Total				Total Load (kg)	Fraction of Total				Total Load (kg)
	NW	W	QF	BF		NW	W	QF	BF		NW	W	QF	BF	
HCO ₃ ⁻	0.61	0.39	0.15	0.85	63373	0.60	0.40	0.39	0.61	406652	0.61	0.39	0.33	0.67	365016
Cl ⁻	0.47	0.53	0.14	0.86	119528	0.26	0.74	0.31	0.69	881209	0.34	0.66	0.28	0.72	947527
NO ₃ ⁻	0.61	0.39	0.14	0.86	4740	0.45	0.55	0.26	0.74	6271	0.51	0.49	0.23	0.77	11019
SO ₄ ²⁻	0.61	0.39	0.15	0.85	10559	0.53	0.47	0.36	0.64	83413	0.61	0.39	0.22	0.78	92566
Na ⁺	0.43	0.57	0.14	0.86	54293	0.24	0.76	0.31	0.69	473416	0.30	0.70	0.28	0.72	403511
K ⁺	0.61	0.39	0.15	0.85	5594	0.63	0.37	0.53	0.47	23327	0.63	0.37	0.42	0.58	12982
Mg ²⁺	0.55	0.45	0.13	0.87	13259	0.48	0.52	0.31	0.69	50729	0.53	0.47	0.28	0.72	78592
Ca ²⁺	0.56	0.44	0.14	0.86	21106	0.55	0.45	0.38	0.62	169202	0.61	0.39	0.41	0.59	306783
SiO ₂	0.62	0.38	0.14	0.86	31667	0.60	0.40	0.34	0.66	40432	0.61	0.39	0.27	0.73	88081
Discharge	0.61	0.39	0.15	0.85	47820 (m/yr)	0.63	0.37	0.54	0.46	131125 (m/yr)	0.62	0.38	0.43	0.57	144293 (m/yr)

6. Figures

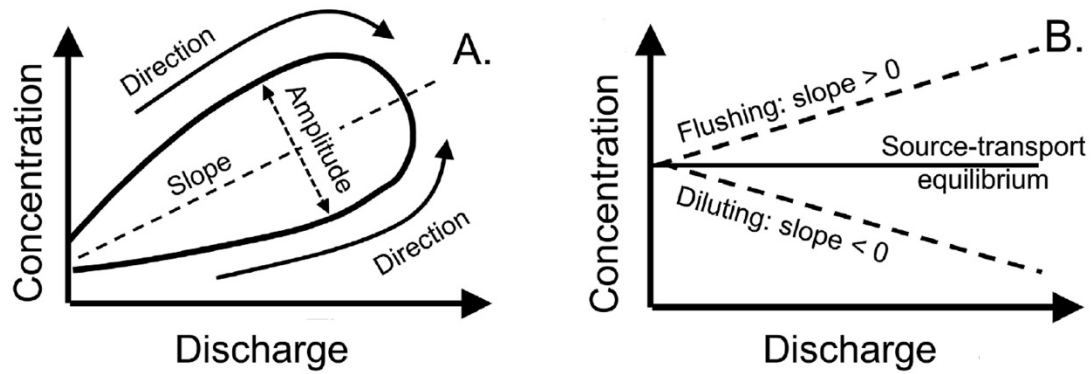


Figure 1. Representations of hysteresis patterns showing (A) general characteristics, including rotational direction, slope, and amplitude, and (B) interpretations of slope. Figure modified from Long (2017).

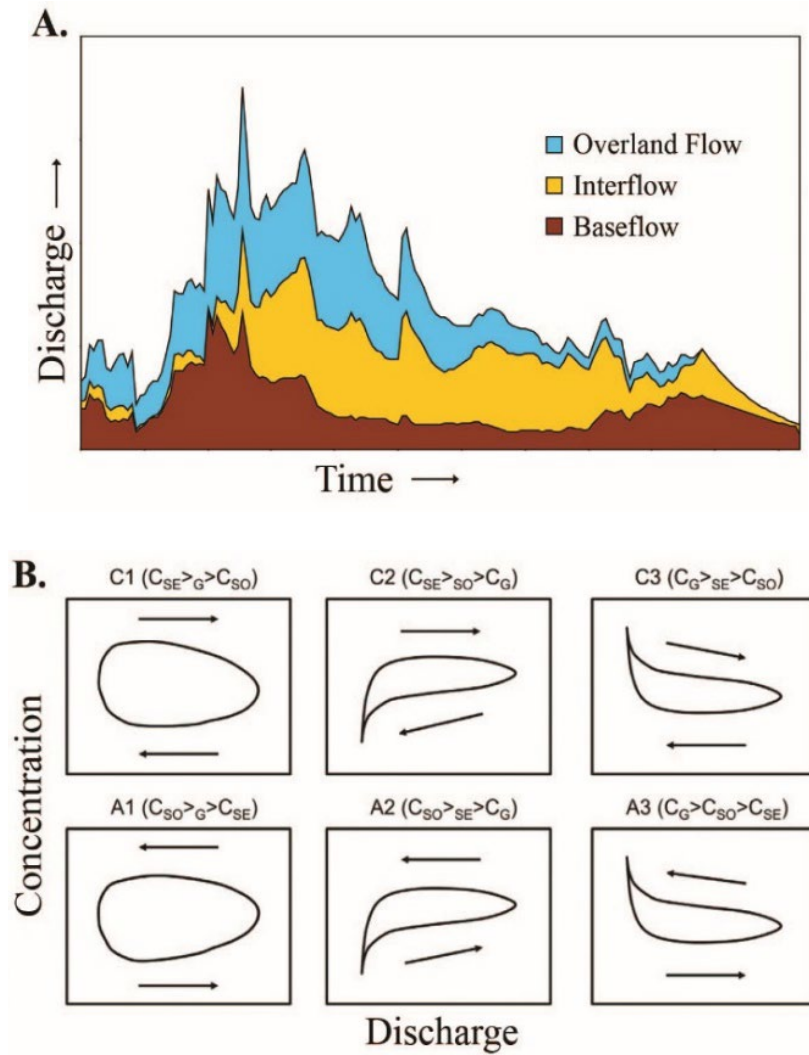


Figure 1. (A) An example of a three-component end-member mixing model adapted from Liu et al. (2004) showing hydrograph contributions of overland flow, interflow, and baseflow over time. (B) Theoretical hysteresis patterns that were proposed by Evans and Davies (1998).

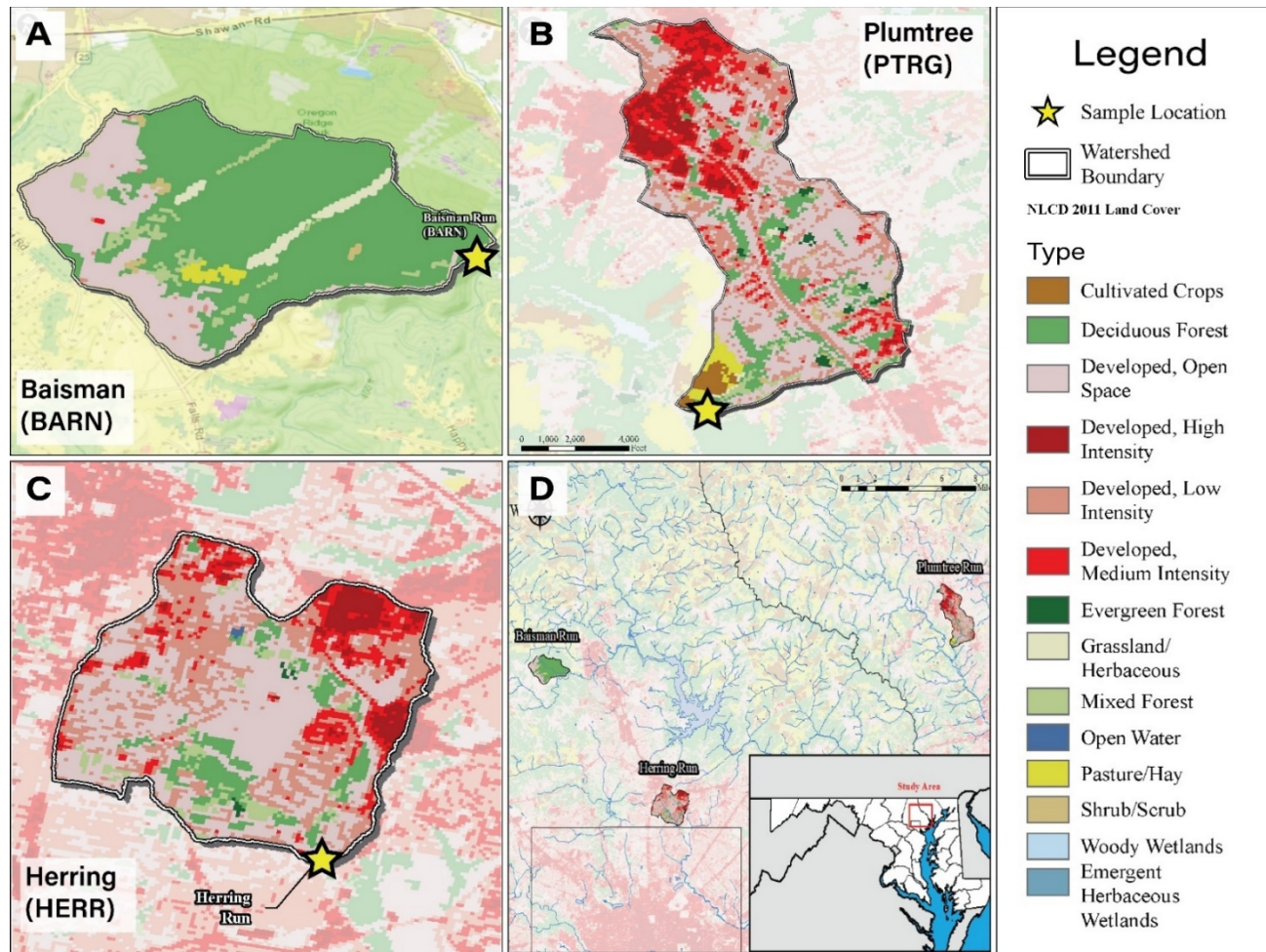


Figure 2. Watershed land cover map of (A) Baisman Run (BARN), (B) Plumtree Run (PTRG), and (C) West Branch Herring Run (HERR); (D) land cover map of the Baltimore metropolitan region. Watersheds are similarly sized ($<7 \text{ km}^2$).

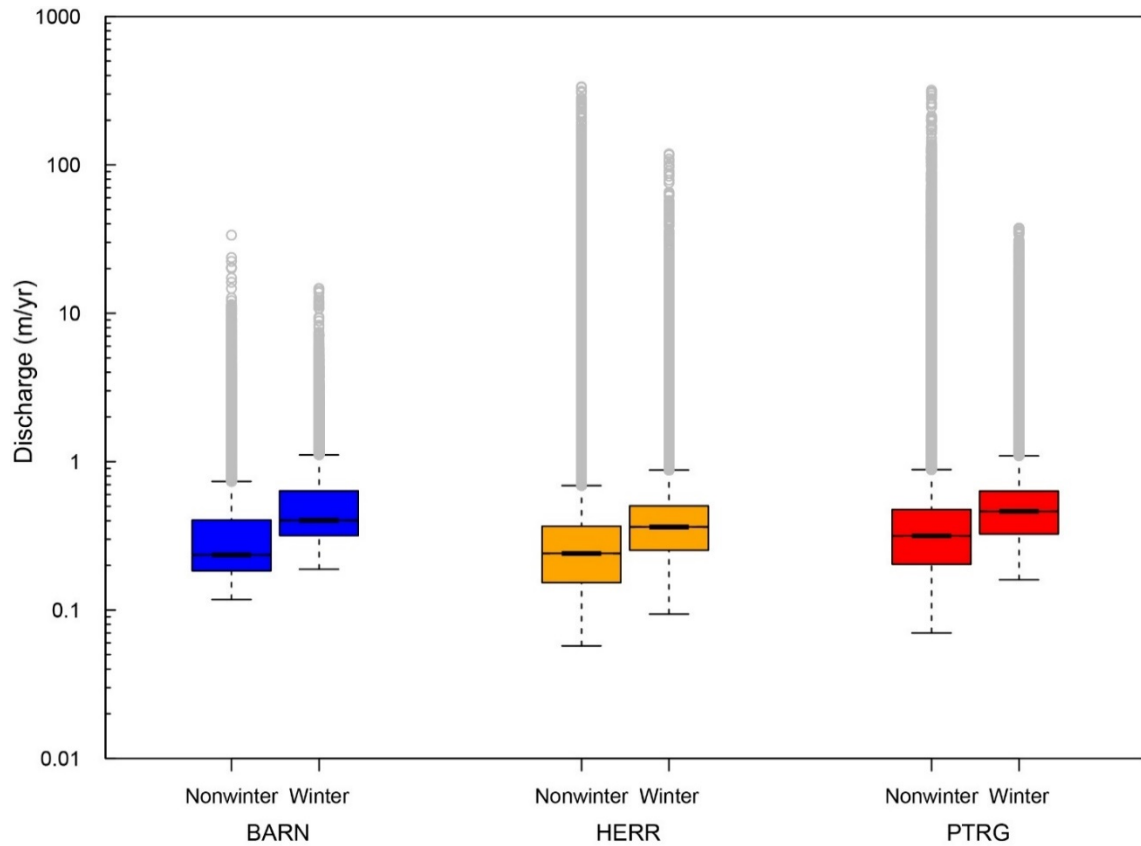


Figure 4: High-frequency discharge normalized to watershed area by season (m/yr). Seasonal medians were similar across all sites. Winter months showed higher median discharge, while the lowest and highest discharge values were recorded during nonwinter months. Discharge spanned >2 orders of magnitude at BARN and >3 order of magnitude at HERR and PTRG. Discharge measurements were collected from January 2019-January 2021 at BARN; measurements were recorded at 15-minute intervals before June 2020 and 5-minute intervals thereafter. Discharge measurements were collected at 5-minute intervals from January 2018-January 2021 at HERR and PTRG. Nonwinter was defined as Apr-Nov. Winter was defined as Dec-Mar, the period during which deicing salts are commonly applied.

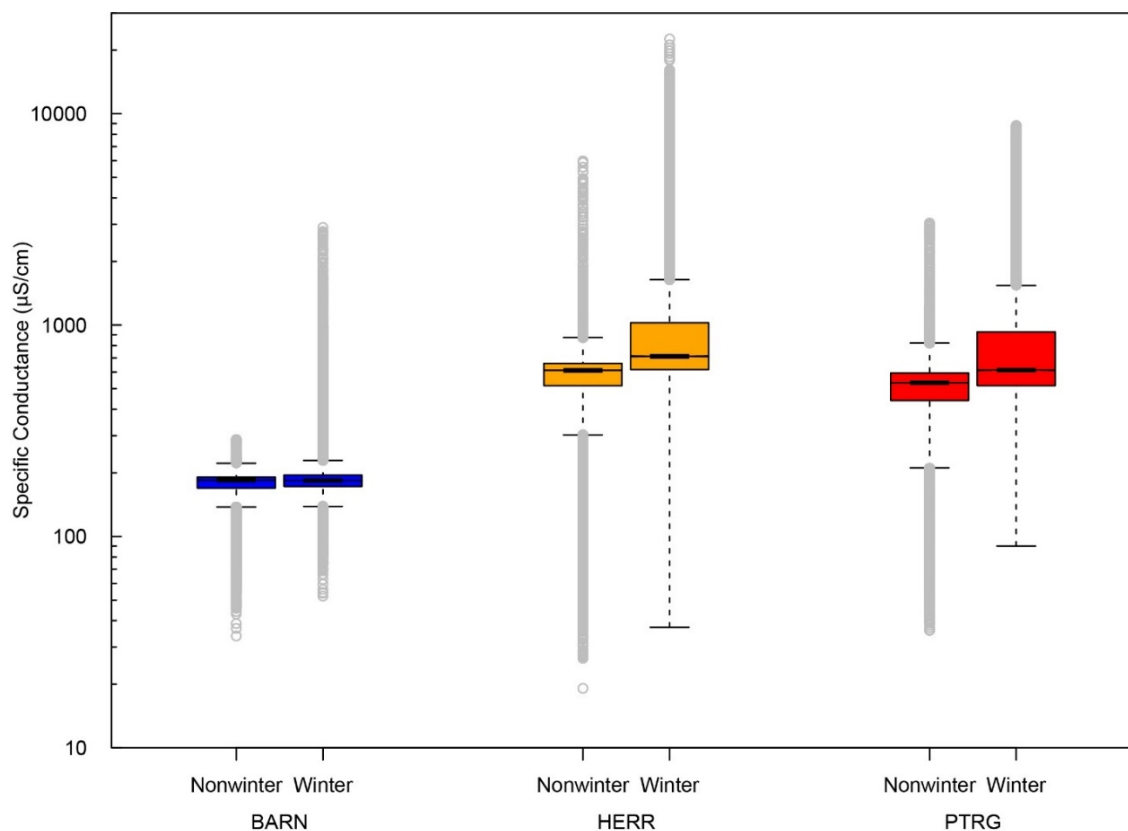


Figure 5: High-frequency specific conductance (SC) by season ($\mu\text{S}/\text{cm}$). Median SC was significantly higher at HERR and PTRG (urban) relative to BARN (mostly forested suburban) across seasons. Median SC during winter was significantly higher than nonwinter at the urban sites but not at BARN. SC measurements spanned >1 , >2 , and >3 orders of magnitude at BARN, PTRG, and HERR, respectively, with the highest values recorded during winter. SC measurements were collected from January 2019-January 2021 at BARN; measurements were recorded at 15-minute intervals before June 2020 and 5-minute intervals thereafter. SC measurements were collected at 5-minute intervals from January 2018-January 2021 at HERR and PTRG. Nonwinter was defined as Apr-Nov. Winter was defined as Dec-Mar, the period during which deicing salts are commonly applied.

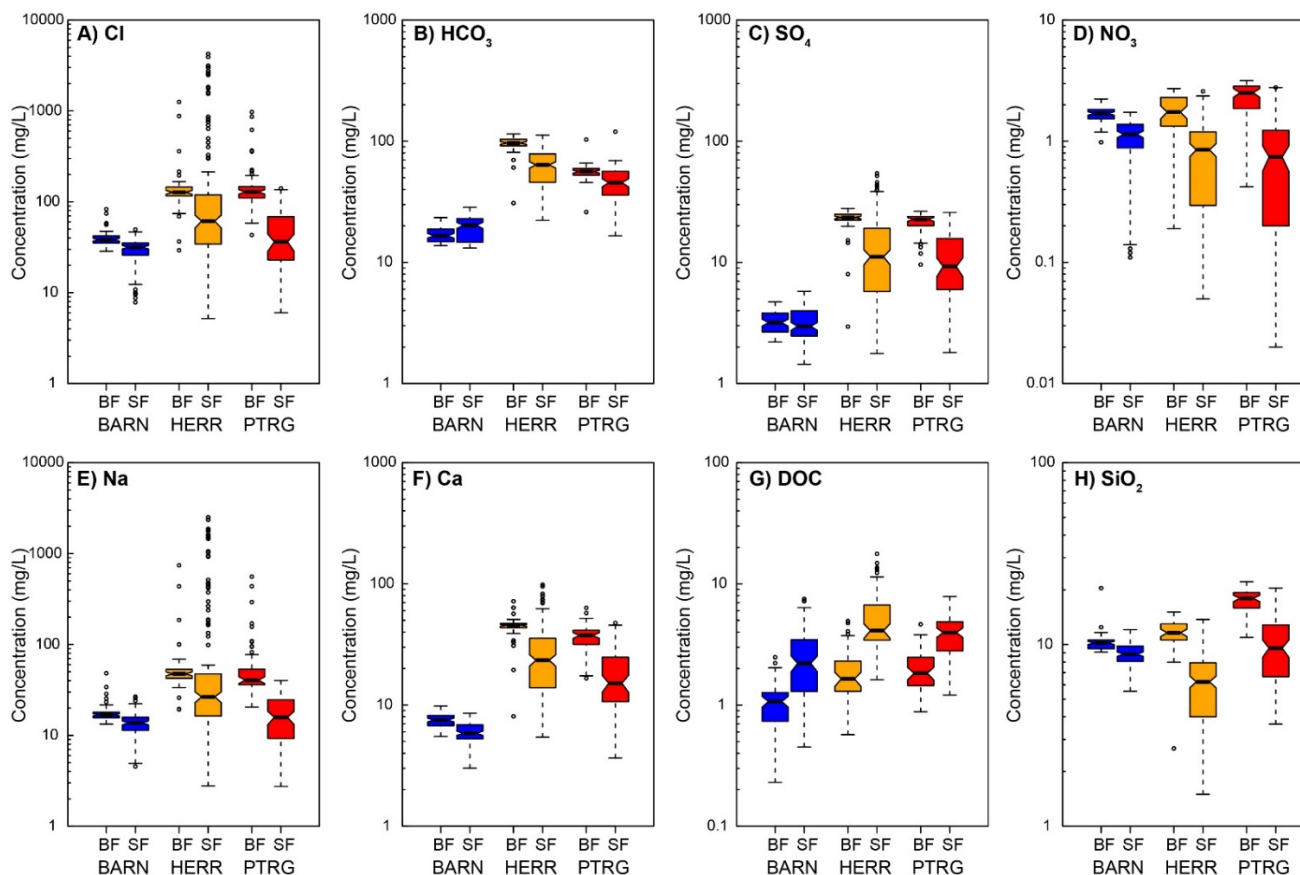


Figure 6: Concentrations (mg/L) of A) Cl^- , B) HCO_3^- , C) SO_4^{2-} , D) NO_3^- , E) Na^+ , F) Ca^{2+} , G) DOC, and H) SiO_2 of discrete samples collected during baseflow (BF) and stormflow (SF) at (blue) BARN, (orange) HERR, and (red) PTRG. Baseflow concentrations of most dissolved species were significantly higher at HERR and PTRG (urban) relative to BARN (mostly forested suburban). Concentrations of most major ions and SiO_2 decreased during stormflow; DOC increased during stormflow. At BARN, behavior of HCO_3^- (significant increase during stormflow) and SO_4^{2-} (no significant difference from baseflow) differed from the urban sites. K^+ , Mg^{2+} , and TDN are not shown; concentrations are reported in Tables 5 and 7.

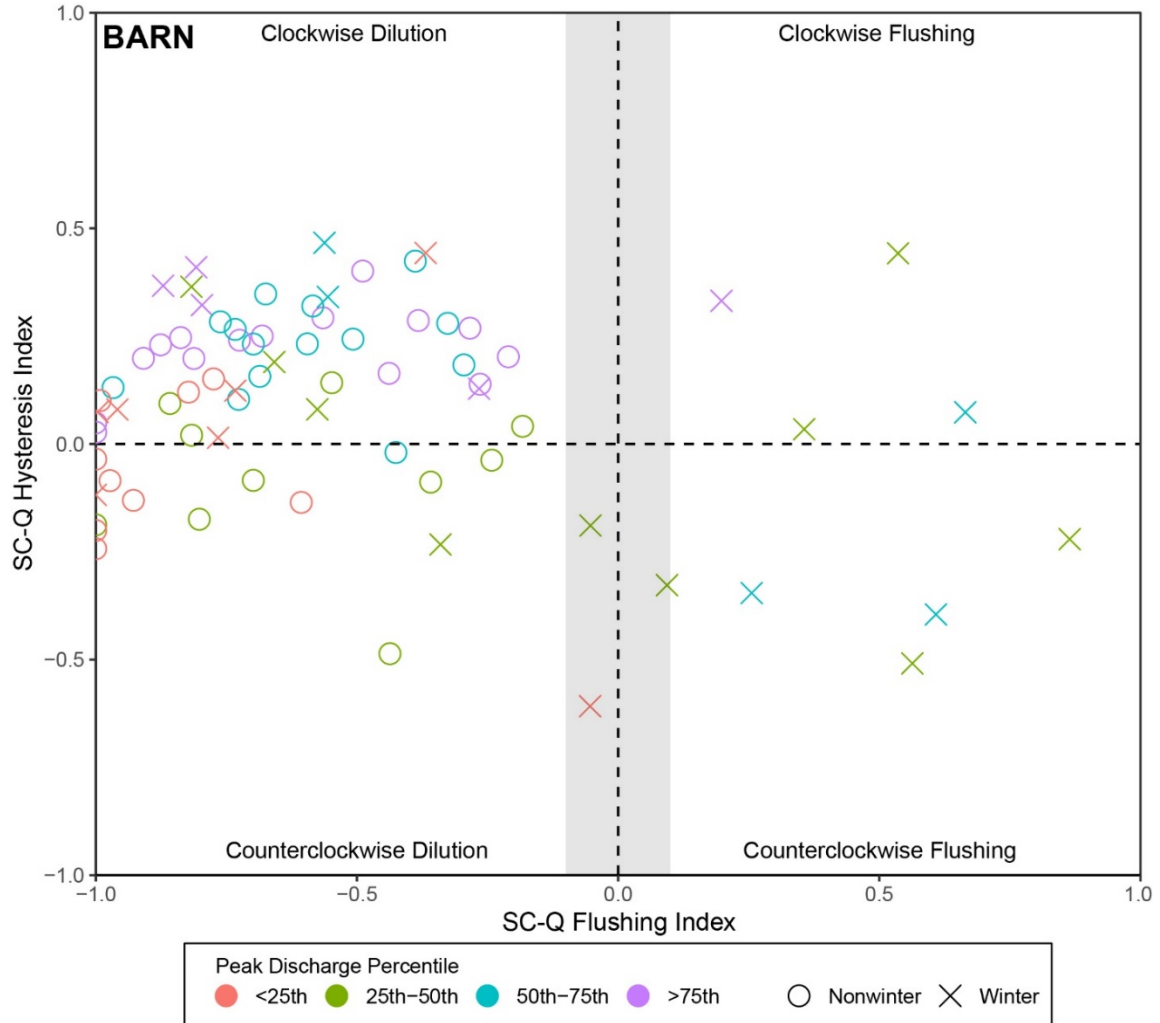


Figure 7: Hysteresis index (HI) versus flushing index (FI) of specific conductance-discharge (SC - Q) relationships at BARN. Color corresponds to the percentile of peak discharge for 75 storm events examined at BARN; values are reported in Table 9. Shape corresponds to season. Nonwinter was defined as Apr–Nov. Winter was defined as Dec–Mar, the period during which deicing salts are commonly applied. The shaded region ($-0.1 \leq FI \leq 0.1$) indicates chemostasis (little to no change in concentration on storm rising limb). Clockwise dilution was the dominant SC response during storm events at BARN. Chemostatic and flushing patterns occurred only during winter months.

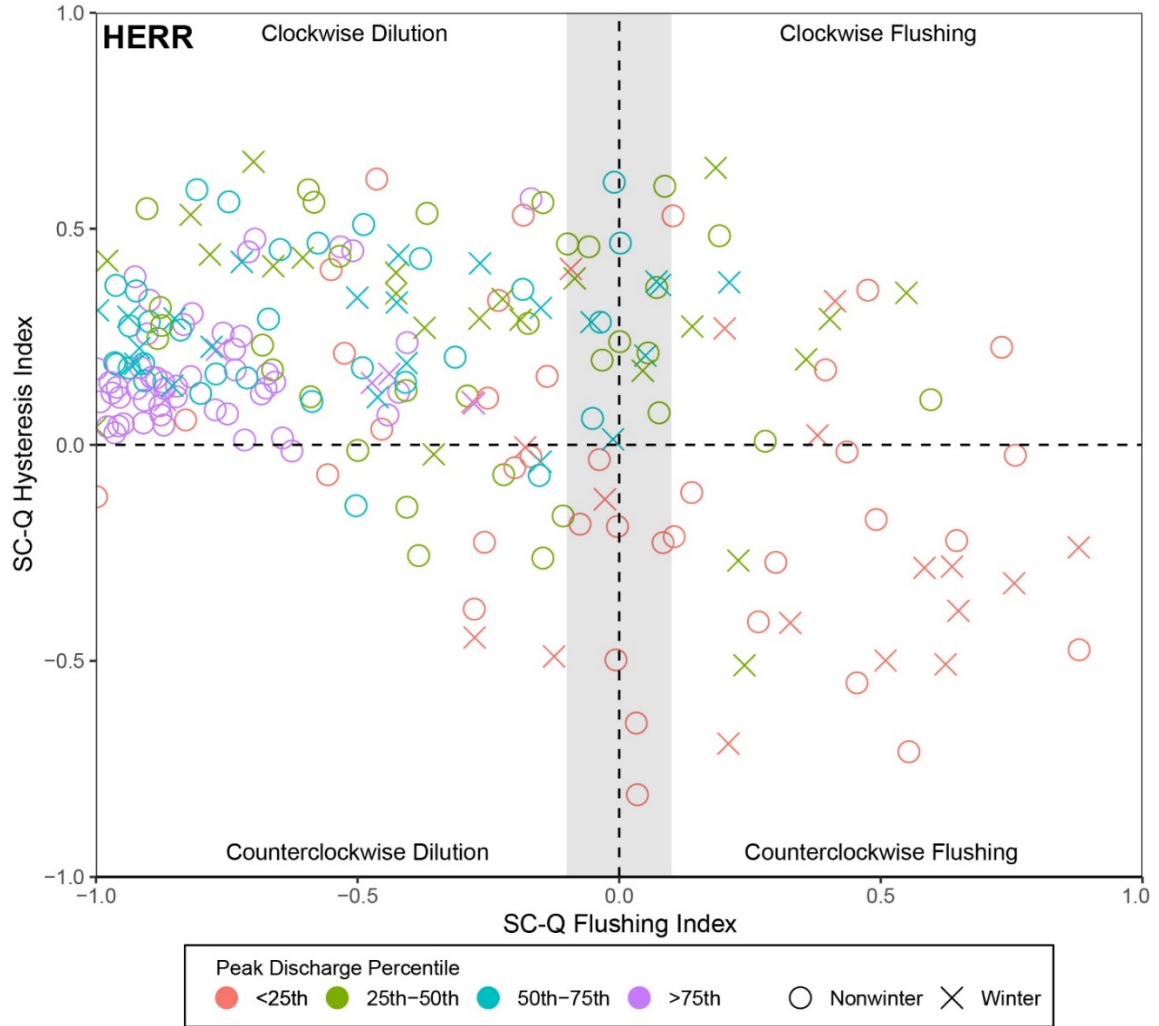


Figure 8: Hysteresis index (HI) versus flushing index (FI) of specific conductance-discharge (SC-Q) relationships at HERR. Color corresponds to the percentile of peak discharge for 219 storm events examined at HERR; values are reported in Table 9. Shape corresponds to season. Nonwinter was defined as Apr-Nov. Winter was defined as Dec-Mar, the period during which deicing salts are commonly applied. The shaded region ($-0.1 \leq FI \leq 0.1$) indicates chemostasis (little to no change in concentration on storm rising limb). Clockwise dilution was the dominant SC response at HERR, particularly during large storm events. Chemostatic and flushing patterns were generally associated with small storm events and showed no seasonal pattern.

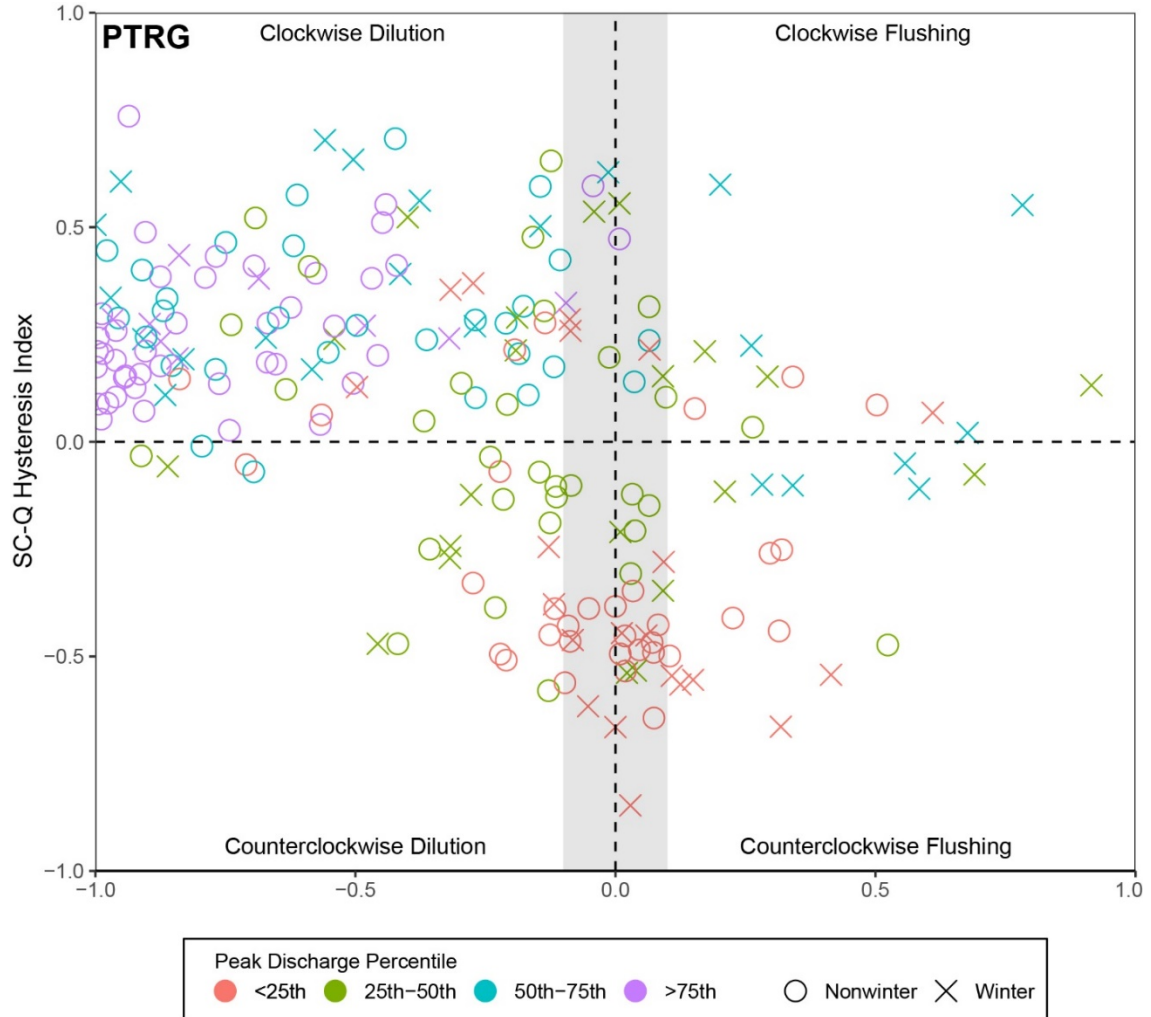


Figure 9: Hysteresis index (HI) versus flushing index (FI) of specific conductance-discharge (SC-Q) relationships at PTRG. Color corresponds to the percentile of peak discharge for 209 storm events examined at PTRG; values are reported in Table 9. Shape corresponds to season. Nonwinter was defined as Apr-Nov. Winter was defined as Dec-Mar, the period during which deicing salts are commonly applied. The shaded region ($-0.1 \leq FI \leq 0.1$) indicates chemostasis (little to no change in concentration on storm rising limb). Clockwise dilution was the dominant SC response at PTRG, particularly during large storm events. Chemostatic and flushing patterns were generally associated with small storm events and showed no seasonal pattern.

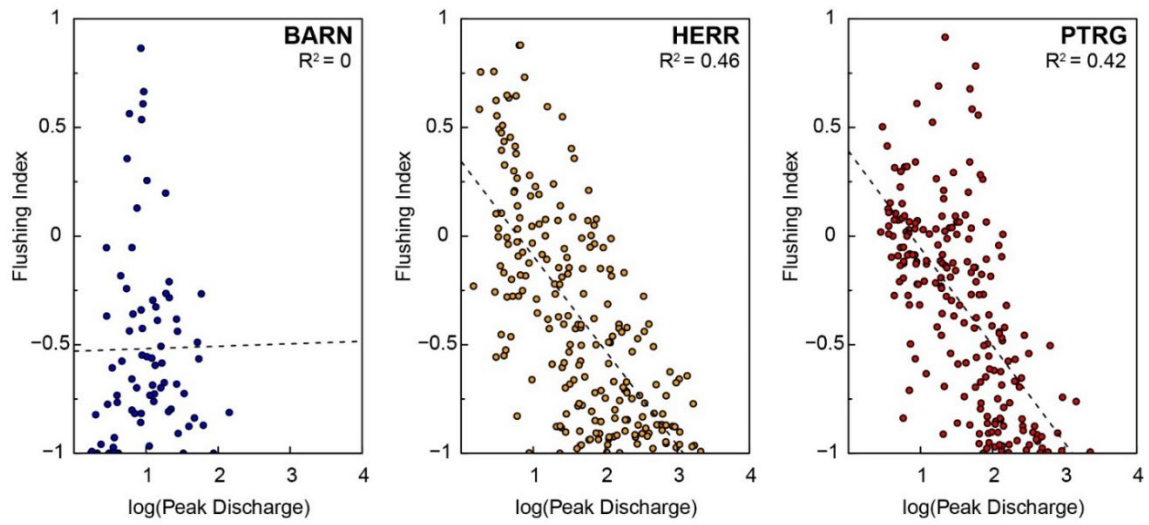


Figure 10: Storm event flushing index (FI) versus the logarithm of peak discharge for 75, 219, and 209 individual events at (blue) BARN, (orange) HERR, and (red) PTRG, respectively. FI was not correlated with peak discharge values at BARN but generally decreased with increasing peak discharge at HERR and PTRG.

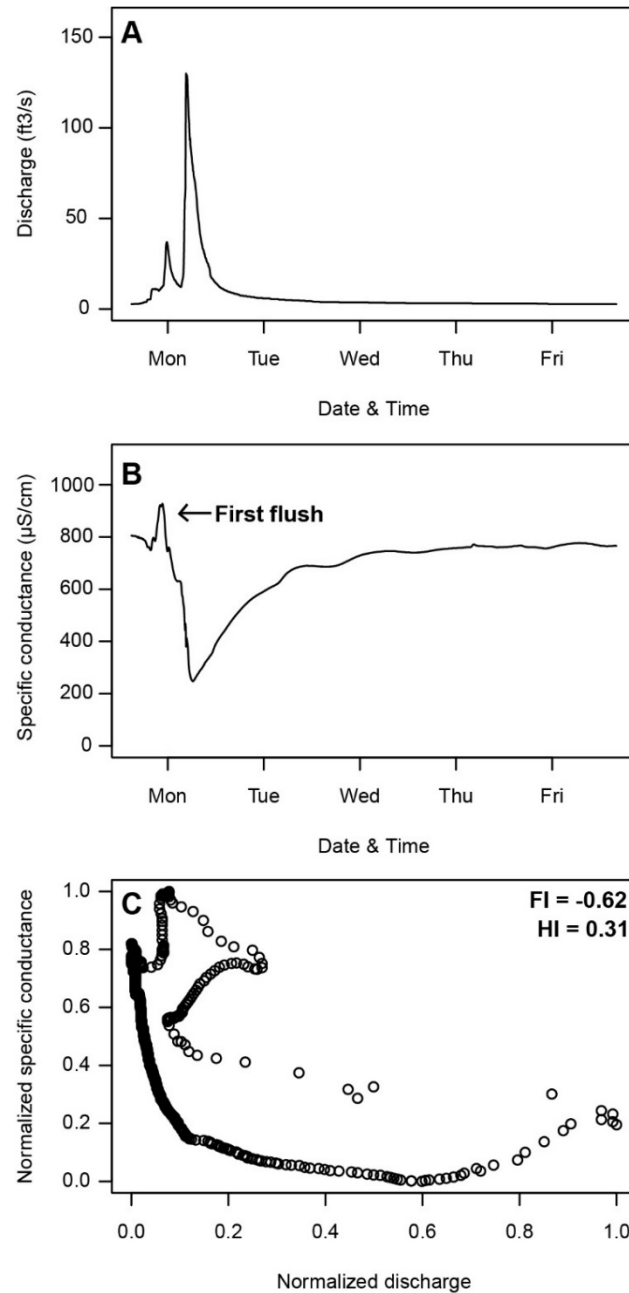


Figure 11: Example of the first flush effect during a moderately-sized storm event at PTRG. A) Hydrograph of storm event on Apr 15, 2018; B) 5-minute SC data shows initial decrease in SC at the storm onset, followed by a sharp increase in SC indicative of the flushing of solutes accumulated on impervious surfaces; SC sharply decreases once solutes are depleted; C) Normalized SC versus normalized discharge; start of the storm is at ~ 0.8 (normalized SC) and 0 (normalized Q), then proceeds in clockwise direction; FI (-0.62) reflects the difference between the initial SC value and the value at peak discharge and can, therefore, obscure the first flush effect.

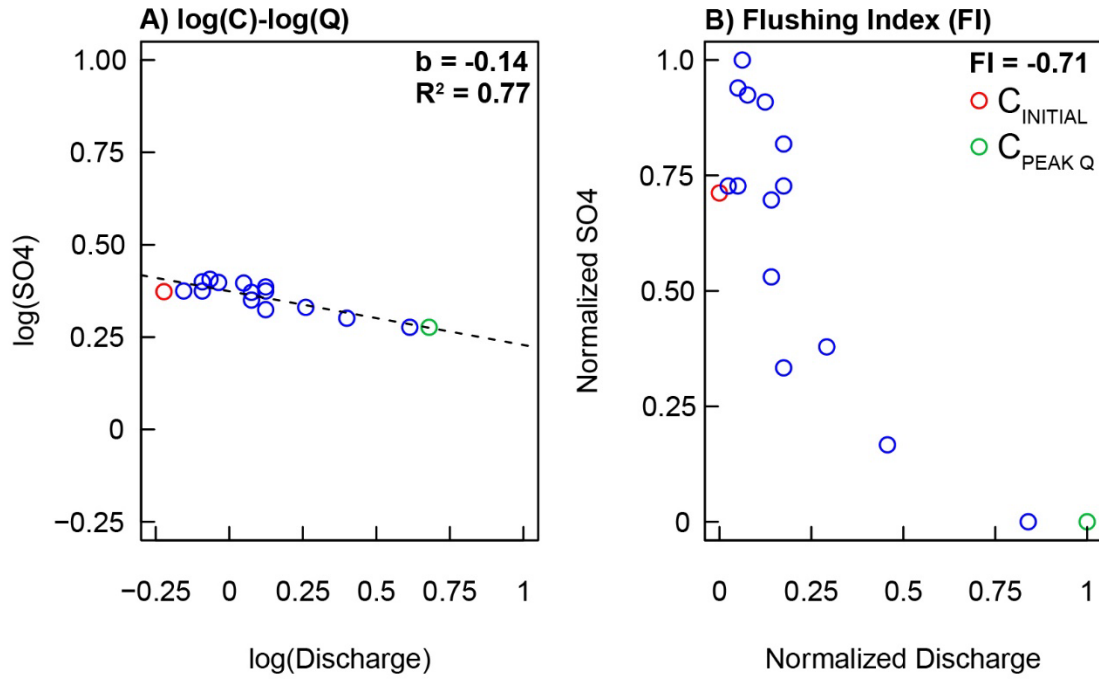


Figure 12: Comparison of C-Q behavior characterization for an example event at BARN using A) the C-Q slope (b) of the $\log(C)$ - $\log(Q)$ regression and B) the flushing index (FI). The initial concentration of SO_4 is shown in red; the concentration at peak discharge is shown in green. While b indicates chemostatic (weak dilution) for SO_4 , the FI yields a highly negative value (-0.71) that may be interpreted as substantial dilution on the rising limb. Given that concentrations SO_4 varied by $<0.5\text{mg/L}$ on the storm rising limb, b provided a better characterization of event-scale behavior.

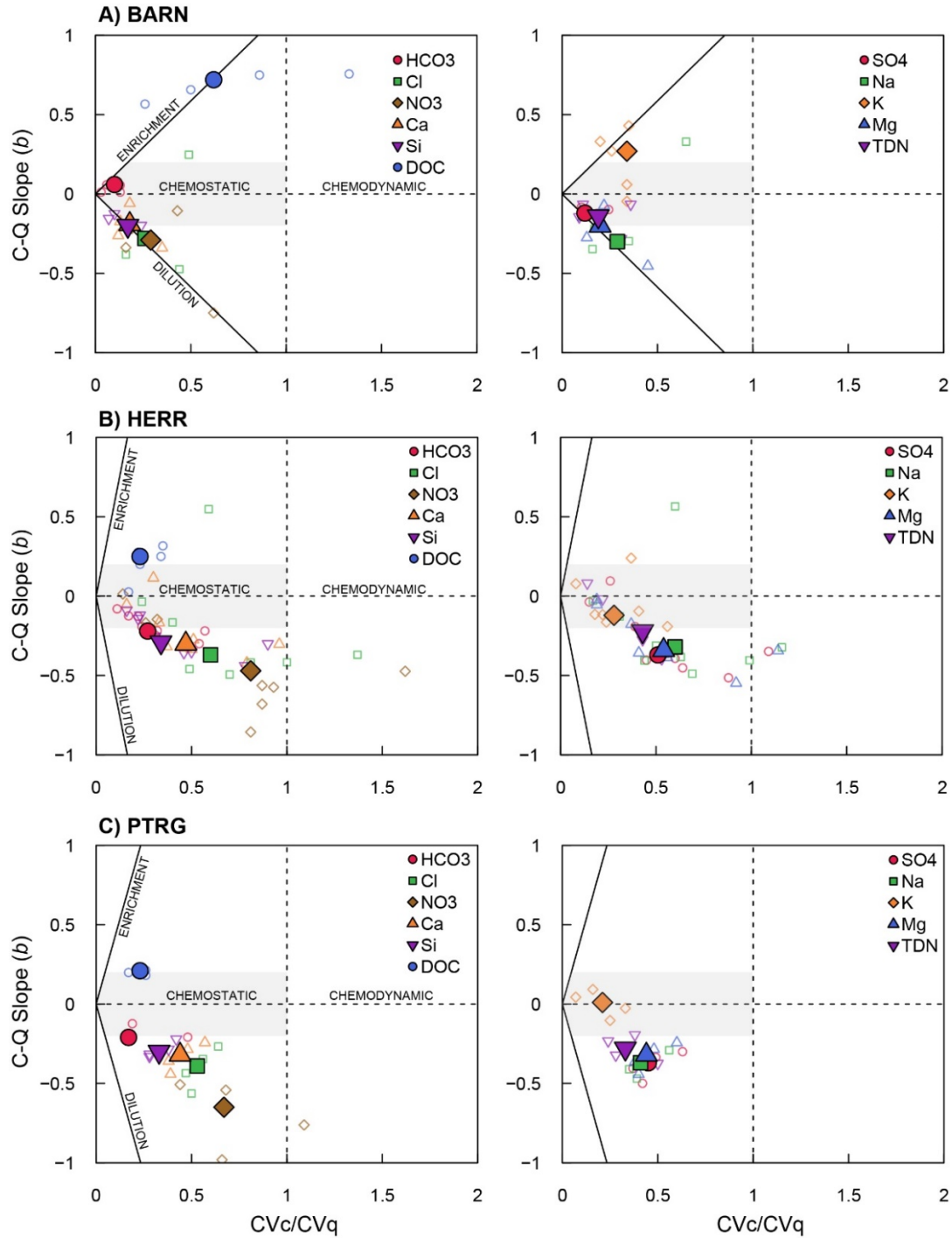


Figure 13: C-Q slope (b) versus CV_c/CV_Q of dissolved solutes for discretely sampled storm events at A) BARN, B) HERR, and C) PTRG. Open symbols represent individual discretely sampled storm events. Filled symbols reflect median storm event b and CV_c/CV_Q for each solute. Diagonal bounds reflect discharge variability at each site across the entire study period; $CV_Q = 1.17$ (BARN), 6.11 (HERR), and 4.29 (PTRG). Shaded area indicates range of chemostatic behavior ($-0.2 \leq b \leq 0.2$, $CV_c/CV_Q < 1$).

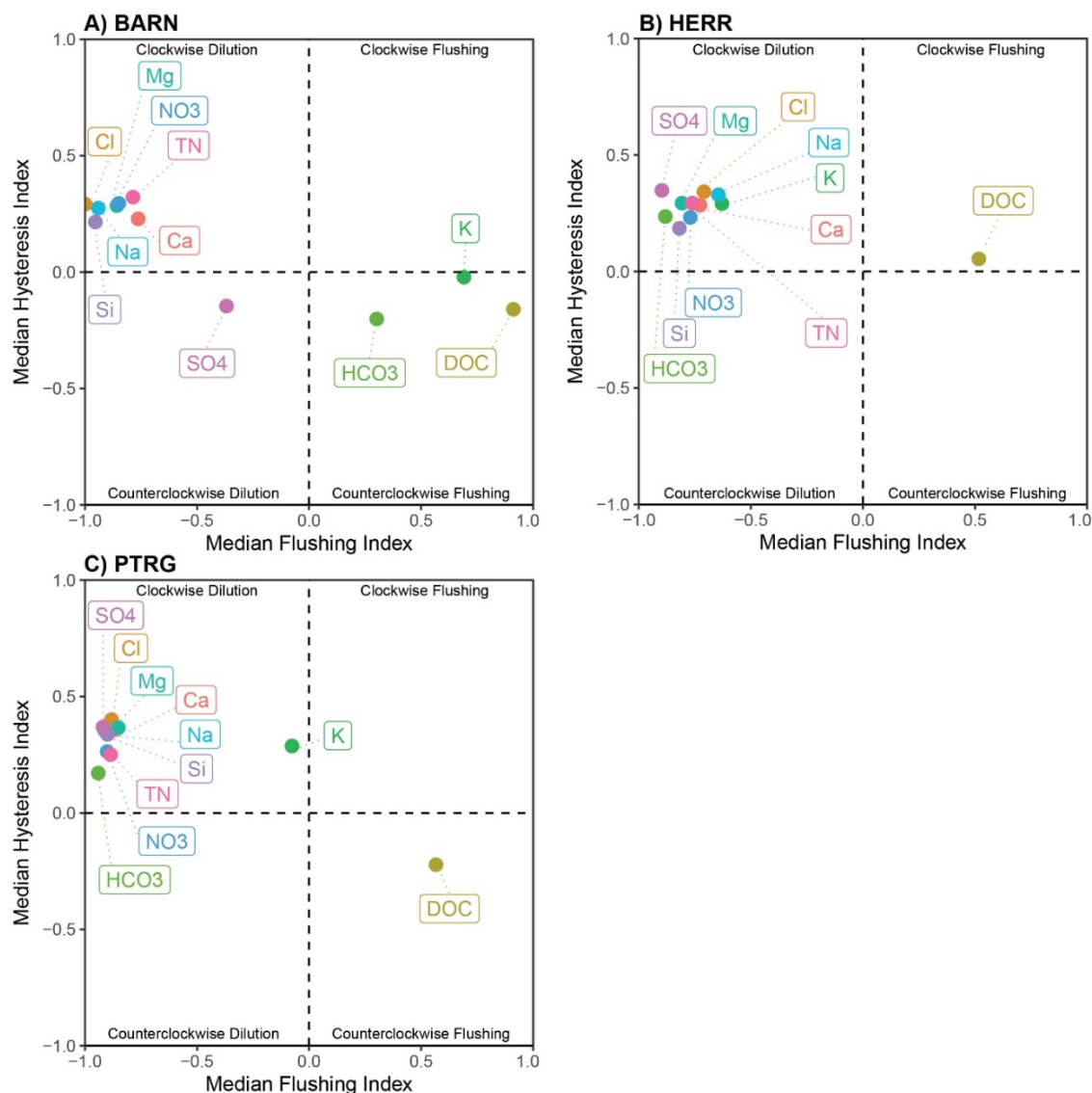


Figure 14: Median *HI* versus median *FI* of dissolved solutes for discretely sampled storm events at A) BARN, B) HERR, and C) PTRG. Biologically associated species (DOC, K) generally exhibited chemostatic or enrichment patterns. Geogenic and exogenous species generally exhibited clockwise dilution across all sites. SO_4 and HCO_3 exhibited distinctly different behavior at BARN. The *FIs* of most solutes show a greater degree of dilution than indicated with the C-Q slope (*b*).

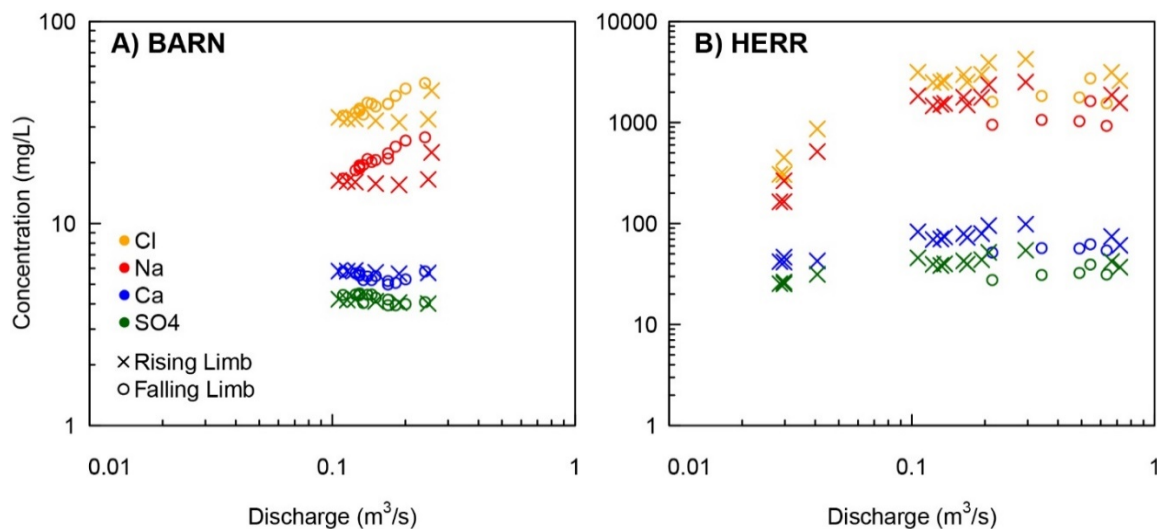


Figure 15: Concentration-discharge behavior of select geogenic and exogenous solutes during discretely sampled winter storm events at A) BARN and B) HERR. While dilution was the dominant behavior of most geogenic and exogenous species, (orange) chloride and (red) sodium exhibited enrichment patterns during winter storm events at both sites. At HERR, (blue) calcium and (green) sulfate also exhibited enrichment patterns. Enrichment patterns for these solutes were not observed during nonwinter months. Higher falling limb concentrations at BARN reflect longer transport times from developed headwaters; higher rising limb concentrations at HERR reflect rapid transport. Storm dates: 03/09/2019 at BARN; 01/23/2018 at HERR

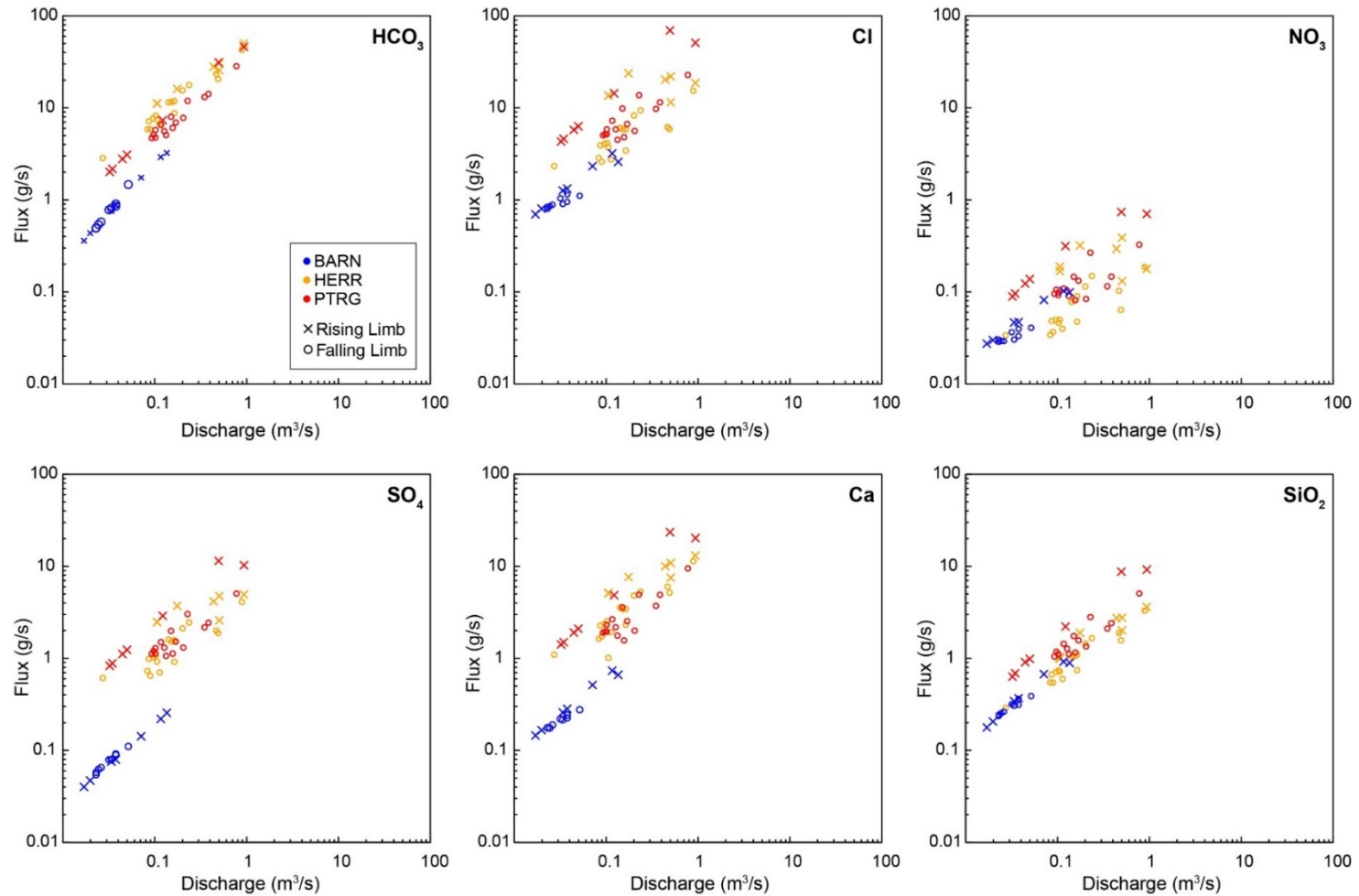


Figure 16: Fluxes (g/s) of select dissolved constituents for a discretely sampled storm event on 10-11-2020 at (blue) BARN, (orange) HERR, and (red) PTRG. Across all sites and solutes, flux increased with discharge regardless of event-scale C-Q behavior. Solute loads are generally higher at HERR and PTRG (urban) relative to BARN (mostly forested suburban).

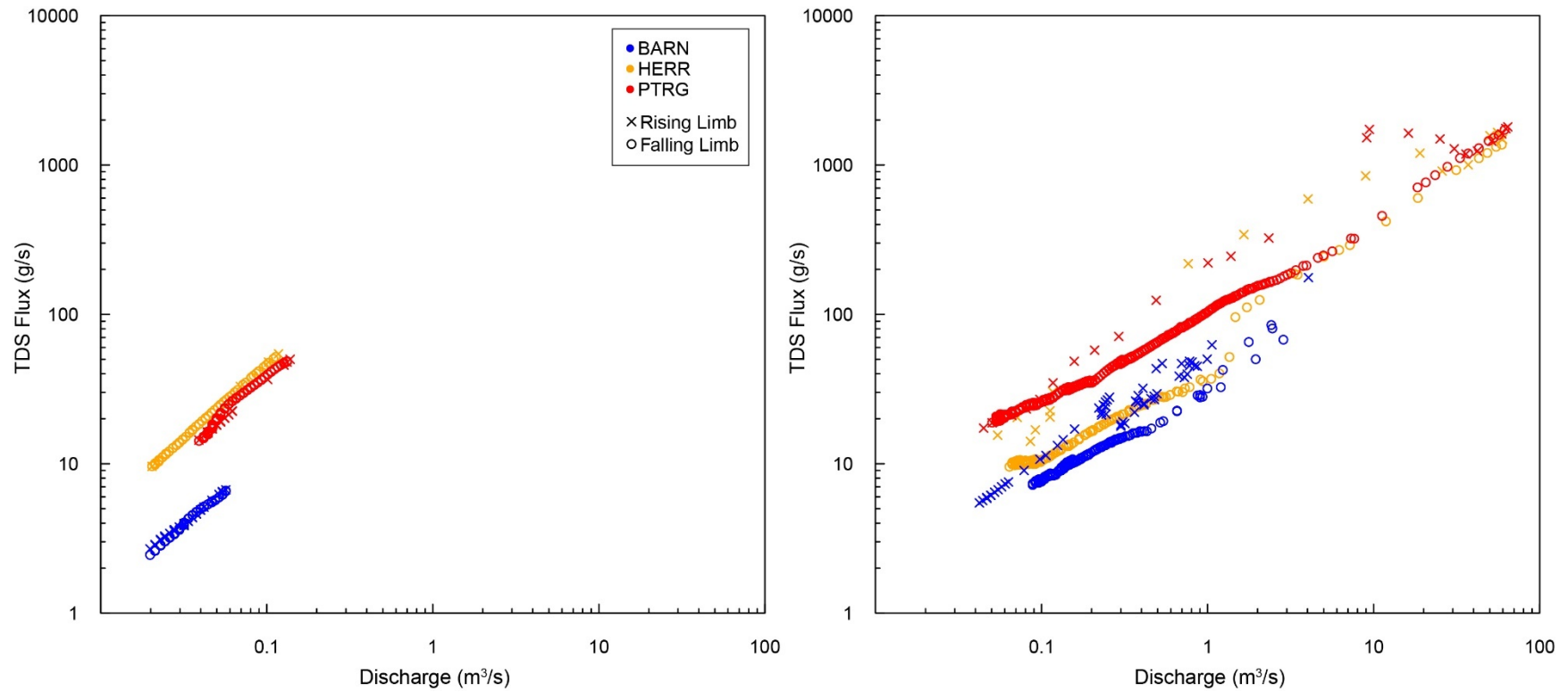


Figure 17: Total dissolved solids (TDS) flux for (left) the smallest storm events (peak $Q < 10$ th percentile) and (right) the largest storm events at (blue) BARN, (orange) HERR, and (red) PTRG. At all sites, solute fluxes appear to increase with discharge regardless of storm size. Peak discharge of largest storm event: 4.05 m³/s (BARN); 59.7 m³/s (HERR); 64.3 m³/s (PTRG)

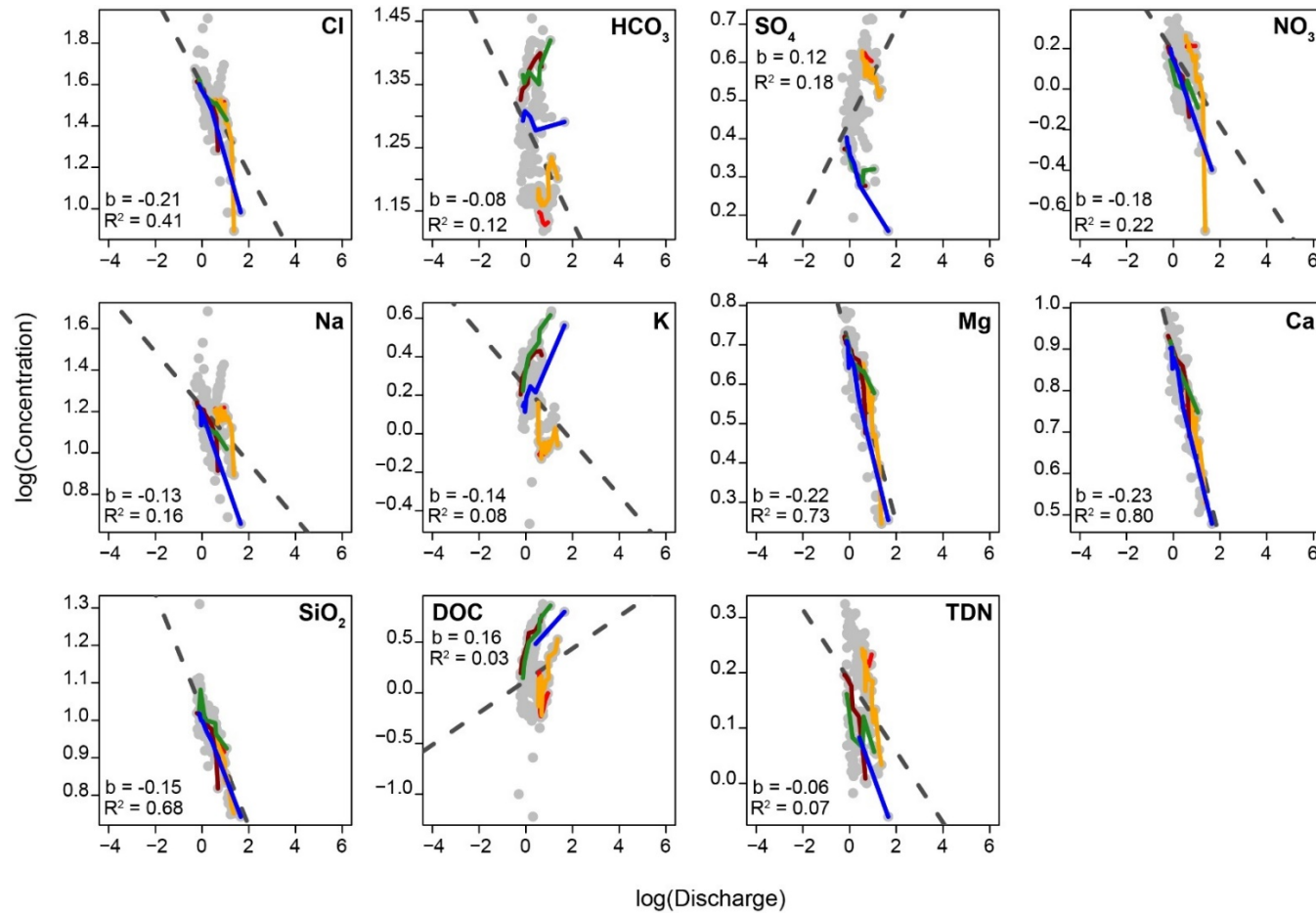


Figure 18: Long-term C-Q behavior of dissolved constituents at BARN (data points shown in gray; dashed line indicates the power-law fit) compared to the C-Q behavior of individual storm events (colored lines; indicate changes in concentration on the rising limb). Most solutes exhibit a dilution pattern on both long-term and event scales. Inter-event variability is more common for some solutes (e.g., HCO₃, SO₄, K) than for others (e.g., Mg, Ca, SiO₂).

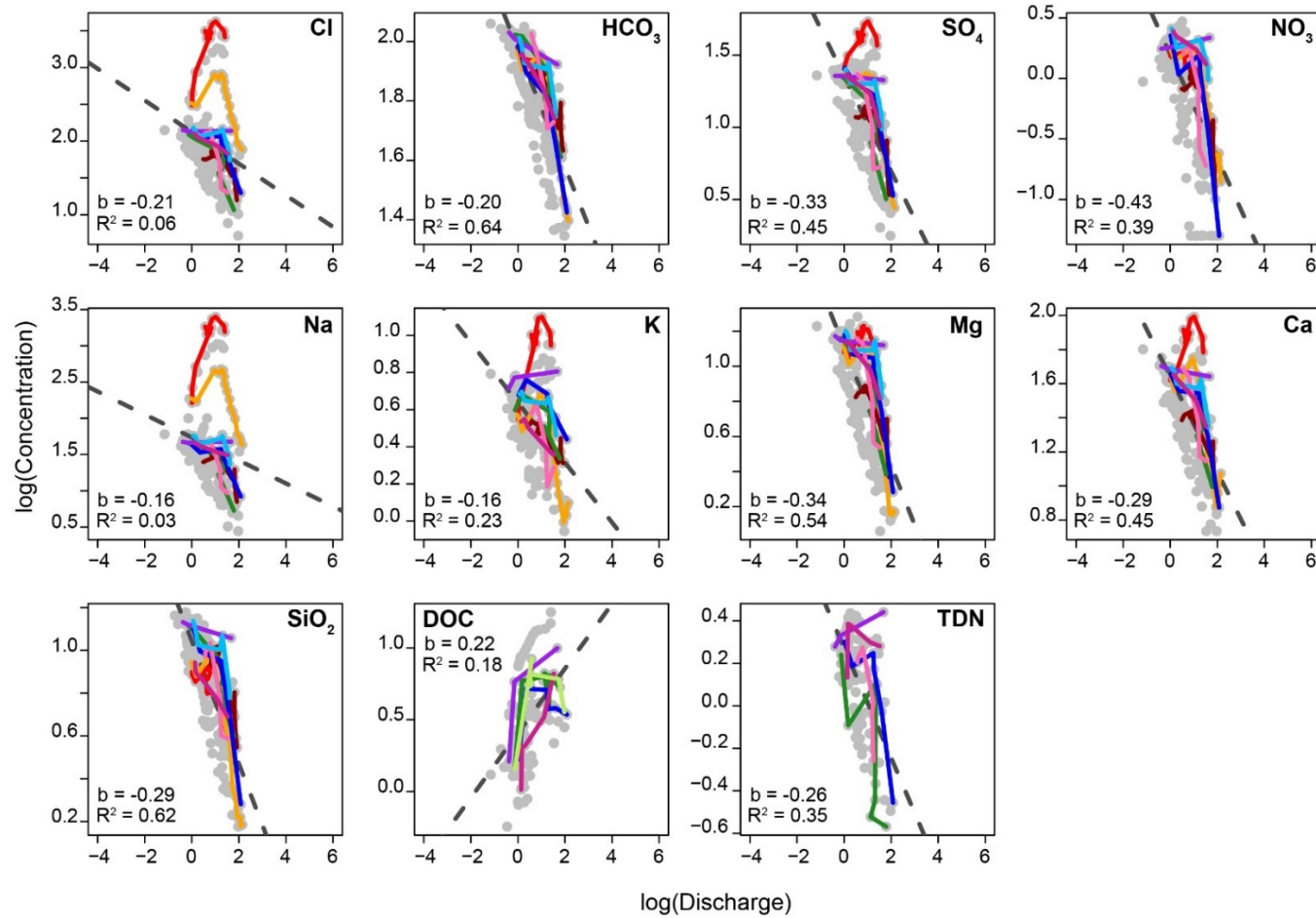


Figure 19: Long-term C-Q behavior of dissolved constituents at HERR (data points shown in gray; dashed line indicates the power-law fit) compared to the C-Q behavior of individual storm events (colored lines; indicate changes in concentration on the rising limb). Most solutes exhibit a dilution pattern on both long-term and event scales. Inter-event variability is more common for some solutes (e.g., Na, Cl, K) than for others (e.g., HCO₃, Mg, SiO₂).

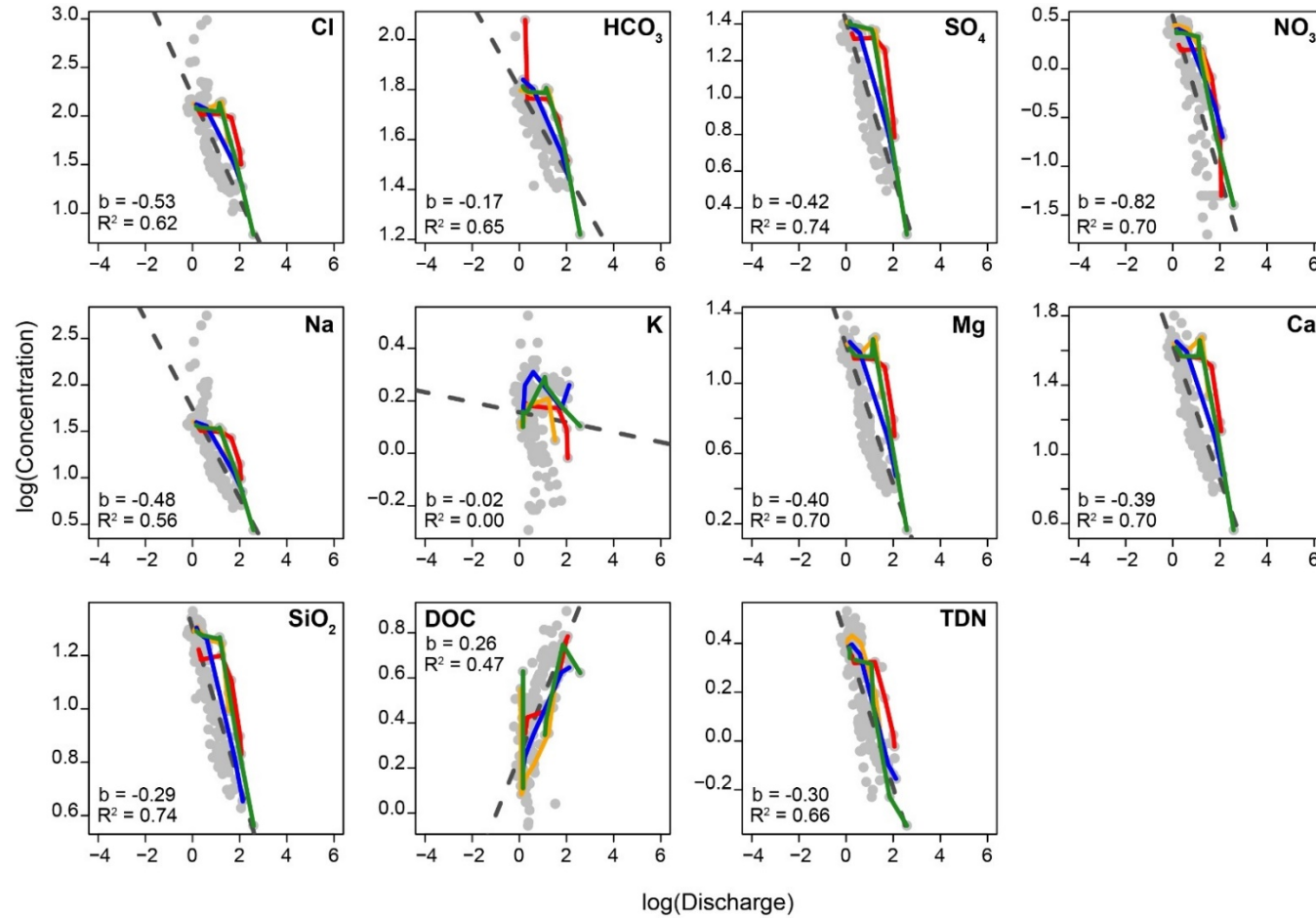


Figure 20: Long-term C-Q behavior of dissolved constituents at PTRG (data points shown in gray; dashed line indicates the power-law fit) compared to the C-Q behavior of individual storm events (colored lines; indicate changes in concentration on the rising limb). Most solutes exhibit a dilution pattern on both long-term and event scales. Long-term C-Q relationships were more well-defined at PTRG relative to BARN and HERR.

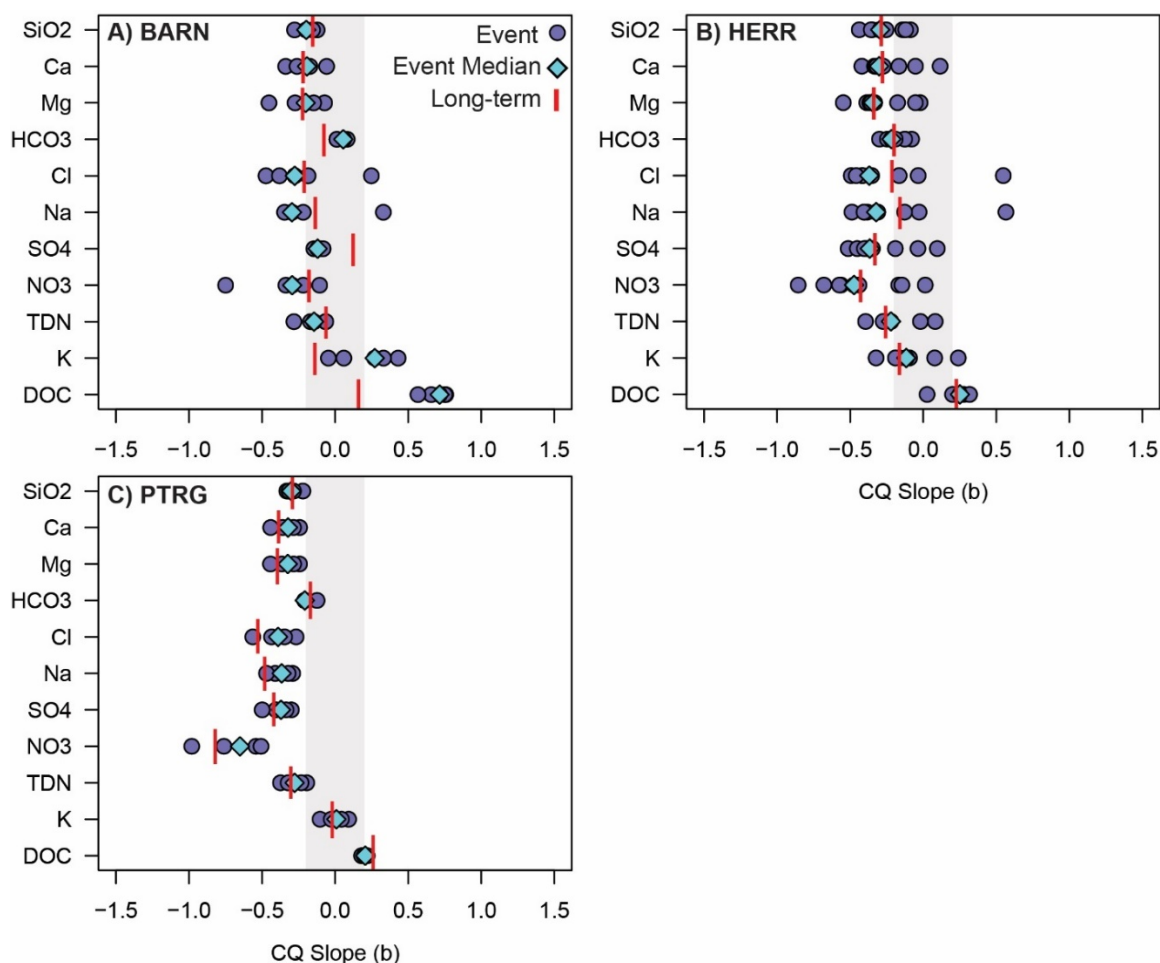


Figure 21: Comparison of event-scale and long-term (4-year) C-Q slopes (b) of dissolved constituents at A) BARN, B) HERR, and C) PTRG. Dark blue circles represent the C-Q slopes of individual discretely sampled storm events; light blue diamonds represent the median C-Q slope of individual events; red bars represent the long-term C-Q slope; shaded region represents chemostatic behavior ($-0.2 \leq b \leq 0.2$). If the red bar (long-term) overlaps the light blue diamond (event median), the long-term slope is a good approximation of event-scale behavior. Long-term slopes were a close approximation of event-scale behavior (± 0.2) for most solutes, particularly geogenic species.

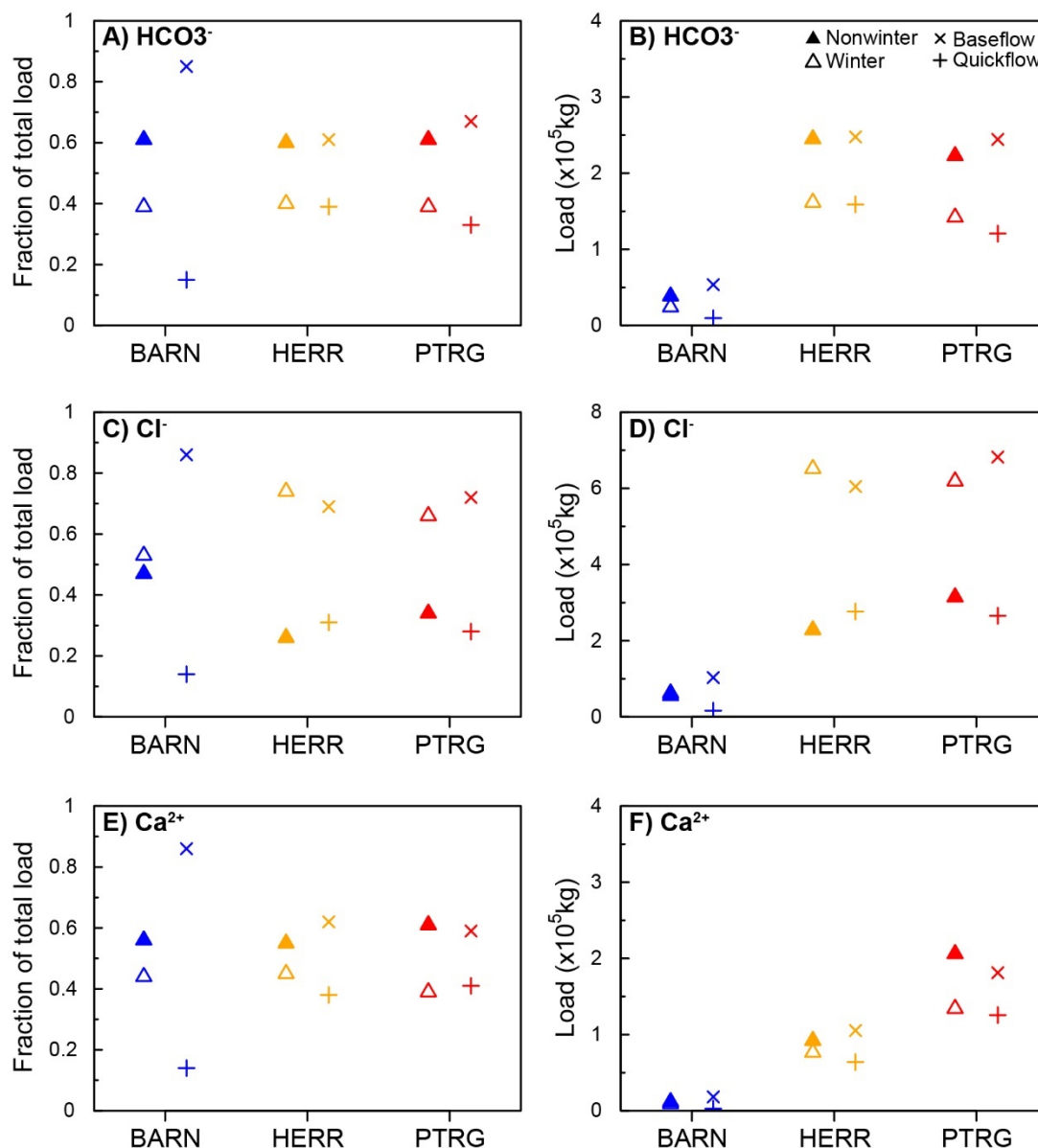


Figure 22: Results from hydrograph separation showing (left) fraction of total load and (right) total load ($\times 10^5 \text{ kg}$) attributed to nonwinter and winter periods, and baseflow and quickflow components as determined from baseflow separation. Load estimates were calculated using high-frequency concentration datasets generated from solute-specific regression models using discrete concentration measurements and either SC or discharge. Load estimates reflect the period from Jan. 2019 through Dec. 2020. Most of the solute export was attributed to baseflow across all sites. Loads of all solutes were substantially higher at HERR and PTRG (urban) relative to BARN (mostly forested suburban). Results for all solutes are reported in Table 16.

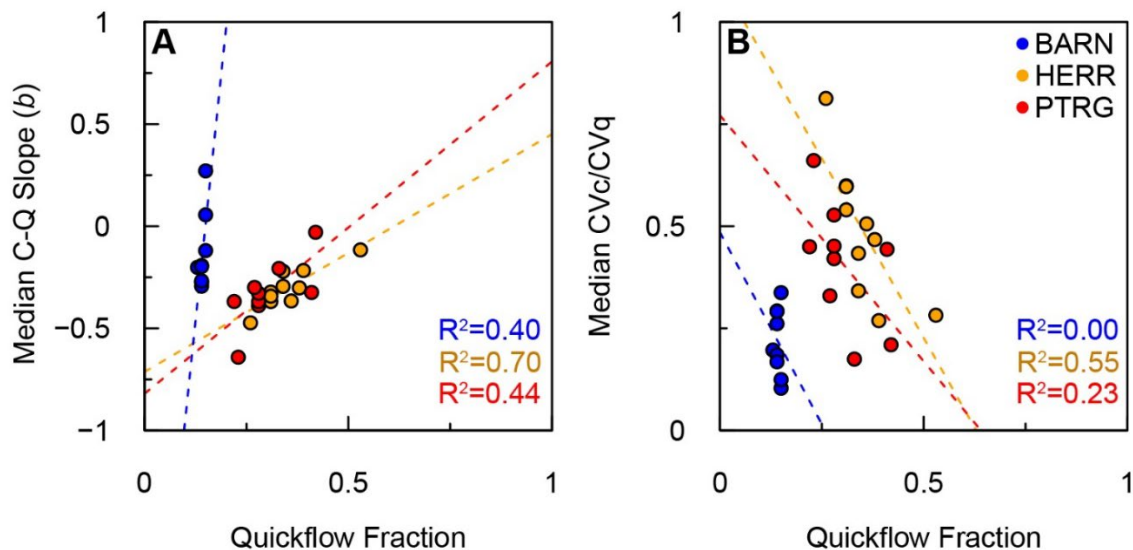


Figure 23: A) Median event-scale C-Q slope (b) versus the fraction of export attributed to quickflow for each solute at (blue) BARN, (orange) HERR, and (red) PTRG. Greater quickflow export is associated with higher C-Q slopes. B) Median event-scale CV_c/CV_q versus the fraction of solute export attributed to quickflow. Quickflow export increases with decreased solute variability at the urban sites, albeit with weak correlation statistics.

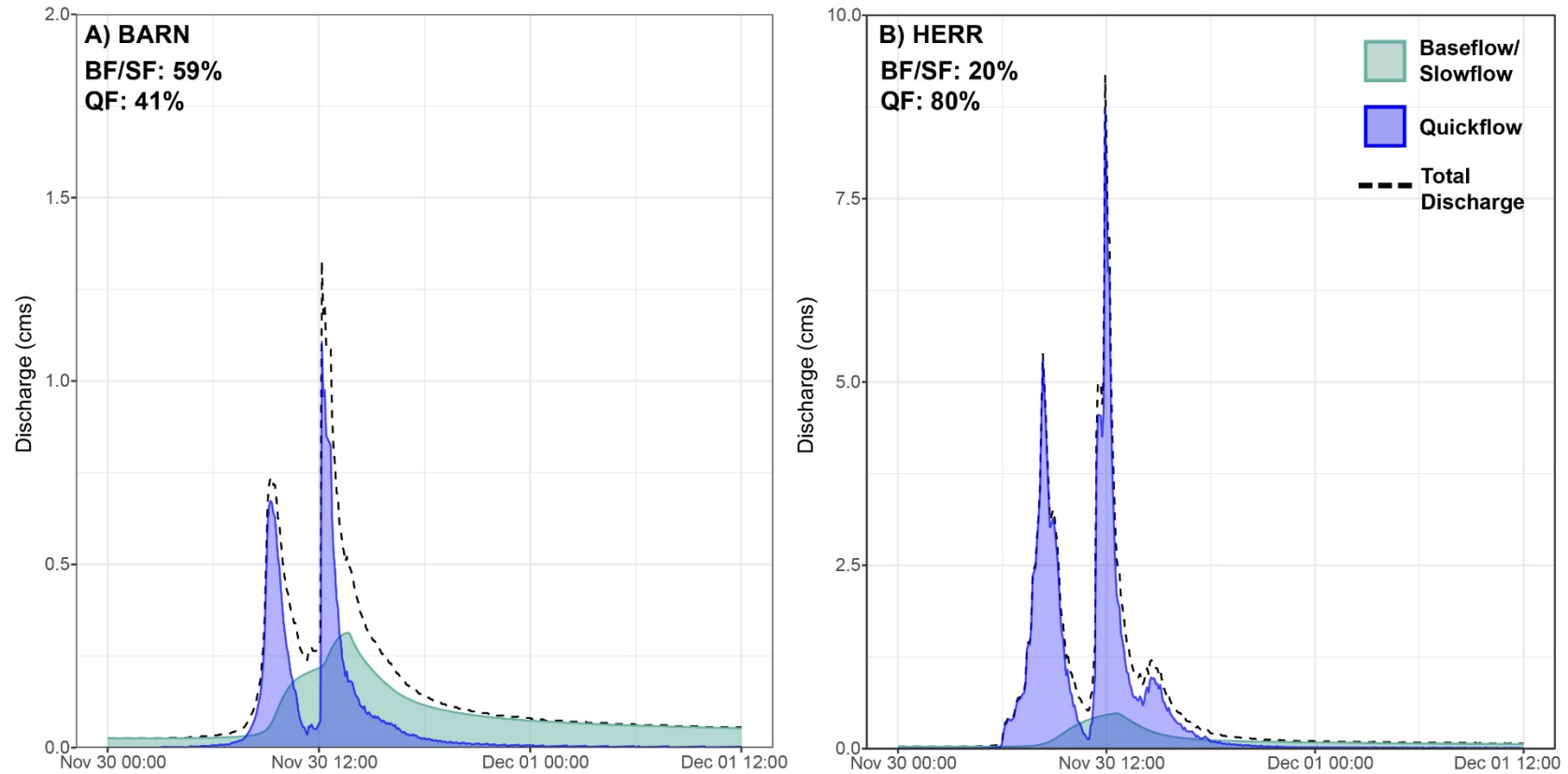


Figure 24: Discharge for an individual storm event in 2020 at A) BARN and B) HERR demonstrating baseflow separation results using the *EcoHydRology* package in R. A filter parameter of 0.925 with nine passes produced reasonable results (across entire study period). Note the y-axis limits for HERR are five times larger. For this event, stormflow contributions were ~59% from baseflow/slowflow (BF/SF) and ~41% from quickflow (QF) at BARN compared to 20% and 80%, respectively, at HERR.

7. References

- Aguilera, R., & Melack, J. M. (2018). Concentration-discharge responses to storm events in coastal California watersheds. *Water Resources Research*, 54(1), 407–424.
<https://doi.org/10.1002/2017WR021578>
- Arora, B., Burrus, M., Newcomer, M., Steefel, C. I., Carroll, R. W. H., Dwivedi, D., Dong, W., Williams, K. H., & Hubbard, S. S. (2020). Differential C-Q analysis: A new approach to inferring lateral transport and hydrologic transients within multiple reaches of a mountainous headwater catchment. *Frontiers in Water*, 2(24), 1–20.
<https://doi.org/10.3389/frwa.2020.00024>
- Bach, P. M., McCarthy, D. T., & Deletic, A. (2010). Redefining the stormwater first flush phenomenon. *Water Research*, 44, 2487–2498.
<https://doi.org/10.1016/j.watres.2010.01.022>
- Baker, E. B., & Showers, W. J. (2019). Hysteresis analysis of nitrate dynamics in the Neuse River, NC. *Science of the Total Environment*, 652, 889–899.
<https://doi.org/10.1016/j.scitotenv.2018.10.254>
- Balerna, J. A., Melone, J. C., & Knee, K. L. (2021). Using concentration–discharge relationships to identify influences on surface and subsurface water chemistry along a watershed urbanization gradient. *Water*, 13(5), 662.
- Barthold, F. K., Tyralla, C., Schneider, K., & Vache, K. B. (2011). How many tracers do we need for end member mixing analysis (EMMA)? A sensitivity analysis. *Water Resources Research*, 47, 1–14. <https://doi.org/10.1029/2011WR010604>

- Benettin, P., McGuire, K. J., Bailey, S. W., Botter, G., Rinaldo, A., & Likens, G. E. (2017). Young runoff fractions control streamwater age and solute concentration dynamics. *Hydrological Processes*, 1–5. <https://doi.org/10.1002/hyp.11243>
- Blaszcak, J. R., Bernhardt, E. S., Delesantro, J. M., Zhong, Y., & Urban, D. L. (2019). Watershed urban development controls on urban streamwater chemistry variability. *Biogeochemistry*, 144(1), 61–84. <https://doi.org/10.1007/s10533-019-00572-7>
- Booth, D B, & Jackson, C. R. (1997). Urbanization of aquatic systems: Degradation thresholds, stormwater detection, and the limits of mitigation. *Journal of the American Water Resources Association*, 33(5), 1077–1090.
- Booth, Derek B. (1991). Urbanization and the natural drainage system: Impacts, solutions, and prognoses. *The Northwest Environmental Journal*, 7(1), 93–118.
- Buttle, J. M. (1994). Isotope hydrograph separations and rapid delivery of pre-event water from drainage basins. *Progress in Physical Geography: Earth and Environment*, 18(1), 16–41. <https://doi.org/10.1177/030913339401800102>
- Butturini, A., Alvarez, M., Bernal, S., Vazquez, E., & Sabater, F. (2008). Diversity and temporal sequences of forms of DOC and NO₃- discharge responses in an intermittent stream: Predictable or random succession? *Journal of Geophysical Research: Biogeosciences*, 113(3), 1–10. <https://doi.org/10.1029/2008JG000721>
- Butturini, A., Gallart, F., Latron, J., Vazquez, E., & Sabater, F. (2006). Cross-site comparison of variability of DOC and nitrate C-Q hysteresis during the autumn-winter period in three Mediterranean headwater streams: A synthetic approach. *Biogeochemistry*, 77(3), 327–349. <https://doi.org/10.1007/s10533-005-0711-7>

- Carey, J. C., & Fulweiler, R. W. (2012). Human activities directly alter watershed dissolved silica fluxes. *Biogeochemistry*, 111(1), 125–138.
<https://doi.org/10.1007/s10533-011-9671-2>
- Chanat, J. G., Rice, K. C., & Hornberger, G. M. (2002). Consistency of patterns in concentration-discharge plots. *Water Resources Research*, 38(8), 1–10.
<https://doi.org/10.1029/2001WR000971>
- Chorover, J., Derry, L. A., & McDowell, W. H. (2017). Concentration-discharge relations in the critical zone: Implications for resolving critical zone structure, function, and evolution. *Water Resources Research*, 53, 8654–8659.
- Christophersen, N., & Hooper, R. P. (1992). Multivariate analysis of stream water chemical data: The use of principal components analysis for the end-member mixing problem. *Water Resources Research*, 28(1), 99–107.
<https://doi.org/10.1029/91WR02518>
- Corsi, S. R., De Cicco, L. A., Lutz, M. A., & Hirsch, R. M. (2015). River chloride trends in snow-affected urban watersheds: Increasing concentrations outpace urban growth rate and are common among all seasons. *Science of the Total Environment*, 508, 488–497. <https://doi.org/10.1016/j.scitotenv.2014.12.012>

- Creed, I. I. F., Mcknight, D. D. M., Pellerin, B. A., Green, M. B., Bergamaschi, B. A., Aiken, G. R., Burns, D. A., Findlay, S. E. G., Shanley, J. B., Striegl, R. G., Aulenbach, B. T., Clow, D. W., Laudon, H., Mcglynn, B. L., Mcguire, K. J., Smith, R. A., & Stackpoole, S. M. (2015). The river as a chemostat: Fresh perspectives on dissolved organic matter flowing down the river continuum. *Canadian Journal of Fisheries and Aquatic Sciences*, 14(April), 1–14.
<https://doi.org/10.1139/cjfas-2014-0400>
- Crowley, W. P., Reinhardt, J., & Cleaves, E. T. (1975). *Geologic Map of the Cockeysville Quadrangle, Maryland, 1:24,000; Maryland Geological Survey: Baltimore Maryland*.
- Diamond, J. S., & Cohen, M. J. (2018). Complex patterns of catchment solute–discharge relationships for coastal plain rivers. *Hydrological Processes*, 32, 388–401.
<https://doi.org/10.1002/hyp.11424>
- Driscoll, C. T., Driscoll, K. M., Fakhraei, H., & Civerolo, K. (2016). Long-term temporal trends and spatial patterns in the acid-base chemistry of lakes in the Adirondack region of New York in response to decreases in acidic deposition. *Atmospheric Environment*, 146, 5–14. <https://doi.org/10.1016/j.atmosenv.2016.08.034>
- Duncan, J. M., Welty, C., Kemper, J. T., Groffman, P. M., & Band, L. E. (2017). Dynamics of nitrate concentration-discharge patterns in an urban watershed. *Water Resources Research*, 53(8), 7349–7365. <https://doi.org/10.1002/2017WR020500>

- Dunne, T., & Black, R. D. (1970). An experimental investigation of runoff production in permeable soils. *Water Resources Research*, 6(2), 478–490.
<https://doi.org/10.1029/WR006i002p00478>
- Evans, C., & Davies, T. D. (1998). Causes of concentration-discharge hysteresis and its potential as a tool for analysis of episode hydrochemistry. *Water Resources Research*, 34(1), 129–137. <https://doi.org/10.1029/97WR01881>
- Farrick, K. K., & Branfireun, B. A. (2015). Flowpaths, source water contributions and water residence times in a Mexican tropical dry forest catchment. *Journal of Hydrology*, 529, 854–865. <https://doi.org/10.1016/j.jhydrol.2015.08.059>
- Finlay, J. C. (2003). Controls of streamwater dissolved inorganic carbon dynamics in a forested watershed. *Biogeochemistry*, 62, 231–252.
- Flint, K. R., Davis, A. P., & Asce, F. (2007). Pollutant mass flushing characterization of highway stormwater runoff from an ultra-urban area. *Journal of Environmental Engineering*, June, 616–627.
- Fork, M. L., Blaszcak, J. R., Delesantro, J. M., & Heffernan, J. B. (2018). Engineered headwaters can act as sources of dissolved organic matter and nitrogen to urban stream networks. *Limnology and Oceanography Letters*, 3, 215–224.
<https://doi.org/10.1002/lol2.10066>

- Fovet, O., Humbert, G., Dupas, R., Gascuel-odoux, C., Gruau, G., Jaffrezic, A., Thelusma, G., Fauchaux, M., Gilliet, N., Hamon, Y., & Grimaldi, C. (2018). Seasonal variability of stream water quality response to storm events captured using high-frequency and multi-parameter data. *Journal of Hydrology*, 559, 282–293. <https://doi.org/10.1016/j.jhydrol.2018.02.040>
- Fuka, D. R., Walter, M. T., Archibald, J. A., Steenhuis, T. S., & Easton, Z. M. (2018). Package “EcoHydRology.” <https://cran.r-project.org/web/packages/EcoHydRology/index.html>
- Godsey, S. E., Kirchner, J. W., & Clow, D. W. (2009). Concentration-discharge relationships reflect chemostatic characteristics of US catchments. *Hydrological Processes*, 23, 1844–1864. <https://doi.org/10.1002/hyp.7315>
- Goldyn, R., Szpakowska, B., Dariusz, Ś., Domek, P., Buxakowski, J., Dondajewska, R., Baralkiewicz, D., & Sajnóg, A. (2018). Influence of stormwater runoff on macroinvertebrates in a small urban river and a reservoir. *Science of the Total Environment*, 625, 743–751. <https://doi.org/10.1016/j.scitotenv.2017.12.324>
- Gwenzi, W., Chinyama, S. R., & Togarepi, S. (2017). Concentration-discharge patterns in a small urban headwater stream in a seasonally dry water-limited tropical environment. *Journal of Hydrology*, 550, 12–25. <https://doi.org/10.1016/j.jhydrol.2017.04.029>

- Hatt, B. E., Fletcher, T. D., Walsh, C. J., & Taylor, S. L. (2004). The influence of urban density and drainage infrastructure on the concentrations and loads of pollutants in small streams. *Environmental Management*, 34(1), 112–124.
<https://doi.org/10.1007/s00267-004-0221-8>
- Herlihy, A. T. (1993). The effects of acidic deposition on streams in the Appalachian Mountain and Piedmont region of the Mid-Atlantic United States. *Water Resources Research*, 29(8), 2687–2703. <https://doi.org/10.1029/93WR01072>
- Herndon, E. M., Dere, A. L., Sullivan, P. L., Norris, D., Reynolds, B., & Brantley, S. L. (2015). Landscape heterogeneity drives contrasting concentration–discharge relationships in shale headwater catchments. *Hydrology and Earth System Sciences*, 19, 3333–3347. <https://doi.org/10.5194/hess-19-3333-2015>
- Hershfield, D. M. (1971). The frequency of dry periods in Maryland. *Chesapeake Science*, 12(2), 72–84.
- Hoagland, B., Russo, T. A., Brantley, S. L., Gu, X., Hill, L., Kaye, J., & Forsythe, B. (2017). Hyporheic zone influences on concentration-discharge relationships in a headwater sandstone stream. *Water Resources Research*, 53, 4643–4667.
<https://doi.org/10.1002/2016WR019717>.
- Hornberger, G. M., Scanlon, T. M., & Raffensperger, J. P. (2001). Modelling transport of dissolved silica in a forested headwater catchment: The effect of hydrological and chemical time scales on hysteresis in the concentration-discharge relationship. *Hydrological Processes*, 15(10), 2029–2038. <https://doi.org/10.1002/hyp.254>

- Hunsaker, C. T., & Johnson, D. W. (2017). Concentration-discharge relationships in headwater streams of the Sierra Nevada, California. *Water Resources Research*, 53, 7869–7884. <https://doi.org/10.1002/2016WR019693>
- Inamdar, S., Dhillon, G., Singh, S., Dutta, S., Levia, D., Scott, D., Mitchell, M., Stan, J. Van, & Mchale, P. (2013). Temporal variation in end-member chemistry and its influence on runoff mixing patterns in a forested, Piedmont catchment. *Water Resources Research*, 49, 1828–1844. <https://doi.org/10.1002/wrcr.20158>
- Inserillo, E. A., Green, M. B., Shanley, J. B., & Boyer, J. N. (2017). Comparing catchment hydrologic response to a regional storm using specific conductivity sensors. *Hydrological Processes*, 31, 1074–1085. <https://doi.org/10.1002/hyp.11091>
- Kaushal, S. S., Groffman, P. M., Likens, G. E., Belt, K. T., Stack, W. P., Kelly, V. R., Band, L. E., & Fisher, G. T. (2005). Increased salinization of fresh water in the northeastern United States. *Proceedings of the National Academy of Sciences*, 102(38), 13517–13520. <https://doi.org/10.1073/pnas.0506414102>
- Kaushal, Sujay S., Duan, S., Doody, T. R., Haq, S., Smith, R. M., Newcomer Johnson, T. A., Newcomb, K. D., Gorman, J., Bowman, N., Mayer, P. M., Wood, K. L., Belt, K. T., & Stack, W. P. (2017). Human-accelerated weathering increases salinization, major ions, and alkalinization in fresh water across land use. *Applied Geochemistry*, 83, 121–135. <https://doi.org/10.1016/j.apgeochem.2017.02.006>

- Kaushal, Sujay S., Groffman, P. M., Band, L. E., Elliott, E. M., Shields, C. A., & Kendall, C. (2011). Tracking nonpoint source nitrogen pollution in human-impacted watersheds. *Environmental Science and Technology*, 45(19), 8225–8232. <https://doi.org/10.1021/es200779e>
- Knapp, J. L. A., Freyberg, J. Von, Studer, B., Kiewiet, L., & Kirchner, J. W. (2020). Concentration–discharge relationships vary among hydrological events, reflecting differences in event characteristics. *Hydrology and Earth System Sciences*, 24, 2561–2576.
- Koenig, L. E., Shattuck, M. D., Snyder, L. E., Potter, J. D., & McDowell, W. H. (2017). Deconstructing the effects of flow on DOC, nitrate, and major ion interactions using a high-frequency aquatic sensor network. *Water Resources Research*, 53(10), 655–673. <https://doi.org/10.1002/2017WR020739>
- Ladson, T., Brown, R., Neal, B., & Nathan, R. (2013). A standard approach to baseflow separation using the Lyne and Hollick filter. *Australian Journal of Water Resources*, 17(1), 25–34. <https://doi.org/10.7158/W12-028.2013.17.1>
- Lakoba, V., Wind, L., DeVilbiss, S., Lofton, M., Bretz, K., Weinheimer, A., Moore, C., Baciocco, C., Hotchkiss, E., & Hession, W. C. (2021). Salt dilution and flushing dynamics of an impaired agricultural–urban stream. *ACS ES&T Water*, 1(2), 407–416. <https://doi.org/10.1021/acsestwater.0c00160>

- Lawler, D. M., Petts, G. E., Foster, I. D. L., & Harper, S. (2006). Turbidity dynamics during spring storm events in an urban headwater river system: The Upper Tame, West Midlands, UK. *Science of the Total Environment*, 360(1–3), 109–126.
<https://doi.org/10.1016/j.scitotenv.2005.08.032>
- Lee, J. H., Bang, K. W., Ketchum, L. H., Choe, J. S., & Yu, M. J. (2002). First flush analysis of urban storm runoff. *The Science of the Total Environment*, 293, 163–175.
- Lin, H. (2010). Earth's critical zone and hydrogeology: Concepts, characteristics, and advances. *Hydrology and Earth System Sciences*, 14, 25–45.
- Liu, F., Conklin, M. H., & Shaw, G. D. (2017). Insights into hydrologic and hydrochemical processes based on concentration-discharge and end-member mixing analyses in the mid-Merced River Basin, Sierra Nevada, California. *Water Resources Research*, 53, 832–850.
<https://doi.org/10.1002/2016WR019437>. Received
- Lloyd, C. E. M., Freer, J. E., Johnes, P. J., & Collins, A. L. (2015). Using hysteresis analysis of high-resolution water quality monitoring data, including uncertainty, to infer controls on nutrient and sediment transfer in catchments. *Science of the Total Environment*, 543, 388–404. <https://doi.org/10.1016/j.scitotenv.2015.11.028>
- Lloyd, C. E. M., Freer, J. E., Johnes, P. J., & Collins, A. L. (2016). Technical note: Testing an improved index for analysing storm discharge-concentration hysteresis. *Hydrology and Earth System Sciences*, 20(2), 625–632. <https://doi.org/10.5194/hess-20-625-2016>

- Long, D. T., Voice, T. C., Chen, A., Xing, F., & Li, S.-G. (2015). Temporal and spatial patterns of Cl⁻ and Na⁺ concentrations and Cl/Na ratios in salted urban watersheds. *Elementa: Science of the Anthropocene*, 3, 000049. <https://doi.org/10.12952/journal.elementa.000049>
- Long, D. T., Voice, T. C., Xagaroraki, I., Chen, A., Wu, H., Lee, E., Oun, A., & Xing, F. (2017). Patterns of C-Q hysteresis loops and within an integrative pollutograph for selected inorganic and organic solutes and E. coli in an urban salted watershed during winter-early spring periods. *Applied Geochemistry*, 83, 93–107. <https://doi.org/10.1016/j.apgeochem.2017.03.002>
- Masoner, J. R., Kolpin, D. W., Cozzarelli, I. M., Barber, L. B., Burden, D. S., Foreman, W. T., Forshay, K. J., Furlong, E. T., Groves, J. F., Hladik, M. L., Hopton, M. E., Jaeschke, J. B., Keefe, S. H., Krabbenhoft, D. P., Lowrance, R., Romanok, K. M., Rus, D. L., Selbig, W. R., Williams, B. H., & Bradley, P. M. (2019). Urban stormwater: An overlooked pathway of extensive mixed contaminants to surface and groundwaters in the United States. *Environmental Science and Technology*, 53(17), 10070–10081. <https://doi.org/10.1021/acs.est.9b02867>
- McGrane, S. J. (2016). Impacts of urbanisation on hydrological and water quality dynamics, and urban water management: A review. *Hydrological Sciences Journal*, 61(13), 2295–2311. <https://doi.org/10.1080/02626667.2015.1128084>
- McMahon, P., Beauchamp, V. B., Casey, R. E., Salice, C. J., Bucher, K., Marsh, M., & Moore, J. (2021). Effects of stream restoration by legacy sediment removal and floodplain reconnection on water quality. *Environmental Research Letters*, 16.

- Miller, A., Dere, A., & Coleman, T. (2021). High-frequency data reveal differential dissolved and suspended solids behavior from a mixed restored prairie and agricultural catchment. *Science of the Total Environment*, 753. <https://doi.org/10.1016/j.scitotenv.2020.141731>
- Miller, J. D., & Hess, T. (2017). Urbanisation impacts on storm runoff along a rural-urban gradient. *Journal of Hydrology*, 552, 474–489. <https://doi.org/10.1016/j.jhydrol.2017.06.025>
- Minor, J., Pearl, J. K., Barnes, M. L., Colella, T. R., Murphy, P. C., Mann, S., & Barron-Gafford, G. A. (2020). Critical zone science in the Anthropocene: Opportunities for biogeographic and ecological theory and praxis to drive earth science integration. *Progress in Physical Geography*, 44(1), 50–69. <https://doi.org/10.1177/0309133319864268>
- Moatar, F., Abbott, B. W., Minaudo, C., Curie, F., & Pinay, G. (2017). Elemental properties, hydrology, and biology interact to shape concentration-discharge curves for carbon, nutrients, sediment, and major ions. *Water Resources Research*, 53, 1270–1287. <https://doi.org/10.1002/2016WR019635>.Received
- Moore, J., Bird, D. L., Dobbis, S. K., & Woodward, G. (2017). Nonpoint source contributions drive elevated major ion and dissolved inorganic carbon concentrations in urban watersheds. *Environmental Science & Technology Letters*, 4(6), 198–204. <https://doi.org/10.1021/acs.estlett.7b00096>

- Moore, J., Fanelli, R. M., & Sekellick, A. J. (2020). High-frequency data reveal deicing salts drive elevated specific conductance and chloride along with pervasive and frequent exceedances of the U.S. Environmental Protection Agency aquatic life criteria for chloride in urban streams. *Environmental Science and Technology*, 54(2), 778–789. <https://doi.org/10.1021/acs.est.9b04316>
- Murphy, J. C., Hornberger, G. M., & Liddle, R. G. (2012). Concentration–discharge relationships in the coal mined region of the New River basin and Indian Fork sub-basin, Tennessee, USA. *Hydrological Processes*, 28(3), 718–728.
- Musolff, A., Schmidt, C., Selle, B., & Fleckenstein, J. H. (2015). Catchment controls on solute export. *Advances in Water Resources*, 86, 133–146. <https://doi.org/10.1016/j.advwatres.2015.09.026>
- Nathan, R. J., & McMahon, T. A. (1990). Evaluation of automated techniques for base flow and recession analyses. *Water Resources Research*, 26(7), 1465–1473.
- National Research Council. (2001). *Basic research opportunities in earth science*. National Research Council.
- Neurath, R. (2007). *Comparative baseflow hydrochemistry of various septic system density groups within the Yellow River Watershed, Gwinnett County, Georgia*. Georgia State University.
- Newcomer, T. A., Kaushal, S. S., Mayer, P. M., Shields, A. R., Canuel, E. A., Groffman, P. M., Gold, A. J., Groffman, P. M., & Gold, A. J. (2012). Influence of natural and novel organic carbon sources on denitrification in forest, degraded urban, and restored streams. *Ecological Monographs*, 82(4), 449–466.

- Nicolau, R., Lucas, Y., Merdy, P., Raynaud, M., Var, T., & Cedex, L. G. (2012). Base flow and stormwater net fluxes of carbon and trace metals to the Mediterranean sea by an urbanized small river. *Water Research*, 46(20), 6625–6637.
<https://doi.org/10.1016/j.watres.2012.01.031>
- O'Driscoll, M., Clinton, S., Jefferson, A., Manda, A., & McMillan, S. (2010). Urbanization effects on watershed hydrology and in-stream processes in the southern United States. *Water*, 2(3), 605–648. <https://doi.org/10.3390/w2030605>
- Olshansky, Y., White, A. M., Moravec, B. G., McIntosh, J., & Chorover, J. (2018). Subsurface pore water contributions to stream concentration-discharge relations across a snowmelt hydrograph. *Frontiers in Earth Science*, 6(181), 1–18.
<https://doi.org/10.3389/feart.2018.00181>
- Pellerin, B. A., Wollheim, W. M., Feng, X., & Vörösmarty, C. J. (2008). The application of electrical conductivity as a tracer for hydrograph separation in urban catchments. *Hydrological Processes*, 22(12), 1810–1818. <https://doi.org/10.1002/hyp.6786>
- Peters, N. E. (2009). Effects of urbanization on stream water quality in the city of Atlanta, Georgia, USA. *Hydrological Processes*, 23, 2860–2878.
<https://doi.org/10.1002/hyp.7373>
- Pinder, G. F., & Jones, J. F. (1969). Determination of the ground-water component of peak discharge from the chemistry of total runoff. *Water Resources Research*, 5(2), 438–445.

- Pratt, J. M., Coler, R. A., & Godfrey, P. J. (1981). Ecological effects of urban stormwater runoff on benthic macroinvertebrates inhabiting the Green River, Massachusetts. *Hydrobiologia*, 83, 29–42.
- Raymond, P. A., & Saiers, J. E. (2010). Event controlled DOC export from forested watersheds. *Biogeochemistry*, 100, 197–209.
<https://doi.org/10.1007/s10533-010-9416-7>
- Rice, K. C., Scanlon, T. M., Lynch, J. A., & Cosby, B. J. (2014). Decreased atmospheric sulfur deposition across the southeastern U.S.: When will watersheds release stored sulfate? *Environmental Science & Technology*, 48, 10071–10078.
- Rose, L. A., Karwan, D. L., & Godsey, S. E. (2018). Concentration–discharge relationships describe solute and sediment mobilization, reaction, and transport at event and longer timescales. *Hydrological Processes*, 32(18), 2829–2844.
<https://doi.org/10.1002/hyp.13235>
- Rose, S. (2003). Comparative solute-discharge hysteresis analysis for an urbanized and a “control basin” in the Georgia (USA) Piedmont. *Journal of Hydrology*, 284(1–4), 45–56. <https://doi.org/10.1016/j.jhydrol.2003.07.001>
- Sansalone, J. J., Hird, J. P., Cartledge, F. K., Marty, E., Sansalone, J. J., Hird, J. P., Cartledge, F. K., & Tittlebaum, M. E. (2005). Event-based stormwater quality and quantity loadings from elevated urban infrastructure affected by transportation. *Water Environment Research*, 77(4). <https://doi.org/10.2175/106143005X51932>
- Shanley, J. B. (1994). Effects of ion exchange on stream solute fluxes in a basin receiving highway deicing salts. *Journal of Environment Quality*, 23(5), 977–986.

Shanley, James B, Kendall, C., Smith, T. E., Wolock, D. M., & McDonnell, J. J. (2002).

Controls on old and new water contributions to stream flow at some nested catchments in Vermont, USA. *Hydrological Processes*, 16, 589–609.

<https://doi.org/10.1002/hyp.312>

Siwek, J. P., Mirosław, Ż., Siwek, J., & Szymański, W. (2017). Effect of land use,

seasonality, and hydrometeorological conditions on the K⁺ concentration–discharge relationship during different types of floods in Carpathian Foothills catchments (Poland). *Water, Air, and Soil Pollution*, 228(11), 445.

<https://doi.org/10.1007/s11270-017-3585-0>

Sklash, M. G., & Farvolden, R. N. (1979). The role of groundwater in storm runoff.

Journal of Hydrology, 43(1–4), 45–65.

Smith, B. K., & Smith, J. A. (2015). The flashiest watersheds in the contiguous United States. *Journal of Hydrometeorology*, 16, 2365–2381.

<https://doi.org/10.1175/JHM-D-14-0217.1>

Southwick, D. L., & Owens, J. P. (1968). *Geologic Map of Harford County, Maryland 1:62,500; Maryland Geological Survey: Baltimore Maryland*.

Taka, M., Kokkonen, T., Kuoppamaki, K., Niemi, T., Sillanpaa, N., Valtanen, M.,

Warsta, L., & Setälä, H. (2017). Spatio-temporal patterns of major ions in urban stormwater under cold climate. *Hydrological Processes*, 31(8), 1564–1577.

The World Bank Group. (2019). *Urban population (% of total)*.

<https://data.worldbank.org/indicator/SP.URB.TOTL.IN.ZS>

- Thompson, S. E., Basu, N. B., Lascurain, J., Aubeneau, A., & Rao, P. S. C. (2011). Relative dominance of hydrologic versus biogeochemical factors on solute export across impact gradients. *Water Resources Research*, 47(7), 1–20.
<https://doi.org/10.1029/2010WR009605>
- Vaughan, M. C. H., Bowden, W. B., Shanley, J. B., Vermilyea, A., Sleeper, R., Gold, A. J., Pradhanang, S. M., Inamdar, S. P., Levia, D. F., Andres, A. S., Birgand, F., & Schroth, A. W. (2017). High-frequency dissolved organic carbon and nitrate measurements reveal differences in storm hysteresis and loading in relation to land cover and seasonality. *Water Resources Research*, 53(7), 5345–5363.
<https://doi.org/10.1002/2017WR020491>
- Vaughan, M. C. H., & Schroth, A. W. (2019). Shining light on the storm: In-stream optics reveal hysteresis of dissolved organic matter character. *Biogeochemistry*, 143(3), 275–291. <https://doi.org/10.1007/s10533-019-00561-w>
- Walsh, C. J., Roy, A. H., Feminella, J. W., Cottingham, P. D., Groffman, P. M., & Morgan, R. P. (2005). The urban stream syndrome: Current knowledge and the search for a cure. *Journal of the North American Benthological Society*, 24(3), 706–723.
- Walsh, C. J., Sharpe, A. K., Breen, P. F., & Sonneman, J. A. (2001). Effects of urbanization on streams of the Melbourne region, Victoria, Australia. *Freshwater Biology*, 46, 535–551.
- Walton, N. R. G. (1989). Electrical conductivity and total dissolved solids: What is their precise relationship? *Desalination*, 72(3), 275–292.

- Wymore, A. S., Leon, M. C., Shanley, J. B., & McDowell, W. H. (2019). Hysteretic response of solutes and turbidity at the event scale across forested tropical montane watersheds. *Freshwater Biology*, 7(126), 1–13.
<https://doi.org/10.3389/feart.2019.00126>
- Zhi, W., Li, L., Dong, W., & Brown, W. (2019). Distinct source water chemistry shapes contrasting concentration-discharge patterns. *Water Resources Research*, 55, 1–19.
<https://doi.org/10.1029/2018WR024257>
- Zhong, J., Li, S., Tao, F., Yue, F., & Liu, C. (2017). Sensitivity of chemical weathering and dissolved carbon dynamics to hydrological conditions in a typical karst river. *Scientific Reports, March*. <https://doi.org/10.1038/srep42944>
- Zuecco, G., Penna, D., Borga, M., & Van Meerveld, H. J. (2016). A versatile index to characterize hysteresis between hydrological variables at the runoff event timescale. *Hydrological Processes*, 30, 1449–1466. <https://doi.org/10.1002/hyp.10681>
- Zuecco, G., Rinderer, M., Penna, D., Borga, M., & van Meerveld, H. J. (2019). Quantification of subsurface hydrologic connectivity in four headwater catchments using graph theory. *Science of the Total Environment*, 646, 1265–1280.
<https://doi.org/10.1016/j.scitotenv.2018.07.269>

8. Curriculum Vitae

MELINDA MARSH



EDUCATION

Towson University, Towson MD

Master of Science in Environmental Science | GPA: 4.0 | August 2021

Towson University, Towson MD

Bachelor of Science in Geology, *summa cum laude* | 2019

Drexel University, Philadelphia PA

Bachelor of Science in Interior Design | 2009

RESEARCH & WORK EXPERIENCE

Towson University, Environmental Science & Studies Department

Graduate Research Assistant | August 2019 – August 2021

Advisor: Dr. Joel Moore

- Investigated concentration-discharge relationships for major ions, dissolved silica, and dissolved organic carbon in urbanized watersheds using a combination of high-frequency specific conductance data and discrete baseflow sampling and storm sampling with automated samplers
- Performed laboratory analyses on collected samples
- Quantified source contributions to stormflow using hydrograph separation and end-member mixing analysis techniques
- Compared annual and event-scale nutrient and sediment loads pre- and post-restoration using high-frequency nutrient and sediment concentration data sets generated from regression relationships developed from discrete data
- Trained undergraduate students to perform fieldwork and use analytical instrumentation

Towson University, Department of Physics, Astronomy, & Geosciences

Undergraduate Research Assistant | May 2017 – August 2019

Advisor: Dr. Joel Moore

- Collected and processed surface water samples during baseflow and stormflow conditions
- Analyzed water samples for concentrations of major ions, dissolved inorganic carbon, dissolved organic carbon, nutrients, and dissolved silica
- Provided field and laboratory assistance to graduate students, including measuring stream discharge via salt dilution gaging and measuring total suspended solids

Jacobs Technology | Aberdeen Proving Ground, MD

Scientific Data Collector | January 2010 – May 2015

- Collected in-field qualitative and quantitative data during developmental and operational testing of automotive, robotic, and communications platforms for the U.S. Army
- Documented incidents and failures, and any subsequent modifications or repairs made to the platform during test operations
- Produced technical reports detailing test methods and results

PUBLICATIONS

P. McMahon, V. B. Beauchamp, R. A. Casey, C. J. Salice, K. Bucher, M. Marsh, J. Moore (2020) Effects of stream restoration by legacy sediment removal and floodplain reconnection on water quality. *Environmental Research Letters*

POSTER PRESENTATIONS

Marsh M. & Moore J. (2019) Using high-frequency data and concentration-discharge relationships to describe solute mobilization and transport in suburban and urban watersheds. *American Geophysical Union Fall Meeting*, San Francisco, CA.

Marsh M. & Moore J. (2019) Using high-frequency data and concentration-discharge relationships to describe solute mobilization and transport in suburban and urban watersheds. *Maryland Water Monitoring Council Annual Conference*, Baltimore, MD.

Marsh M., Bucher K., Moore J. (2018) Investigating concentration-discharge relationships for urban watersheds in Maryland. *American Geophysical Union Fall Meeting*, Washington, DC.

Marsh M., Bucher K., Moore J. (2018) Characterizing storm event concentration-discharge relationships in urban watersheds using high-frequency data. *Maryland Water Monitoring Council Annual Conference*, Baltimore, MD. *Awarded 2nd place for undergraduate student poster.*

FELLOWSHIPS & GRANTS

Maryland Water Resources Research Center Graduate Research Fellowship (\$6000) | 2020
University of Maryland, College Park

Fisher College of Science & Mathematics Undergraduate Research Grant (\$700) | 2019
Towson University

Fisher College of Science & Mathematics Undergraduate Research Grant (\$500) | 2018
Towson University

HONORS & AWARDS

Geosciences Achievement Award | 2019, 2018
Towson University Department of Physics, Astronomy, & Geosciences

William F. Pelham Award for Outstanding Junior | 2017
Towson University Department of Physics, Astronomy, & Geosciences

Mineralogical Society of America Undergraduate Prize | 2017
Mineralogical Society of America

